Department of Chemistry

Synthesis, Characterisation and Functionalisation of Magnetic Nanoparticles for Biomedical Applications

Thesis submitted in accordance with the requirements of the University of Liverpool for the degree of Doctor of Philosophy

By

Ian Robinson

2009

I certify that all material in this thesis that is not my own work has been clearly identified and no material is included for which a degree has previously been awarded

Dedicated to the memory of my Dad, Arthur 'Billy' Robinson

1935 - 2006

Acknowledgments

I would like to thank my supervisors, Dr. Nguyen TK Thanh and Professor David G Fernig for their support and guidance during this project.

Many thanks to Dr Le Duc Tung in the Department of Physics, University of Liverpool, for carrying out the SQUID experiments and for useful discussion in interpreting the data. I would also like to thank Dr Ian Prior, Ms Cornelia Muncke and Ms Alison Beckett of the Department of Physiology, University of Liverpool for all their assistance using the TEM. Thanks also to Ms Marion Pope, School of Veterinary Science and various members of staff at the Department of Engineering for use of TEM.

Special thanks to Prof Cameron Alexander of the School of Pharmacy, University of Nottingham, for kindly providing the thermo-responsive polymers, Dr Stefano Zacchini of the Department of Physical and Inorganic Chemistry, University of Bologna for kindly providing the bimetallic carbonyl clusters, Dr Christoph Walti, School of Electronic and Electrical Engineering, University of Leeds, for providing the thiolated DNA, Dr Martin Volk of the Department of Chemistry, University of Liverpool for provision of the laser, Dr Gabriel Caruntu, Advanced Materials Research Institute, University of New Orleans, and Dr Shinya Maenosono, School of Materials Science, Japan Advanced Institute of Science and Technology for X-ray diffractometery.

Thanks also to Prof Don Bethell, Prof Brian Heaton, Dr Peter Hawkins, Mr John Michells, Dr Richard Hodgson, Dr Laura Parkes, Prof Jon Dobson and Dr Neil Farrow for their collaborative research and useful discussions. I also like to thank the past and current members of Nanomag Lab, Department of Chemistry and Lab D in the School of Biological Sciences and the administration and support staff in the Department of Chemistry and School of Biological Sciences.

Thanks to the EPSRC for my funding and the Royal Society and the North West Cancer Research Fund for funding the research.

And finally thanks go to my wife Joanne and our children Emily and Sam for help and comfort through the tough times.

Abstract

The synthetic techniques used to produce magnetic nanoparticles have been greatly refined in recent years to the point where very fine control over the size, shape and composition of the particles is now achievable. The focus of much research now is to produce magnetic nanoparticles for specific applications. For use in biomedical applications, the initial step is to synthesise nanoparticles that are water soluble and stable in biological solutions. This can be achieved by tailoring the surface of the nanoparticles with various organic coatings such as polymers and peptides or inorganic coatings such as noble metals or silica. Modification of the nanoparticle surface is also essential for the biofunctionalisation of these particles.

Water soluble, monodisperse, cobalt and maghemite nanoparticles were made by a one-step organic synthesis method, with a mean diameter of 7 ± 1 nm and 8 ± 1 nm, respectively, and coated with a stimuli-sensitive polymer. The nanoparticles are superparamagnetic at room temperature and stable in different media such as phosphate buffer solution and water. The nanoparticles were also stable across a wide pH range. With the stimuli-sensitive polymer coating, the nanoparticles also exhibit 'smart behaviour' in response to the changing temperature. The stability of the nanoparticles and their ability to dissolve in aqueous solution makes them potential candidates for biomedical application.

Using pulsed laser irradiation to decompose cobalt carbonyl in a solution of stabilising ligands it was possible to produce sub 4 nm cobalt nanoparticles. By modifying the reaction conditions such as the ligand concentration and wavelength of light used it was possible to change the size and size distribution of the synthesised nanoparticles. Controlling these conditions also gave an insight into the formation mechanism of the nanoparticles.

The thermal decomposition of bimetallic carbonyl clusters offered a unique method for the synthesis of alloy magnetic nanoparticles. The composition of nanoparticles produced very closely matched the atomic arrangement of the carbonyl cluster used to synthesise them. Changing the reaction conditions, such as ligand concentration, ligand type and reaction temperature had very little effect upon the physical characteristics of the synthesised nanoparticles.

The latter two methods produced magnetic nanoparticles with a hydrophobic coating that needs to be modified to make them water soluble if they are to be used in biomedical applications. One approach used to overcome this was to manipulate the surface of the magnetic nanoparticles which involved the exchange of, or addition to, the hydrophobic ligand shells to make the nanoparticles more hydrophilic. Monodisperse cobalt and iron oxide nanoparticles of various sizes were synthesised in organic solvent and coated with hydrophobic oleic acid. Several synthesised polymers were used, each with its own exchange or addition technique. Using thermo-responsive polymers produced water stable dispersions of both cobalt and iron oxide stable up to 0.2 M and 0.5 M, respectively. However, where the iron oxide nanoparticles remained discrete in solution the cobalt nanoparticles formed larger spherical aggregates (100 to 150 nm in diameter). The stability of iron oxide nanoparticles in aqueous solution was further improved by the use of phosphine oxide-polyethyleneglycol polymer. However, this polymer did not stabilise cobalt nanoparticles in water. The addition of Pluronic F127 to the oleic acid layer produced very water-stable iron oxide nanoparticles, but again was not suitable for use with cobalt nanoparticles. Since the ligand exchange/addition techniques did not work well with cobalt nanoparticles an alternative method for the functionalisation of the magnetic nanoparticles was sought. This method was to reduce a gold salt on the surface of preformed magnetic nanoparticles to give them a layer of gold in a core-shell structure. This gold shell provided a versatile platform for the functionalisation of the nanoparticles. It was found that the gold layer did not easily form on the cobalt nanoparticles surface and instead formed an alloy, making stabilisation of these particles in aqueous solution difficult. However, a gold layer did form on the surface of magnetite nanoparticles and it was possible to disperse these core-shell nanoparticles in aqueous solution and furthermore, they could be functionalised with thiolated DNA.

List of Publications

Robinson, I.; Zacchini, S.; Tung, L.D.; Maenosono, S.; Thanh, N.T.K. Synthesis and characterization of magnetic nanoalloys from bimetallic carbonyl clusters. *Chemistry of Materials* **2009**, *21*, 3021-3026.

Robinson, I.; Volk, M.; Tung, L. D.; Carnutu, G.; Kay, N.; Thanh, N. T. K. Synthesis of Co nanoparticles by pulsed laser irradiation of cobalt carbonyl in organic solution. *Journal of Physical Chemistry C* **2009,** *113*, 9497-9501.

Robinson, I.; Alexander, C.; Tung, L. D.; Fernig, D. G.; Thanh N. T. K., Fabrication of water-soluble magnetic nanoparticles by ligand-exchange with thermo-responsive polymers. *Journal of Magnetism and Magnetic Materials* **2009**, *321*, 1421-1423.

Parkes, L. M.; Hodgson, R.; Lu, L. T.; Tung, L. D.; **Robinson, I.**; Fernig, D. G.; Thanh, N. T. K., Cobalt nanoparticles as a novel magnetic resonance contrast agent-relaxivities at 1.5 and 3 Tesla. *Contrast Media & Molecular Imaging* **2008,** *3*, 150-156.

Lu, L. T.; Tung, L. D.; **Robinson, I.**; Ung, D.; Tan, B.; Long, J.; Cooper, A. I.; Fernig, D. G.; Thanh, N. T. K., Size and shape control for water-soluble magnetic cobalt nanoparticles using polymer ligands. *Journal of Materials Chemistry* **2008**, *18*, 2453 - 2458.

Robinson, I.; Alexander, C.; Lu, L. T.; Tung, L. D.; Fernig, D. G.; Thanh, N. T. K., One-step synthesis of monodisperse water-soluble 'dual-responsive' magnetic nanoparticles. *Chemical Communications* **2007**, *44*, 4602 - 4604.

Thanh, N. T. K.; **Robinson, I.**; Tung, L. D., Magnetic nanoparticles for biomedical applications: synthesis, characterization and uses. *Dekker Encyclopedia of Nanoscience and Nanotechnology* **2007**, *1*, 1 - 10.

In preparation

Robinson, I., Maenosono, S., Walti, C., Tung, L.T., Thanh, N.T.K. Gold coated magnetic nanoparticles: interaction with thiolated DNA. *Journal of Physics D.*

Conference Presentations

Nanoparticles 2009: Synthesis, Properties and Applications of Nanoparticles, Liverpool, UK September 2009. Poster: *"Synthesis and characterization of magnetic nanoalloys from bimetallic carbonyl clusters" (2nd prize for best poster)*

UK Nanoform, London, UK, October 2008. Poster: *"A versatile approach for producing water-stable magnetic nanoparticles: ligand exchange"*

7th International Conference on the Scientific and Clinical applications of Magnetic Carriers, Vancouver, Canada, April 2008. Poster: *"Synthesis of cobalt nanoparticles by laser irradiation in organic solution"*

Nanoparticles 2008: Synthesis, Properties and Applications of Nanoparticles, Bradford, UK, February 2008. Poster: *"One-step organic synthesis of monodisperse water-soluble magnetic nanoparticles"*

MC8: Advancing Materials by Chemical Design, London, UK, July 2007. Poster. *"The synthesis of thermo-responsive polymer coated magnetic nanoparticles"*

Nanoparticles: New Opportunities for Colloid Scientists, Warwick, UK, March 2007. Oral: *"Fabrication of monodispersed, tunable size and shape water-soluble Co magnetic NPs using a simple reduction method in polymer ligands"*
Poster: *"The synthesis of magnetic nanoparticles coated with thermo-responsive polymers"*

6th International Conference on the Scientific and Clinical applications of Magnetic Carriers, Krems, Austria, May 2006. Poster: *"Design and Synthesis of Core-Shell Magnetic Nanoparticles: A Novel Approach"*

Table of Contents

List of Figures

List of Schemes

List of Tables

Abbreviations

AC	Alternating current
ACVA	4,4'-Azo-bis(4-cyanovaleric acid)
AIBN	α,α'-Azo-bis(isobutyronitrile)
B_0	Static magnetic field
CTAB	Cetyltrimethylammonium bromide
d	Density
DCB	1,2-Dichlorobenzene
DMSA	Dimercaptosuccinic acid
DNA	Deoxyribonucleic acid
EDX	Energy dispersion X-ray spectroscopy
FC	Field cooled
HRTEM	High resolution transmission electron microscope
HSP	Heat shock proteins
$KAuCl_4$	Potassium tetrachloroaurate
LCST	Lowest critical solubility temperature
MagFFF	Magnetic field flow fractionation
MALDI-TOF	Matrix assisted laser desorption ionization time-of-flight
3-MPA	3-Mercaptopropanoic acid
MRI	Magnetic resonance imaging
Mw	Molecular weight
NaAOT	Sodium bis(2-ethylhexyl) sulfosuccinate
Nd:YAG	Neodymium-doped yttrium aluminium garnet
NiPAm	N-isopropylacrylamide
NMPO	1-Methyl-2-pyrrolidinone

NMR	Nuclear magnetic resonance
NPs	Nanoparticles
N-t-BAm	N-tert-butylacrylamide
OA	Oleic acid
OLA	Oleyl amine
PBS	Phosphate buffer solution
PEG	Polyethylene glycol
PEI	Polyethyleneimide
PEO	Polyethylene oxide
PO-PEG	Phosphine oxide-polyethylene glycol
PPO	Polypropylene oxide
r	Radius
r_1	Longitudinal or spin relaxation rate
r_2	Transverse or spin-spin relaxation rate
rf	Radio frequency
RNA	Ribonucleic acid
rt-PA	Recombinant tissue plasminogen activator
SQUID	Super-conducting quantum interference device
T_1	Longitudinal or spin relaxation time
T_2	Transverse or spin-spin relaxation time
T_b	Blocking temperature
TEA	Tetraethyl amine
TEM	Transmission electron microscopy
TEOS	Tetraethoxysilane
THF	Tetrahydrofuran

TMBA	Trimethylbenzyl amine
TMA	Tetramethyl amine
TOP	Trioctyl phosphine
TOPO	Trioctyl phosphine oxide
UV/vis	Ultra-violet/visible spectroscopy
v	Volume
VEGF	Vascular endothelial growth factor
XRD	X-ray diffraction
ZFC	Zero field cooled

Chapter 1

Introduction

1.1 Overview

Nanotechnology can be described as the development materials at the atomic and molecular level in order to instil them with special physical and chemical properties[1]. Nanoparticles (NPs) represent an area within nanotechnology, which deals with particles typically between 1 and 100 nm in size. These NPs can be divided into different types according to their physical and chemical properties. For example, semiconductor NPs fabricated from materials such as CdSe, CdS and ZnS, which exhibit atom-like energy states due to confinement effects, can be described as quantum dots[2]. The electronic properties of these particles allows them to be used as active materials in single electron transistors[3]. Furthermore, the atom-like energy states also play a role in the special optical properties observed in these materials, such as particle-size dependent wavelength of fluorescence[1]. Metallic NPs represent another class of nanomaterial that have been studied since the mid-1800s. For instance, gold NPs have been used in the past for medical applications[4] and the optical properties of these particles have been found to differ greatly from the bulk material[5]. Metallic NPs of particular interest are the magnetic NPs that can consist of metals such as iron[6, 7], cobalt[8] and nickel[9], alloys such as CoPt[10, 11] and FeCo[12] as well as iron oxides.

Interest in magnetic NPs has grown rapidly in recent years due to their diverse applications in biomedicines[13], novel materials for engineering[14] and devices[14], which arise from the unique combination of small size, exotic properties and processability of these materials. Magnetic NPs can be extremely useful due to their potential biomedical applications in areas such as magnetic

resonance imaging (MRI)[15], targeted drug delivery[16], hyperthermia treatment[13] of solid tumours and cell separation[13].

The physical properties can be attributed to the size and surface effect of the NPs as well as inter-particle interactions and unusual electron transport properties[1]. These include a large surface area to volume ratio and ubiquitous tissue accessibility making the particles very suitable for use in *in vitro* diagnostic applications[13]. The magnetic properties of the NPs is particularly important for *in vivo* applications where superparamagnetic particles are preferred as these do not retain any magnetism upon the removal of a magnetic field as opposed to ferromagnetic material that aggregate after exposure to a similar field[17, 18].

As mentioned above, the physical properties of these nanostructures (optical, electrical, chemical, magnetic, etc) are dependent upon their size, composition and crystal structural ordering. Therefore, the fabrication of tailored NPs reliably and predictably is highly desirable. One of the ways to produce well defined NPs is to tailor the surface properties of the particles, often by coating or encapsulating them in a shell of a particular material[19]. This coating and encapsulation can also protect the core from extraneous chemical and physical changes[6, 14, 20]. Various substances have been used to form the protective shell of NPs e.g. silica[7], polymer[21], peptide[22, 23] and noble metals[24, 25], however achieving long term stability of the particles still remains a problem.

Modification of the surface properties is particularly important when considering *in vivo* applications to ensure that particles are biocompatible, non-toxic and stable to the reticulo-endothelial system: the body's major defence

mechanism[13]. Particles possessing a hydrophobic surface are readily coated with plasma components in the blood stream and are therefore easily removed from the circulation, while more hydrophilic particles can resist coating and are cleared much more slowly[26]. Many common hydrophilic coatings used on NPs include derivatives of dextran, polyethylene glycol, polyethylene oxide, poloxamers and polyoxamines[27]. The dense brushes of polymers can inhibit the opsonisation (the process that causes foreign bodies to be recognised by the body's reticulo-endothelial system) of the particles, thereby increasing their circulation time.

1.2 Magnetism

Magnetic moments arise from electrons having a negative charge and spin. A rotating, electrically charged body causes a magnetic dipole effect, thus creating magnetic poles in equal but opposite directions. Therefore, all materials are magnetic to some extent and the magnetism depends upon the atomic structure of the material and temperature. However, most materials only exhibit a low level of magnetism, and even then only in an externally applied magnetic field[13]. These materials can be described as either diamagnetic or paramagnetic. Diamagnetic material displays a weak repulsion from a magnetic field and arises because all the paired electrons in a material will make a weak contribution to its response. Diamagnetism is overpowered in materials that display other forms of magnetism. Paramagnetic material has unpaired electron spins and, in an external magnetic field, has a small induced magnetism, due to the small number of spins orientated by the field. It does not retain any residual magnetism after the

removal of an external magnetic field as the thermal motion causes the spins to become randomly orientated (Figure 1.1).

Other materials display ordered magnetic states and some are magnetic in the absence of an external magnetic field; these materials can be described as ferromagnetic, ferrimagnetic and antiferromagnetic (Figure 1.1)[28]. Each type of magnetism has different coupling interaction between the electrons within the material that gives rise to large spontaneous magnetisations[28]. Ferromagnetic material becomes magnetised in an externally applied magnetic field and remains magnetised for a period after removal of the field. Atoms with partially filled atomic orbitals (i.e. unpaired electrons) can experience a net magnetic moment in the absence of a magnetic field. Ferromagnetic material has many such electrons giving rise to permanent dipoles or 'spins' that can align in parallel spontaneously, even in the absence of an external magnetic field. Adjacent magnetic moments can align in opposite directions; in ferrimagnetic material the opposing moments are of unequal strength, resulting in a net magnetic field lower than that expected for ferromagnetic material. If the opposing moments are of equal strength, giving rise to a zero net magnetisation, the material is described as antiferromagnetic. All these effects are temperature dependent and only occur below the Curie temperature[28] in ferro- and ferrimagnetic material and the Néel temperature[28] in antiferromagnets. Above this temperature the thermal energy is sufficient to overcome the energy within the magnetic field and the moments are free to move out of alignment and the material becomes paramagnetic. To minimise energy losses ferromagnetic material tends to form magnetic domains, where each domain is magnetised in a different direction. However, particles less than approximately 100 nm in diameter are composed of

a single magnetic domain. When magnetic particles are cooled below a certain temperature, the magnetic moment becomes blocked. This temperature is known as the blocking temperature (T_b)[28]. Blocking temperature is dependent up on the size and composition of the particle (larger particles have larger blocking temperatures). Unblocked material that responds to a magnetic field is described as superparamagnetic. This material can display paramagnetic behaviour below the Curie or Néel temperature; however superparamagnetic material has a higher magnetic susceptibility per atom than paramagnetic material. This phenomenon occurs in material composed of small crystallites and while the thermal energy is not enough to overcome the coupling forces between neighbouring atoms it is sufficient to change the magnetisation of the whole crystallite.

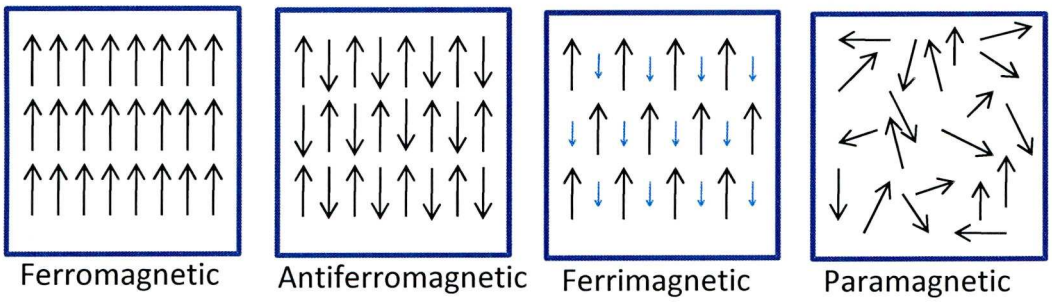

Figure 1.1. Schematic diagram of the arrangement of magnetic spins (symbolised by arrows) in materials showing different types of magnetism.

1.3 Biomedical applications

Magnetic NPs, in the form of ferrofluids, have potential use in a wide range of applications in biomedicine, for example MRI[15], controlled drug delivery[29, 30], biological targeting and cell separation[31], cancer diagnosis and treatment[32]. Each application requires NPs that are tailored specifically for that function. Some of the applications are discussed in more detail in the following sections.

1.3.1 Magnetic fluid hyperthermia

Thermotherapy of tumours includes thermoablation[33] and hyperthermia[34] treatment. In thermoablation therapy the tumour is heated above 46 °C for a relatively short period of time to induce necrosis and coagulation or carbonisation of the cancer cells. Hyperthermia treatment heats the tumour to a lower temperature (42 –46 °C) for an extended period of time to cause cancer cell death. Thermotherapy has the potential to be very effective for targeted treatment of cancer as tumours are more susceptible to the effects of heating than healthy tissue because of the poor and disorganised blood supply[33]. The poor blood supply means that the heat is not dissipated from the tumour as rapidly as healthy tissue. Not only this, but the hypoxic cells of the tumour have a lower thermal resistance due to higher levels of lactic acid[34]. Magnetic NPs have the potential for use in these treatments, in conjunction with chemotherapy, radiotherapy and surgery[35-37]. The treatment is based on the response of the magnetic NPs to an alternating current (AC) magnetic field where heat is generated by hysteresis loss and Ohmic loss as well as Néel relaxation (reorientation of the magnetisation) and Brownian relaxation (frictional forces)[38, 39]. For superparamagnetic material the main source of energy loss is via Brownian relaxation[40]. Upon exposure to elevated temperatures, the cancer cells will release heat shock protein (HSP) that will try to refold proteins that have been denatured by the heat. Therefore, thermotherapy should be used in conjunction with HSP inhibitors[41]. The control of the temperature of the magnetic NPs *in vivo* can also help avoid healthy tissue damage. By designing materials in such a way that they display temperature sensitive magnetic properties, it may be possible to control the temperature of the

particles. A material with a suitable Curie temperature (T_C ~ 42 – 56 °C) would be ideally suited for this purpose. Below the Curie temperature, exposing the material to an AC magnetic field will generate heat and the heating will stop once the temperature exceeds this temperature[42]. This way the material can act as an *in vivo* temperature-controlling switch. Amongst the more promising material for this use are ferrites such as $Mn_{0.4}Zn_{0.6}Fe_2O_4$[42].

1.3.2 Magnetic resonance imaging contrast enhancement

MRI is based on the response of protons from water in tissues and organs to the combined effects of a strong static magnetic field (B_0) and a transverse radiofrequency field (rf field)[43]. After rf excitation the protons attempt to return to their ground states through two independent relaxation processes. In longitudinal (spin-lattice) relaxation, or T_1 recovery, the energy absorbed by the protons is released into the surrounding tissue (lattice) as they try to re-align with B_0 and is quickly dispersed. The other process is transverse (spin-spin) relaxation, or T_2 decay, where the energy is dispersed between spinning protons in the tissue and is therefore a much slower process. A computer collects the relaxation data and a two-dimensional Fourier transformation is applied to give the amplitudes of nuclear magnetic resonance (NMR) signals[44-46]. The intrinsic differences in relaxation times between different tissues is usually small, however, the addition of magnetic material as contrast agents can shorten these relaxation times (Figure 1.2)[15] and thus improve the diagnostic value of MRI for improved delineation of organs.[47]

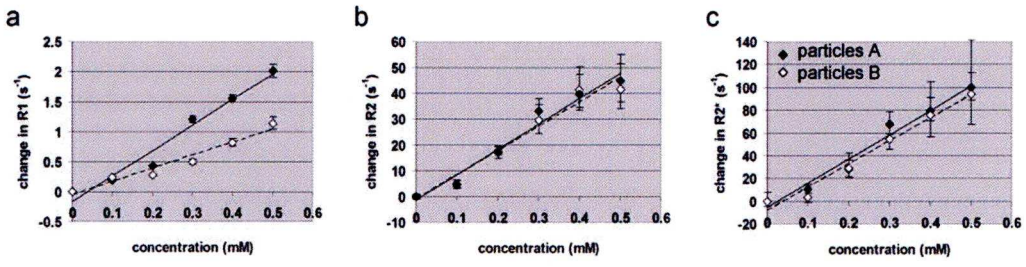

Figure 1.2. Relaxation rates R1 (a), R2 (b) and R2* (c) plotted for different concentrations of cobalt (from Parkes *et al*[15]).

The detection of metastases has proved difficult in the detection of invasive tumours. Using magnetic NPs as contrast agents in MRI it is possible visualise metastases in lymph nodes, backbone, brain, liver, spleen, urine bladder, throat, lungs, kidney, and rectum in mice that were not palpable by physical examination nor visualised using non-enhanced MRI[48].

1.3.3 Drug carrying and release

Magnetic drug delivery is based on the concept that magnetic nanoparticle-drug conjugates are injected into a patient and then guided to a specific site by localised magnetic field gradients, held there until the therapy is complete and removed[49]. In this way, large doses of drug can be localised to achieve a high local concentration and released over a long time period, improving efficacy, and thus reducing systemic toxicity and other adverse side effects associated with high drug doses[50-52] (Figure 1.3). For example, the anti-cancer drug, Melphalan, has been bound to dextran coated ferrite NPs and as a result, it was found that the activity of the drug increased[53]. Magnetic nanoparticle uptake in cancer cells is much faster than in healthy cells[53-57]. In addition, the magnetic fluid can also be used to locally heat a tumour by applying an external AC magnetic filed in a combined therapy known as

'magnetohydrodynamic thermochemotherapy'[48]. Elsewhere, monodisperse magnetite particles have been embedded into silica with CdSe/ZnS quantum dots and then used for the uptake and controlled release of ibuprofen, with the release controlled by the surface properties of the mesoporous silica spheres[58].

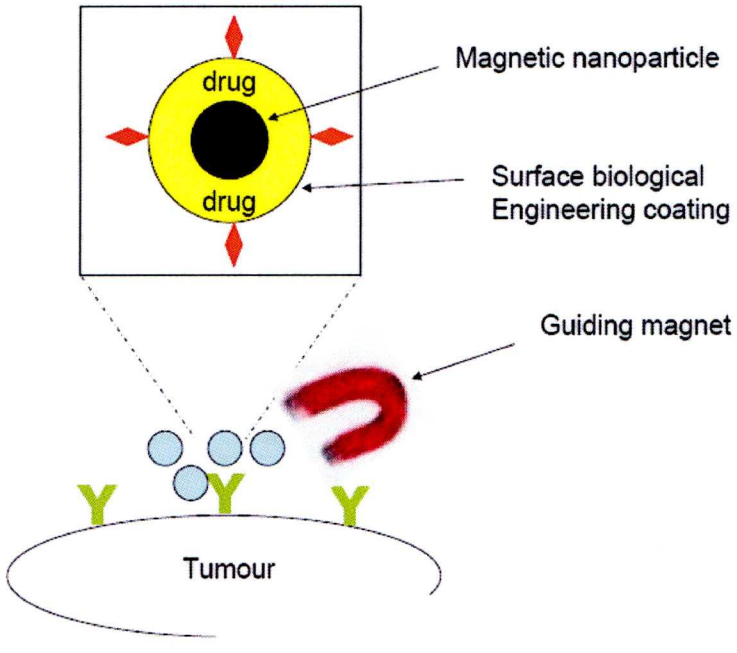

Figure 1.3. Schematic view of the use of magnetic nanoparticles for guided drug delivery (Adapted from Moore.[59]).

As well as anti-cancer therapy, magnetic nanoparticle-drug conjugates can be used in other therapies such as the treatment of ischemic thrombosis. Recombinant tissue plasminogen activator (rt-PA) has been shown to effectively restore or improve perfusion in thromboembolic diseases such as ischemic stroke[60, 61]. It works by strongly binding to newly formed thrombi, exerting serine protease activity and converts plasminogen to plasmin, resulting in fibrinolysis at the site of the thrombus. However, systemic administration of rt-PA often results in haemorrhage, with serious consequences for the patient. By implanting a permanent magnet into an embolic rat model, it has been possible to retain magnetic nanoparticle-rt-PA conjugates in the vicinity of a blood clot

resulting in the thrombolysis of the clot[62]. This approach allows a lower amount of drug to be administered, while increasing the effective drug concentration at the site of activity, resulting in reduced side effects.

1.3.4 Magnetohistopathology

Histopathology is the principle method for the diagnosis of disease, particularly cancer[63]; however the assessment tends to be subjective and not automated or quantifiable. Immunohistochemistry utilises the specificity of antibodies for their target antigens[64]. A vast number of antibodies are commercially available that can be used as diagnostic and prognostic indicators leading to an equally large number of immunohistochemical assays. The simplest assay is the direct conjugation of the antibody to the reporter molecule. However, this requires a large copy number of the marker to relay the signal. More complex methods involve an amplification step to produce a signal. This uses the addition of layers composed of antibodies and complexes that physically increase the mass to boost the signal. Magnetic NPs offer a unique method to detect the expression of clinically significant marker molecules in the histopathological examination of tissue samples used to identify cancer (Figure 1.4). Biotinylated or streptavidin coated magnetic NPs can be introduced into a standard immunohistochemical assay, that uses a biotin/streptavidin system and thereby get caught up in the globular complex formation[65]. The presence of the magnetic NPs can be detected by using magnetic force microscopy and has the potential to automate the screening process as well as categorising expression levels of cellular markers semi-quantitatively.

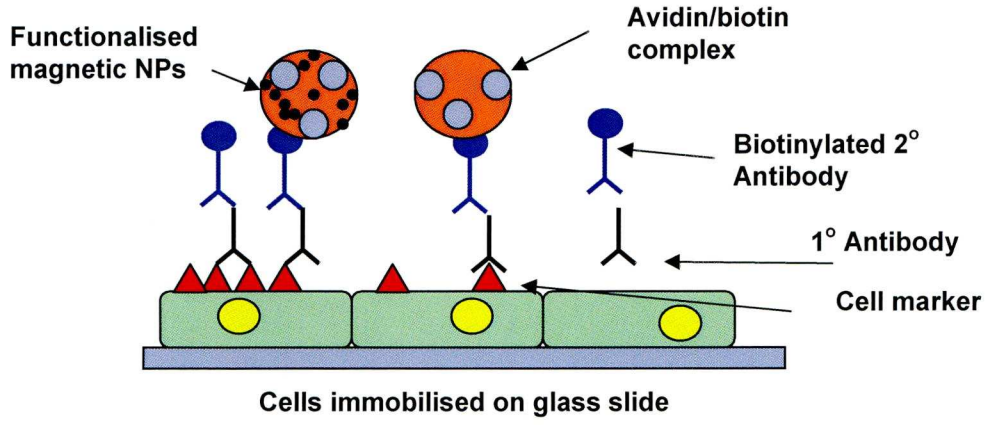

Figure 1.4. Schematic of the magnetic-immunohistochemical assay. Approximately 2 μm tissue sections are incubated with a primary (1°) antibody specific to the marker of interest. A secondary (2°) biotinylated antibody specific to the 1° antibody is added followed by an avidin/biotin complex. Other biotinylated or streptavidin coated molecules can be added in the process such as horseradish peroxidase or magnetic NPs. Amplification is achieved by altering the complex formation parameters resulting in an increased number of magnetic reporter molecules being deposited on the 1° antibody. (adapted from Mitchells *et al*[65]).

1.3.5 Nucleic acid/gene delivery

Nucleic acid delivery into cells, also known as transfection (in the case of nonviral vectors) or transduction (in the case of viral vectors), is in most cases used to achieve the over-expression of introduced genes, the on/off regulation of endogenous genes or gene repair[66]. In a similar way to magnetic drug delivery, magnetic NPs can be used as a non-viral gene delivery vectors[67-69] in a process coined magnetofection[70]. The use of magnetic field promotes the transfection of genetic material-magnetic nanoparticle conjugates into target cells[70]. By using an oscillating magnetic field, transfection rates can be much improved and have been observed to be more efficient than lipid based agents such as Lipofectaimine 2000[70, 71]. For example, polyethyleneimine (PEI) coated magnetic NPs can bind DNA via electrostatic interactions[72] and then by using a magnetic field gradient they can be targeted to a specific tissue[70]. Once the

magnetic nanoparticle-DNA complex has entered the target cell (usually via clatharin-dependent endocytosis[73, 74]), the PEI (itself a non-viral delivery agent) promotes DNA release into the cell by facilitating lysosomal escape.[75] Magnetofection has been used in a variety of cell lines and primary human cells and has also been used to deliver siRNA[74] and antisense oligonucleotides both *in vitro* and *in vivo*[76]. Similarly, streptavidin coated magnetic NPs were used as gene delivery vectors to transfer vascular endothelial growth factor (VEGF) *in vivo*, which can be targeted to the heart by means of an external magnetic field for treatment of cardiovascular disease.[77] Using silica as the protecting and biocompatible layer on a magnetic nanoparticle, Zhao *et al.*[78] used biotin-avidin molecules as linkers for bioconjugating a molecular beacon as a DNA probe. These NPs were able to detect, collect and separate trace amounts of DNA/RNA with a single base difference and can monitor and confirm the collected gene products in real time.

The improved efficiency of the delivery by magnetic NPs compared to other methods may be due to the time taken for the genetic material to get into the tissue. Most non-viral vectors enter cells by slow diffusion, however these vector are subject to time dependent inactivation and can be toxic at high concentrations[79]. In a high gradient magnetic field the full applied magnetic nanoparticle vector dose can sediment onto the cells in a matter of minutes[79]. As well as overcoming the diffusion limitations, magnetofection can be used to synchronise transfection and the vector dose is reduced.

There are some limitations with this technique that involve problems with scale up: it has been shown to work *in vitro* and *in vivo* in small animals. For

targets further from the magnetic field source, higher gradients are required as the field strength quickly diminishes with distance from the magnetic source[80].

1.3.6 Biomagnetic separation and magnetic field flow fractionation

Magnetic field flow fractionation (MagFFF) is a technique similar to chromatography except where chromatography uses the separation between the liquid and solid phases; MagFFF uses the liquid phase only[81]. A typical instrument set-up is depicted in Figure 1.5. By applying a quadrupole magnetic field across a thin-parallel-walled channel, magnetically tagged material in a solution is drawn to the edge of the channel where the fluid is moving very slowly[82]. Material not attracted to the magnetic field remains in the faster flowing fluid in the centre of the channel and is eluted first. The magnetic field is then removed allowing the tagged material to be eluted. An adaptation of this technique has successfully isolated pancreatic islets infused with magnetic NPs[83], which is a requirement for islet transplantation for the treatment of type 1 diabetes[84].

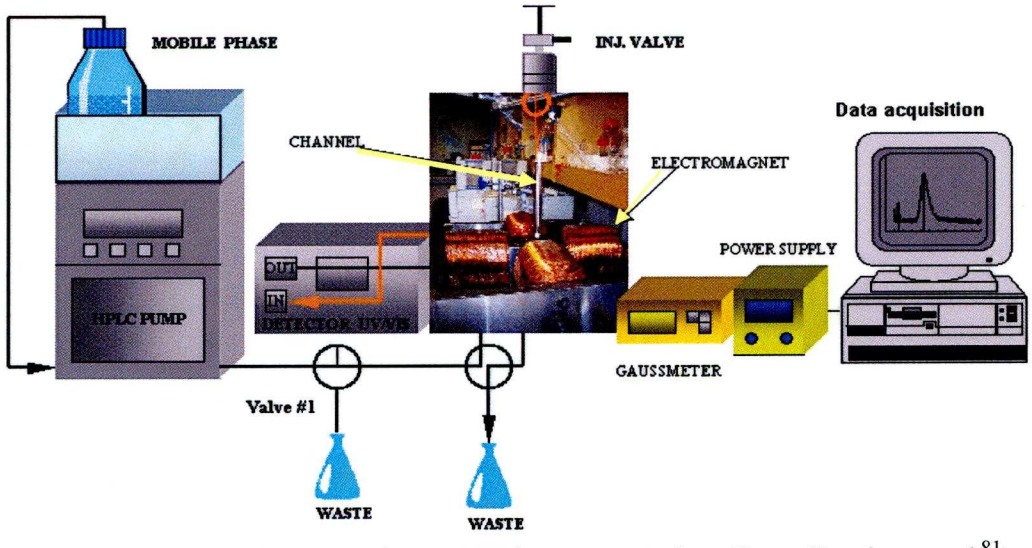

Figure 1.5.A typical set-up of MagFFF instrumentation (from Carpino *et al.*[81]).

1.3.7 Cell tracking

Interest in the use of stem cells and dendritic cells as therapeutic agents has increased greatly over recent years[85]. For the development of clinical cell-based therapies, the location and detection of the cells used needs to be determined in a non-invasive manner. This can be achieved by using magnetic NPs to track the cells through MRI[85]. Magnetic NPs provide the labelled cell with a large magnetic moment that creates substantial disturbances in the local magnetic field leading to a rapid dephasing of the protons, not only in the labelled cell but also those in its immediate vicinity[85]. For example, Bulte *et al.*[86] were able to observe the migration of oligodendrocyte progenitors, that were magnetically labelled using iron oxide NPs, up to a distance of 10 mm in the spinal cord of myelin-deficient mice. They were also able to detect the formation of new myelin in the areas of hypointense magnetic resonance signal, indicating that the presence of magnetic NPs made little difference to the function of the therapeutic cells. This has significance in the treatment of multiple sclerosis, a general feature of which is the failure of patients to regenerate myelin. Other conditions, such as Parkinson's Disease, ischaemic stroke and spinal injuries have the potential to be treated with cell-based therapies[87, 88]. These cells can uptake 10 to 20 ng of iron per cell without any effect upon cell viability and proliferation[89], however, inhibition of cellular differentiation along particular pathways has been reported in certain cell types[90].

Magnetic NPs also have the potential to detect the movement of T-cells by using a SQUID array[91]. This technique has potential as a non-invasive method for determining organ transplant rejection, which is usually monitored by biopsy.

In a similar way lymph node metastasis from breast cancer can be identified by injecting a 'magnetic dye' into the primary tumour[92]. Using this technique a clinician can distinguish the specific lymph nodes to which the cancer has spread and set any treatment accordingly.

An interesting development for the treatment of tumours is the use of a patient's own monocytes that have been genetically modified as gene delivery agents[93]. Once in the tumour the monocytes differentiate into macrophages and accumulate particularly in the treatment resistant hypoxic/perinecrotic areas allowing delivery of genetic material to previously inaccessible areas. However, *ex vivo* manipulated monocytes do not travel to tumour very efficiently when re-administered to the patient[93]. Incorporating magnetic NPs into the monocytes mean they can be attracted to the diseased tissue by use of a magnetic field gradient near the tumour and because the monocytes are magnetically labelled, the degree of infiltration into the tumour can also be monitored by MRI.

1.4 Methods of synthesis of magnetic nanoparticles

The three main synthetic methods for nanoparticle fabrication can be grouped into solid, gas and solution routes (for review see Tartaj *et al.*[94]). Solid routes mainly involve the mechanical milling or the mechanochemical treatment of raw powder to produce NPs[14]. This method has the disadvantage of introducing contamination to the products from the milling equipment and the atmosphere as well as producing large polydisperse particles.

Chemical methods can be split into two main groups: 'phase-transformation'[14] which can be described as the conversion of metal compounds

into metals through thermal decomposition (see below) or chemical reduction[14] and 'phase-buildup' where particles are 'constructed' from building blocks (metal atoms). The process can take place in the gas phase (chemical vapour deposition)[14] or the liquid phase (chemical precipitation)[14]. Gas phase synthesis involves the formation of a supersaturated vapour of condensable gaseous species as a result of a chemical reaction that produces a new species or as a result of a physical process, such as cooling that will reduce the vapour pressure of the condensable species. There are also several methods that use the solution route and are discussed in further detail below. These techniques produce uniform metal particles of different shape by using appropriate precursors and by adding a surfactant/capping ligand during the transformation. The addition of a surfactant/capping ligand can also prevent aggregation of the particles.

In the liquid phase, the chemical precipitation usually occurs from homogeneous solution. When the concentration of the constituent precursor reaches critical supersaturation there is short burst of nucleation (Figure 1.6). This followed by a period of uniform growth as the solutes diffuse from the solution to the surface of the nuclei until the final size is reached. To achieve monodisperse NPs, this process requires the separation of the nucleation and growth phases, with no further nucleation occurring during the growth period. Multiple nucleation events can result in small particles aggregating to form much larger particles[95, 96]. Nucleation, particle growth and particle interaction can be better controlled in a liquid medium, making chemical precipitation a more favourable method for producing uniform particles with well-controlled features.

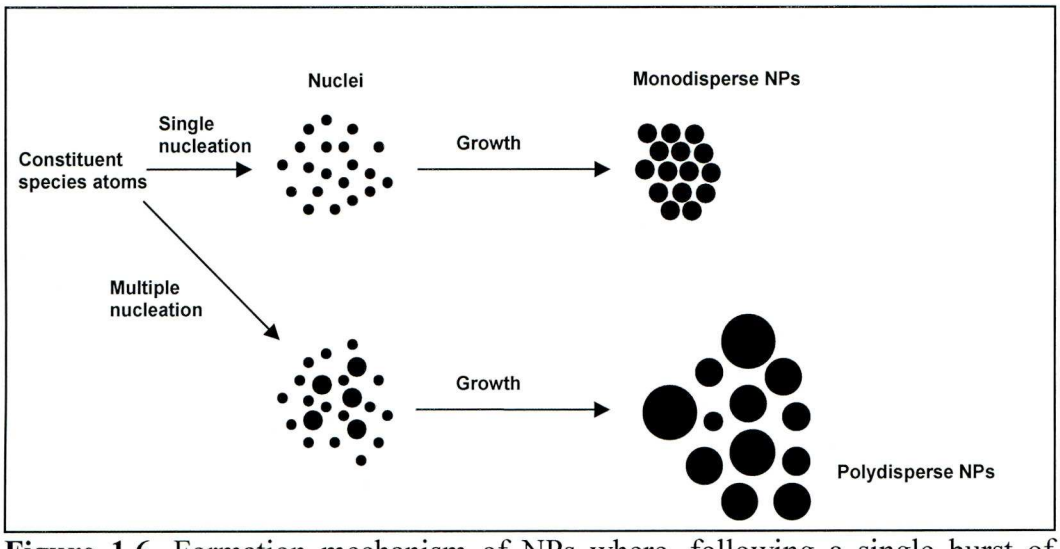

Figure 1.6. Formation mechanism of NPs where, following a single burst of nucleation, a period of uniform growth leads to the formation of monodisperse particle by diffusion. Multiple nucleation events and growth can lead to polydisperse suspensions of NPs (from Thanh *et al*[19]).

1.4.1 Decomposition of organometallic compounds

1.4.1.1 Decomposition at high temperature

In this process organometallic complexes are rapidly broken down in hot solvent containing surfactant, which can form a protecting layer around the nanoparticle. For example the rapid pyrolysis of dicobalt octacarbonyl [$Co_2(CO)_8$] in *o*-dichlorobenzene (DCB), in the presence of trioctyl phosphine oxide (TOPO) and oleic acid (OA) at reflux temperature will produce cobalt NPs (as depicted in Figure 1.7), whose size and shape can be controlled by varying the molar ratios of precursor and surfactant[97, 98]. This method of synthesis can produce NPs of narrow size distribution and highly uniform shape.

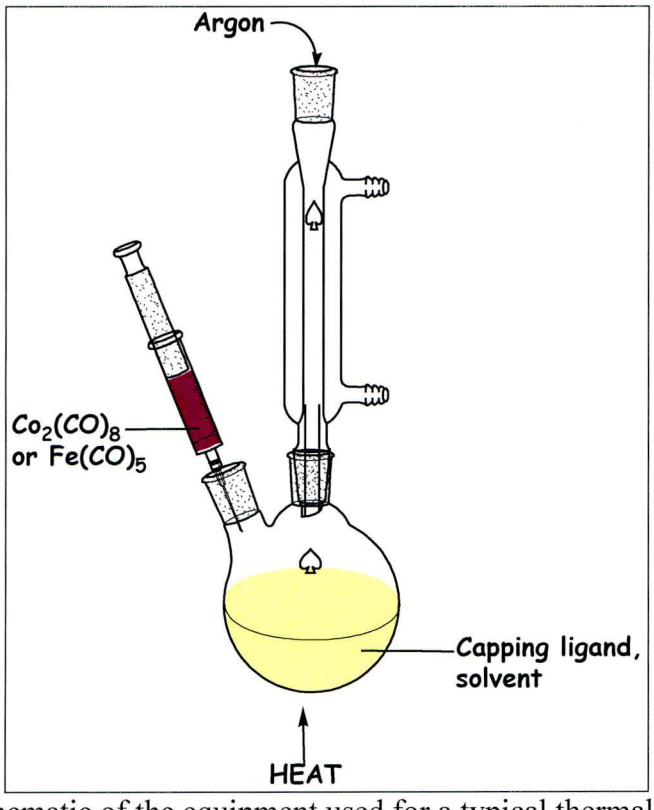

Figure 1.7. Schematic of the equipment used for a typical thermal decomposition nanoparticle synthesis.

The protective layer can also consist of polymers, which can be tailored to improve the biocompatibility of the NPs. For example, Stevenson *et al.*[21] used a poly[dimethylsiloxane-β-(3-cyanopropyl)methylsiloxane-β-dimethylsiloxane] (PDMS-PCPMS-PDMS) family of triblock polymers with controlled length to coat cobalt NPs. The central block (PCPMS) absorbs onto the nanoparticle surface and the hydrophobic end-blocks protrude into the carrier fluid (poly[dimethylsiloxane]), providing suspension stability. Alternatively, Thanh *et al.*[23] used peptides as capping ligands for *in situ* synthesis of water-soluble cobalt NPs with the aim to use these particles for biological applications. The ability to tune the properties of the peptides (by varying the length, and sequence of amino acids) makes them a unique class of ligands for combinatorial nanomaterial synthesis. In addition to the 20 amino acids that occur naturally in proteins, over

100 unnatural amino acids are available for peptide synthesis, which provide access to a huge chemical combinatorial space.

Thermal decomposition has been successfully used to synthesise magnetic NPs oxides of Cr, Mn, Co and Ni from metal fatty acid salts[99]. The particles produced have a very narrow size distribution and sizes that are tuneable over a wide size range (3-50 nm). However, the synthesis is carried out in organic solvent and the particles were capped with fatty acids making them non-dispersible in water. Park *et al.*[100] used a similar technique to produce monodisperse iron oxide NPs using an iron (III) chloride and sodium oleate, which are both inexpensive and non-toxic, to generate an iron oleate complex. The complex was then decomposed at high temperature (240 – 320 °C) in a variety of solvents to produce iron oxide NPs with diameters in the range of 5 – 22 nm depending on the temperature and aging period. The same group produced monodisperse iron NPs by the sequential decomposition of $Fe(CO)_5$ and the iron oleate complex at different temperatures.[101] The reaction is similar to a seed mediated growth process and by using this method is was possible to obtain very fine control over the particle size to within a single nanometre. In both these cases the particles produced were dispersible in organic solvents, but it is unclear if they were dispersible in water.

For biomedical applications, NPs that can be dispersed in water are much more desirable. Water soluble magnetite NPs have been produced by heating a solution of $FeCl_3 \cdot 6H_2O$ in 2-pyrrolidine[102] or α,ω-dicarboxyl-terminated poly(ethylene)[103] under reflux (245 °C). The particle size could be controlled by

the amount of time the solution was heated under reflux (i.e. the longer the time the larger the particle).

Due to their larger magnetisation compared to metal oxides, metallic NPs are much more desirable for many applications. Thus, thermal decomposition of $Fe(CO)_5$, in the presence of polyisobutene, has been used to synthesise iron NPs[104]. By decomposing $Fe\{N[Si(CH_3)_3]_2\}_2$ with H_2 in the presence of hexadecylamine and oleic acid or hexadecylammonium chloride at 150 °C, Dumestre *et al.*[105] produced iron nanocubes between 7 and 8.3 nm that assembled in extended crystalline superlattices. Cobalt nanodisks have been made using the thermal decomposition of in the presence of linear amine that self-assemble into long ribbons[106] and the high temperature decomposition of non carbonyl organometallics, such as $Co(\eta^3\text{-}C_8H_{13})(\ \eta^4\text{-}C_8H_{12})$, have produced cobalt nanorods[107, 108].

Air stable cobalt NPs have been synthesised by the thermolysis of $Co_2(CO)_8$, using aluminium alkyl compounds as the co-ordinating ligand[109]. By varying the alkyl chain length of the co-ordinating ligand it was possible to control the particle size in the range of 3 to 11 nm[109]. The particles were stabilised by the partial oxidation of the cobalt particle surface using synthetic air to produce an oxide shell. Without this oxidation step the particles rapidly lost their magnetisation.

Magnetic alloys such as CoPt and FePt have some advantages over metallic and metal oxide NPs such as high magnetic anisotropy, enhanced magnetic susceptibility and large coercivities[110]. Novel materials, such as FeP and MnP have been synthesised from the reaction iron(III) acetylacetonate and

manganese carbonyl, respectively, with tris(trimethylsilyl)phosphine at high temperature[111, 112]. These materials have been studied for their ferromagnetism, magnetoresistence and magnetocaloric effects[113, 114].

1.4.1.2 Decomposition by laser irradiation

The laser driven pyrolysis of metal compounds, such as carbonyls, can be used to produce magnetic NPs. The synthesis is usually carried out in the vapour phase, with a carrier gas used to transport the nebulised precursor into a reaction chamber where it is irradiated with a laser. The size of the particles can be controlled by changing the flow rate of the vapour through the reaction chamber[115]. For example Co NPs have been produced by the laser pyrolysis of $Co_2(CO)_8$ vapour produced by evaporation of the precursor[116]. This laser evaporation method has been used to produce a variety of nanosized material such as FeCo alloy and silica coated iron oxide NPs[115, 117-119]. Ultra-violet irradiation of a cobalt (II) acetate solution has also been used to synthesise Co NPs which have certain morphologies depending upon the experimental parameters[120]. By using variation of this technique it is possible to use laser irradiation to induce the decomposition of $Co_2(CO)_8$ in organic solution. This will be discussed further in Chapter **3**.

1.4.2 Reduction methods

1.4.2.1 Reduction in solution

Reduction is the transfer of electrons from reducing agent to oxidised metal species in a process driven by the standard redox potential of the reaction,

ΔE^0. The value of ΔE^0 will indicate the likelihood of the reduction proceeding and can predict the rate of the chemical reaction. An increase in its value is associated with faster generation of atoms in the liquid phase. This leads to a higher supersaturation concentration and, therefore, faster nucleation. Thus, finely controlling the redox potential of the reacting species and the overall reaction is vitally important in controlling the properties of the metal particle produced. Complexing or precipitating the oxidised metallic species can alter their electrochemical potential. The degree of change is dependent on the stability constants or the solubility products of the resulting compounds[121].

The simplest form of this type of reaction is the reduction of a metal salt in aqueous solution with a suitable reducing agent. For example, Lu *et al.*[122] used $NaBH_4$ to reduce $CoCl_2$ in an aqueous solution containing synthetic polymers to produce water stable Co NPs. The size and shape of the Co NPs could be controlled by varying the structure, molecular weight and concentration of the polymers in solution. An alternative reduction method is to use the polyol process. In this technique one or more metal salts are dissolved in alkaline polyol and heated to obtain pure or alloy magnetic NPs[123, 124]. Control of the composition, size, size distribution and crystal structure is dictated by the reaction rate of the polyol process. The reaction rate in turn is a function of many experimental parameters such as polyol reduction potential, metal salt concentration, pH and reaction temperature.

The reducing agent can form an intermediate with the oxidised metal species without altering its oxidation state. For example, the reduction process can be initiated by increasing the temperature, producing conditions that lead to

the formation of highly crystalline structures of regular shape. One example is the reduction of iron (II) chloride and platinum acetylacetonate using super-hydride ($LiBEt_3H$) at high temperature (263 °C) to produce 4 nm FePt magnetic NPs[125]. Alternatively, 5 nm CoPt NPs can be produced by co-reduction of cobalt and platinum acetylacetonate in trimethylene glycol[11]. These particles are ferromagnetic at room temperature and by annealing above 550 °C the magnetic properties of the NPs can be enhanced, due to the induction of ordering.

1.4.2.2 Reduction in microemulsion/reverse micelles

Reverse micelles or microemulsions are spherical vesicles formed by surfactants dissolved in organic solvent (Figure 1.8) that can be used as micro-reactors for the synthesis of NPs. Briefly, ions of the metal nanoparticle desired are dissolved in aqueous solution and added to the reverse microemulsion suspension. A reductant (e.g. $NaBH_4$) is added to the mixture and once the

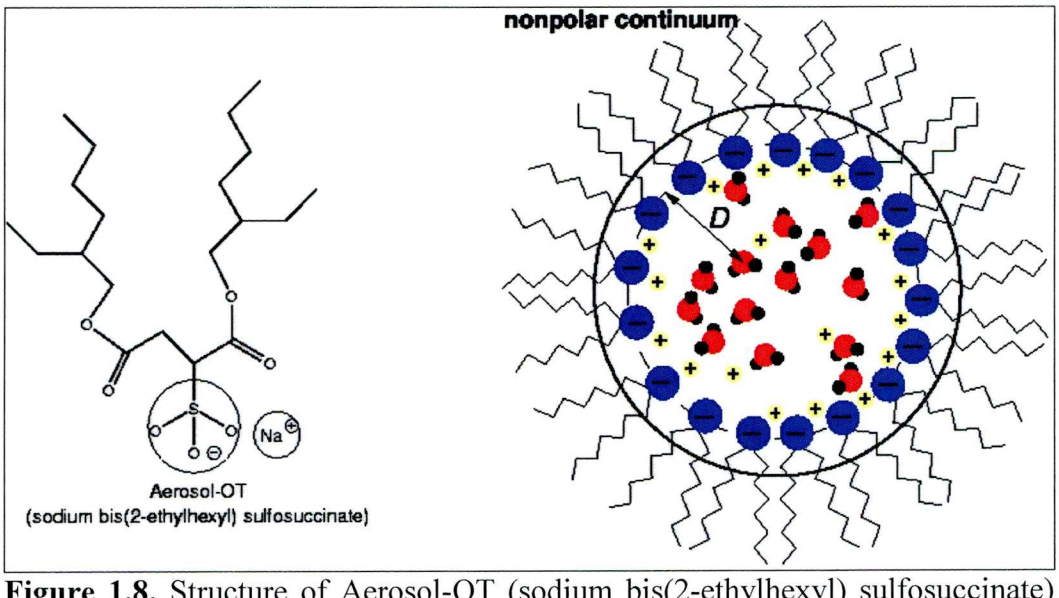

Figure 1.8. Structure of Aerosol-OT (sodium bis(2-ethylhexyl) sulfosuccinate) and a spherical reverse micelle (from Faeder and Ladanyi[126]).

metallic NPs are formed the microemulsion solution is disrupted by adding excess amounts of polar solvent and the particles are collected[127-131].

A variety of magnetic NPs have been produced using the microemulsion technique including cobalt, cobalt/platinum alloys and gold coated cobalt/platinum[132], where cetyltrimethylammonium bromide (CTAB) and 1-butanol were used as the surfactants and the continuous oil phase consisted of octane[132]. Similarly, spinel ferrites, such as $MnFe_2O_4$, with controllable sizes from 4 to 15 nm, have been made using a water in toluene reverse microemulsion, with sodium dodecylbenzenesulfonate as the surfactant[133]. The aqueous surfactant solution was added to an aqueous solution of $Mn(NO_3)_2$ and $Fe(NO_3)_2$, followed by a large volume of toluene to form the reverse microemulsion. The particle size was controlled by the ratio of water to toluene. It has also been possible to produce non-spherical particles using a microemulsion, for example, the iron oxide nanorods synthesised by Woo *et al.*[134]. The reverse microemulsion was formed from oleic acid and benzyl ether, with $FeCl_3 \cdot 6H_2O$ used as the iron source and propylene oxide as the proton scavenger. By varying reaction conditions, such as temperature, atmosphere and hydration state, the phase of the nanorods could be controlled.

Many types of nanoparticle have been made using the microemulsion method[135]. However, the particles produced tend to have a wide size distribution. Furthermore, the working window for the synthesis is narrow leading to a relatively low yield of NPs, compared to other techniques such as thermal decomposition. Also the large volumes of solvent used during the synthesis make the scale-up of this method difficult.

Reverse microemulsions provide unique reaction media as they can solubilise, concentrate, localise and even organise reactants. They also allow the nanoparticle synthesis to take place in aqueous solution. However, control of the size and shape of NPs synthesised by this method is difficult as it reflects the interior of the micelle.

1.4.2.3 Hydrothermal synthesis

Co-precipitation is a technique that has been used for many years to produce iron oxide NPs from aqueous Fe^{3+}/Fe^{2+} salt solutions by the addition of a base under inert atmosphere. The technique is simple to use; however it does tend to produce polydisperse NPs. A variation of the co-precipitation method, known as hydrothermal reduction has produced a broad range of NPs. The technique uses a liquid-solid-solution system where metal ions are reduced by ethanol at the phase interfaces[136]. The phases consist of ethanol-linoleic acid as the liquid phase, sodium linoleate as the solid phase and a water-ethanol solution of metal ions of the desired NPs. The method is based on the instantaneous phase transfer and separation mechanism that occurs at the interfaces of the different phases present during the synthesis and ion exchange that leads to the formation of metal linoleate and sodium ions entering the aqueous phase. At a certain temperature the ethanol in the liquid and solution phases will reduce the metal ions at the liquid-solid or solution solid interfaces. The linoleic acid generated by the reaction is adsorbed onto the developing nanoparticle to form a stabilising shell. A combination of the hydrophobic surface on the particles and their weight means the formed NPs are easily collected. This technique has been used to produce very monodisperse 9 nm Fe_3O_4 and 12 nm $CoFe_2O_4$ NPs[137, 138].

1.4.2.4 Seed mediated growth

Introducing 'seeds' to a reaction mixture can increase the nucleation rate and thus the properties of the resulting metallic particles[121]. The catalytic and/or surface properties of the small solid entities can trigger the reduction of the species and the nucleation process. This is of particular use in systems in which nucleation would not otherwise take place or too slowly. It also has the advantage of artificially separating the nucleation and growth phases of the particle formation. Seeds can be produced '*in situ*' by the rapid reduction of a different, more electropositive element or be in the form of a stable dispersed preformed nanosized particle of the same metal. To form monodisperse metallic particles it is necessary for the nucleation process to be uniform throughout the entire solution, a condition that is difficult to achieve in rapid reductions. This has an effect upon reproducibility and scale up of the process. To avoid this, it is favourable to use systems in which the electron transfer is inhibited when the reactant species are brought into contact, but can be induced by changing the conditions (e.g. pH, temperature, etc) after the systems is already homogenised. For example the solvent used to dissolve the metal salts will become the reducing agent on changing the conditions. Wang *et al.*[24] used Fe_3O_4 NPs as seeding materials for the reduction of gold precursors to synthesise gold coated Fe_3O_4 NPs (Fe_3O_4@Au).

1.4.3 Decomposition and reduction

There is great interest in alloy magnetic NPs due to their magnetic properties such as high saturation magnetisation[124] and their resistance against

oxidation. Alloy magnetic NPs can be produced from the thermal decomposition of a single polynuclear carbonyl clusters (for further details see Chapter **5**) or from the reaction of two separate precursors[123, 124, 139, 140]. In the latter method it is possible to control the size shape and composition of these alloy NPs by controlling the initial concentration of the precursors in the solution. For example FePt NPs have been produced from $Fe(CO)_5$ and $Pt(acac)_2$ in organic solvent[141]. In this example, the control of shape and composition is a result of two reactions taking place in rapid succession. Initially $Fe(CO)_5$ decomposes to give rise to Fe^0 atoms. These then serves as the reductant for the Pt^{2+} ions. The standard redox potentials of Pt^{2+}/Pt^0 and Fe^{2+}/Fe^0 are 1.2 V and -0.44 V, respectively, which supports this hypothesis.

Overall it can be said that thermal decomposition offers the best method for producing magnetic NPs with good control over size, shape and size distribution. Alternatively, microemulsions can be used, however this can result in an increase in the polydispersity of the NPs and large volumes of solvent are required. Hydrothermal reduction is a relatively new technique, which has been used to synthesise monodisperse magnetic oxide NPs, although it has not been used to produce metallic particles. Laser pyrolysis of precursor vapour offers the advantage of "wall-less" production of NPs with narrow size distribution.

1.5 Protection/stabilisation of nanoparticles for biomedical applications

The protective coating for NPs can be split into two groups: organic shells, for example surfactants and polymers[142-146] or coating with an inorganic

layer including silica[147], carbon[148], noble metals (such as Au, Pt and Ag)[149-152] and oxides formed by mild oxidation of the surface of the NPs or additionally deposited, such as Y_2O_3[153]. An alternative method to prevent or minimise aggregation and oxidation of magnetic NPs is to embed or disperse them into a dense matrix, usually a polymer, silica or carbon, to form composites. However this method fixes the particles in space relative to each other, which is often not desired.

1.5.1 Biofunctionalisation

As already mentioned, the protective layer on a magnetic nanoparticle can be used as a platform for the functionalisation of the particles with biological components such as various drugs, nucleic acids, antibodies and enzymes (Figure 1.9). Once functionalised, the magnetic core then allows the easy separation and specific placement of the NPs by means of an external magnetic field.

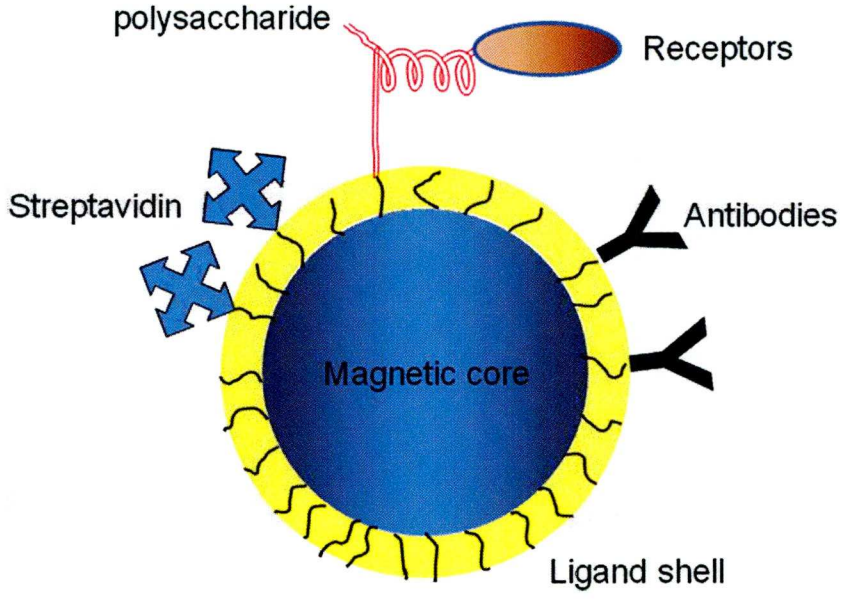

Figure 1.9. Schematic of the functionalisation of magnetic NPs with various biological components.

The functionalisation of magnetic NPs can be achieved by anchoring biotin ligands to the surface of the nanoparticle via their carboxylic acid groups. However, biotin is practically insoluble in water, so it is necessary to anchor a water soluble co-ligand to the surface of the nanoparticle, such as bipyridinium carboxylic acid[154]. These functionalised NPs have been used for affinity isolation of fluorescein labelled avidin. Similarly, dopamine can be bound to the surface of iron oxide NPs, which can then act as an anchor to further attach nitrilotriacetic acid molecules[155]. The composite material has been found to show very high specificity for protein separation as well as having good stability in both high temperature and high salt concentrations. Other functional groups such as –OH, –SH, and $–NH_2$ can be used as anchor sites onto the surface of magnetic NPs. For example the amino groups of the antibiotic vancomycin have been used to attach the drug onto FePt NPs for the detection of enterococci and other Gram-positive bacteria[156]. Immunoglobulins can also be immobilised onto a nanoparticle surface via an ester bond and used for a variety of purposes[157]. The surface of a magnetic nanoparticle also can be modified so that an antibody can bind to the surface. For example polyethylene glycol (PEG)-COOH or *N*-5-azido-2-nitrobenzoyl groups will react with amino groups of an antibody molecule, while 2-pyridyldisuphide or maleimide groups can react with sulphhydryl-modified antibodies[158]. The introduction of PEG molecules (and other natural polymers such as dextrans and protein/peptides) as linkers can benefit *in vivo* application of magnetic NPs since these molecules are non-immunogenic, non-antigenic and protein resistant and can increase the half –life of the NPs in the blood stream.

1.5.2 Organic coatings

1.5.2.1 Surfactant and Polymer coating

Generally, surfactants and polymers can be chemically bound or physically adsorbed onto a magnetic nanoparticle surface, forming a single or a double layer[159, 160]. Steric repulsion forces arising from this layer balances the magnetic and van der Waals forces acting on the NPs, thus stabilising them in solution[161]. A commonly used stabilising ligand for magnetic NPs is oleic acid ([*Z*]-octadec-9-enoic acid). During synthesis, the terminal carboxylic acid group binds strongly to the surface of newly formed Co and iron oxide NPs and by controlling the concentration of oleic acid in the reaction mixture it is possible to control the nanoparticle diameter. While oleic acid provides excellent stability in organic solution, it is hydrophobic and therefore unsuitable for use in aqueous solution and needs to be replaced or modified if the NPs are to be used in biomedical applications.

A variety of hydrophilic ligands have been used to stabilise magnetic NPs in aqueous solution such as dextran[162], dodecylamide[163] and ω-hydroxycarboxylates[164] as well as a wide variety of polymers and co-polymers, many of which contain functional groups such as carboxylic acids, phosphates and sulphates. Certain biocompatible polymers have been used to modify magnetic NPs for use as magnetic field directed drug targeting and in MRI contrast enhancement[165, 166]. In most cases carrying out a polymerisation reaction on the surface of the magnetic NPs forms the polymer layer. For example, Dresco *et al*[167] synthesised 80 nm Fe_3O_4 particles using a reverse micelle method and subsequently added water, the monomers, a cross linker and an initiator to the reaction mixture to produce

polymer coated NPs. In a similar way, polyaniline was used to coat Fe_3O_4 NPs by oxidative polymerisation using ammonium peroxodisulphate as the oxidant[168]. However this method tended to produce polydisperse particles in the 20 – 30 nm range. Using atom transfer radical polymerisation, Vestal and Zhang[169] have coated 15 nm $MnFe_2O_4$ NPs with polystyrene. An alternative approach is to use pre-formed synthetic polymers as a matrix to confine and control the formation of magnetic cores. The physical properties of the polymers can also be retained once they are bound to the nanoparticle surface (Figure 1.10)[170]. This will be discussed in greater depth in Chapter **2**.

While silica has been found to be a relatively simple way to coat NPs, it is also known that it is unstable under basic conditions and contains pores through which oxygen and other species can diffuse. Therefore recent studies have focused on carbon protected systems, which have the advantage of much higher chemical and thermal stability as well as good biocompatibility[161].

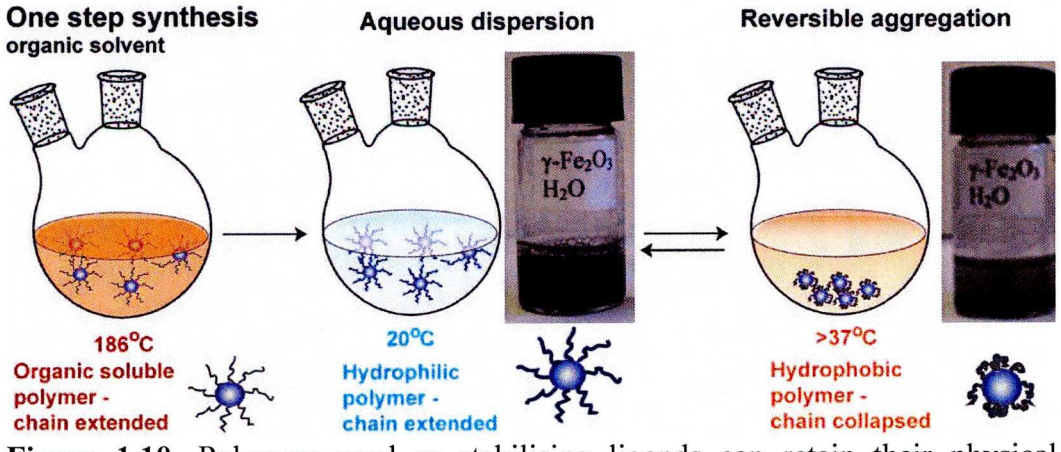

Figure 1.10. Polymers used as stabilising ligands can retain their physical properties.

1.5.2.2 Carbon coating

Graphitised carbon structures such as nanoonions and nanotubes can be formed by laser ablation, arc discharge and electron irradiation in the presence of metallic NPs[171-174]. The carbon coating protects the metal core from oxidation and acid erosion and because they are metal core (as opposed to metal oxides) they have a relatively high magnetic susceptibility[161]. Air stable, carbon coated, Co NPs were synthesised using a sonochemical method[175]. However, while the particles produced were highly stable, they were rather polydisperse. Carbon coated Fe and Fe_3C, which were stable up to 400 °C have been produced by the direct pyrolysis of iron stearate in an inert atmosphere at 900 °C[176]. This single-step process has good potential to be scaled up, but again the particles obtained are polydisperse (20 to 200 nm) with the cores coated with between 20 and 80 graphene layers. Lu *et al.* achieved better control over size distribution when synthesising 11 nm Co NPs[148]. The Co particles were coated with furfuryl alcohol that is firstly converted to poly(furfuryl alcohol) then carbonised to carbon during the pyrolysis step. These NPs were found to be stable against air oxidation and erosion by acids or bases. Similar methods, using polymers as the carbon source, have produced carbon coated Co NPs that are air stable for approximately one year[177, 178].

Carbon coated NPs have several advantages, however the particles obtained are often agglomerated clusters and the synthesis of dispersible carbon coated NPs in an isolated form still remains a challenge to be overcome.

1.5.3 Inorganic coatings

1.5.3.1 Noble metal coating

A pure metal core can be protected from oxidation by depositing a layer of noble metal, such as gold, on the nanoparticle surface. Not only does gold protect reactive metallic cores from oxidation, but also the gold surface can be a versatile platform for the functionalisation of the NPs because of the very well studied thiol chemistry of gold NPs. For example, Lee *et al*[25] coated 6.5 nm Co NPs with a Au shell. This was achieved by heating the Co particles in 1,2-dichlorobenzene, under reflux, with $[(C_8H_{17})_4N]^+[AuCl_4]^-$ containing triocylphosphine (TOP) as a stabiliser. A by-product of the reaction was analysed and found to be $CoCl_2$, indicating the core-shell structure was formed by a process of redox transmetallation between Co^0 and Au^{3+}. A similar process led to the formation of gold-coated iron NPs that are stable under neutral and acidic aqueous conditions[179]. $FeCl_3$, dissolved in *N*-methyl-2-pyrrolidinone (NMP), was reduced by sodium to form the metallic core with benzylpyridine as the capping ligand. The gold layer was deposited by the addition of $HAuCl_4$, also dissolved in NMP. This type of core-shell nanoparticle can also be prepared by a reverse microemulsion method. The inverse micelles were formed with CTAB as the surfactant, 1-butanol as a co-surfactant and octane as the continuous oil phase. $FeSO_4$ was then reduced using $NaBH_4$, followed by the addition of $HAuCl_4$ to coat the iron particles[150]. Cobalt NPs have also been coated with gold by a chemical reduction method. The Co particles were synthesised using 3-(*N,N*-dimethyldodecylammonio)propanesulphonate as the stabiliser and lithium triethylhydridoborate as the reducing agent. Using ultrasonication and an inert

atmosphere, a solution of $KAuCl_4$ in THF was used to form the gold shell via reduction of the Au^{3+} ions on the Co nanoparticle surface[180].

1.5.3.2 Other coatings

1.5.3.2.1 Oxide layer by mild oxidation of the core

The surfaces of magnetic NPs can be passivated by controlled oxidation of the pure metal core. For example Peng *et al.*[181] used a plasma-gas condensation type cluster deposition apparatus to oxidise gas phase NPs and oxygen plasma has been used to produce air stable Co NPs[182]. Alternatively, a stable CoO layer was formed on synthesised Co NPs using synthetic air[109]. This layer was found to stabilise the cobalt NPs from further oxidation. Control of the oxide layer is an important factor in exchange-biased systems, as these systems require a well-defined thickness of the ferromagnetic core and antiferromagnetic oxide layer[161].

1.5.3.2.2 Silica coating

Silica coatings can impart good stability on magnetic NPs in aqueous conditions and also have the advantages of simple surface modification and easy control over inter-particle interactions by variation of the shell thickness[161]. A silica layer avoids direct contact between the magnetic core and any additional agents bound to the silica surface, therefore preventing any undesirable interactions. The modification of the silica surface can introduce functionalisation of the magnetic NPs that facilitates their potential use in applications such as biolabelling and targeted drug delivery[183].

Using the sol-gel method with ammonia and tetraethoxysilane (TEOS) in water, Lu *et al.*[184] have coated the commercially available ferrofluid, EMG 340, with a silica shell. Varying the amount of TEOS in the solution can control the shell thickness. The silica readily bound to the iron oxide due the presence of hydroxyl groups on the particle surface and the negative charge of the silica meant the NPs could easily be dispersed in water, without the use of additional ligands. The iron oxide core, once coated with a mesoporous silica shell can then be reduced to metallic iron, for example, by using hydrogen[6, 185, 186].

Achieving a homogeneous silica shell, with controlled thickness, however, still remains a challenge. Recent research has focused on using a reverse microemulsion method in an attempt realise this[187]. Using this technique, Yi *et al.*[188] have produced uniform silica coated iron oxide NPs with a controlled thickness between 1.8 and 30 nm. Elsewhere, Tartaj and Serna[186] have also used a reverse microemulsion to embed iron oxide NPs into silica. The iron oxide was then reduced to α-Fe NPs with hydrogen at 450 °C. Similar techniques have also been used to coat spinel ferrite NPs of $CoFe_2O_4$ and $MnFe_2O_4$[189].

The lack of OH groups on the surface of metallic NPs makes coating them with silica more difficult than metal oxides. However, Kobayashi *et al.*[147] used 3-aminopropyltrimethoxysilane and TEOS as the silica precursors to coat amorphous Co NPs in an aqueous ethanolic solution. Another problem arises from the ease at which iron and cobalt are oxidised by dissolved oxygen. Applying a method used on precious metals[190], it may be possible to overcome this by use of a primer to make the surface vitreophilic (glasslike)[191].

1.5.3.2.3 Matrix Dispersed Magnetic Nanoparticles

There is a variety of methods that can be used to produce matrix dispersed magnetic NPs: they can be dispersed in a continuous matrix, the coating of another larger particle, or in the form of aggregates of single particles, which are connected via their coating. The last method is particularly useful if isolated particles are not required, they can then be embedded in a matrix, which will stabilise them and proved protection against oxidation[161].

Stoeva *et al.*[192] synthesised magnetic NPs that consisted of a silica core, with Fe_3O_4 and gold as inner and outer shells, respectively. The silica particles were used as templates upon which 15 nm Fe_3O_4 NPs were bound. These composites were then coated with 1 – 3 nm gold nanoparticle seed, which act as nucleation sites in the subsequent reduction of $HAuCl_4$ to form a continuous gold layer around the silica/Fe_3O_4 particle. The gold layer proved a platform for the functionalisation of the NPs, whilst maintaining good magnetic properties. A mixture of magnetic NPs and quantum dots has been dispersed in a silica matrix by a reverse microemulsion method[193]. The 11.8 nm γ-Fe_2O_3 and 3.5 nm CdSe NPs where synthesised separately and dispersed in cyclohexane. The solutions were introduced into the reverse micelles followed by ammonium hydroxide. Finally TEOS was added and left to react to completion. The composite NPs obtained retained both magnetic and optical properties of the components and could be redispersed in water and ethanol, however these solutions were not entirely homogeneous.

1.6 Summary

Magnetic NPs have a variety of potential biomedical applications[13] and can be produced by a range of synthetic methods. In general, each of the applications requires particular properties of the magnetic NPs such as high magnetic susceptibility[194] or very small diameter[195]. The synthesis method of choice can help control these properties[19]. The biocompatibility and stability of magnetic NPs can be controlled by the manipulation of their surface properties[19], for instance by adding a polymer[170] or a carbohydrate[162]. Surface manipulation is also vital with regards to the functionalisation of magnetic NPs e.g. the addition of antibodies[158] or therapeutic agents[156].

1.7 Objectives of the thesis

As previously mentioned, magnetic NPs need to be stable in aqueous solution if they are to be used in biomedical applications and in the second chapter of this thesis, the production of water soluble magnetic NPs using thermo-responsive polymers as stabilising ligands will be discussed. The temperature dependent conformational changes in these polymers affect their hydrophilicity/hydrphobicity[196]. This means it is possible to use these polymers in a facile one-step synthesis method to produce water stable magnetic via the thermal decomposition of organometallic precursors. It would also be advantageous if the attached polymers were to retain their amphiphilic properties and therefore the response of the polymer coated NPs to external stimuli is also investigated.

Many of the applications in which magnetic NPs can be used require NPs with specific properties, for example size; therefore it is desirable to develop new

synthesis methods which can produce required NPs. To this end, Chapter 3 discusses the synthesis of Co NPs produced by the pulsed laser irradiation of $Co_2(CO)_8$ in an organic solution containing stabilising ligands. Controlling the size of the NPS, by changing certain reaction parameters, is of great importance and could give insight to formation mechanism of the Co NPs using this method.

Magnetic alloy NPs are an important class of nanoparticle due to their favourable magnetic properties and resistance to oxidation when compared to those produced from a single component[124]. Chapter 4 studies alloy magnetic NPs synthesised by the thermal decomposition of bimetallic carbonyl clusters. The use of a single bimetallic carbonyl cluster can afford better control over the composition of the synthesised alloy NPs than that achieved when using two or more precursors[197]. It is important that the physical properties of the synthesised NPs can be controlled. Therefore, the effect of changing synthesis conditions, such as stabilising ligand concentration, ligand type and reaction temperature on the characteristic of the NPs is also examined.

Control of the chemical and physical properties of magnetic NPs is easily achieved when they are synthesised in organic solvent, however, this usually renders them hydrophobic and unsuitable for certain applications. Chapter 5 looks at the surface modification of synthesised NPs in an attempt to increase their water solubility and proved a platform for functionalisation. For use biomedical applications, magnetic NPs must be stable in physiological conditions, thus studies are also carried out into the stability of the modified NPs in aqueous electrolyte solution and across a wide pH range. The methods and materials can be found in Chapter 6.

Chapter 2

One step synthesis of water soluble magnetic nanoparticles using thermo-responsive polymers

2.1 Aims and objectives

It is the aim of this chapter to synthesise water soluble magnetic Co and iron oxide NPs using a facile one-step method. This will be achieved by the thermal decomposition of $Co_2(CO)_8$ and $Fe(CO)_5$, respectively, in organic solvent containing thermo-responsive polymers (Scheme 2.1). At room temperature the polymers are water soluble, however as the temperature increases they undergo a conformational change which results in them becoming hydrophobic. This feature can be exploited so that in hot organic solvent, the polymer helps to form discrete NPs during the decomposition of the precursor and, once cooled to room temperature, stabilise the NPs in aqueous solution. The stabilising effect of these polymers will be assessed across a wide pH range and in electrolyte solutions of increasing concentration. The response of the polymer coating to changes in temperature will also be studied.

$$Co_2(CO)_8 \xrightarrow[\text{heat}]{\text{Polymer}} 2Co + 8CO$$

Scheme 2.1. Synthesis of thermo-responsive polymer coated Co NPs

2.2 Introduction

As mentioned in Section **1.3** magnetic NPs have several potential *in vivo* applications in areas such as MRI[15], targeted drug delivery[29, 30] and hyperthermia treatment of solid tumours[13]. In these applications, it is necessary that the particles are superparamagnetic, as opposed to ferromagnetic, so that they do not aggregate upon removal of a magnetic field[17, 18]. At room temperature, superparamagnetism is usually achieved for NPs with a size of approximately 10

nm or less. Due to their very small size, surface effects may play an important role in determining the magnetic properties of the particles and so NP synthesis must be both reliable and predictable.

The most common way to produce well-defined NPs is to tailor the surface properties of the particles, often by coating or encapsulating them in a shell of a particular material[19]. This coating and encapsulation can also protect the core from extraneous chemical and physical changes[6, 14, 20]. Various substances have been used to form the protective shell of NPs such as silica[7], polymer[21], peptide[22, 23] and noble metals[24, 25].

Furthermore, modification of the surface properties is particularly important when considering *in vivo* applications to ensure that particles are biocompatible[36], non-toxic and stable to the reticulo-endothelial system, the body's major defence mechanism[13]. Particles possessing a hydrophobic surface are readily coated with plasma components in the blood stream and are, therefore, easily removed from the circulation[26], while more hydrophilic particles can resist coating and are cleared much more slowly[26]. Many common hydrophilic coatings used on NPs include derivatives of dextran[27], polyethylene glycol[130], polyethylene oxide[198], poloxamers[26] and polyoxamines[26]. The dense brushes of polymers can inhibit the opsonisation (the process that causes foreign bodies to be recognised by the body's reticulo-endothelial system) of the particles, thereby increasing their circulation time[13].

A major problem is the stability of magnetic NPs in aqueous solution. Current solutions are the synthesis NPs either *in situ* with a suitable stabilising ligand (one-step method)[170] or a two-step method using ligand exchange[199]. In

the latter method, the NPs are synthesised in organic solvent, *via* pyrolysis of organometallic compounds, to produce monodisperse particles. Then, in the second step, the NPs are transferred to aqueous solution by using a process of ligand exchange. This method is discussed further in Chapter **5**. The one-step synthesis method can be regarded as simpler than the ligand exchange method, although, when carried out in aqueous solution, it is more difficult to control the particle size as well as the dispersity. In another approach, thermo-responsive polymers have been used to coat NPs using a multi-step method whereby monomers are adsorbed onto a preformed nanoparticle surface and the polymer brushes are then grown via a polymerisation reaction[200, 201].

Using thermo-responsive polymers as stabilising ligands it may be possible to synthesise monodisperse magnetic NPs, in a single step, using the thermal decomposition of organometallic compounds in organic solvent. The thermo-responsive polymers are based on poly(N-isopropyl-co-t-butylacrylamide) containing a thiol ether group and a terminal carboxylic acid, for attachment to the nanoparticle surface (the general structure is shown in Figure 2.1). In water these polymers undergo a sharp coil-to-globule transition change at a Lowest Critical Solution Temperature (LCST)[196]. The coil-to-globule transition means a polymer is water soluble and hydrophilic below the LCST and hydrophobic above it (and thus soluble in organic solvent). Therefore, the polymer is dissolved in hot solvent, facilitating the nanoparticle synthesis by thermal decomposition. Upon cooling the nanoparticle suspension below the LCST, the organic solvent can be removed and replaced with water. Using these polymers, it could be possible to synthesise water soluble magnetic NPs with narrow size distribution and good stability.

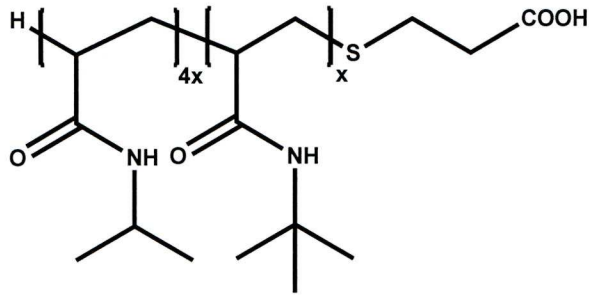

Figure 2.1 The general structure of poly(N-isopropyl-co-t-butylacrylamide)

2.3 Mechanism of thermo-responsive polymer formation

The thermo-responsive polymers were formed by free radical polymerisation mechanism, as depicted in Figure 2.2. In this mechanism the free radical initiator is broken down into two radicals by mild heating. The radical is transferred to the thiol group of 3-mercaptopropanoic acid (3-MPA) (initiation). The 3-MPA radical attacks the double bond of the monomer and the radicalised monomer reacts with another monomer molecule and the subsequent repetition creates the polymer chain (propagation). The polymerisation is terminated by chain disproportionation where two radicals meet and exchange a hydrogen atom which gives a saturated polymer chain.

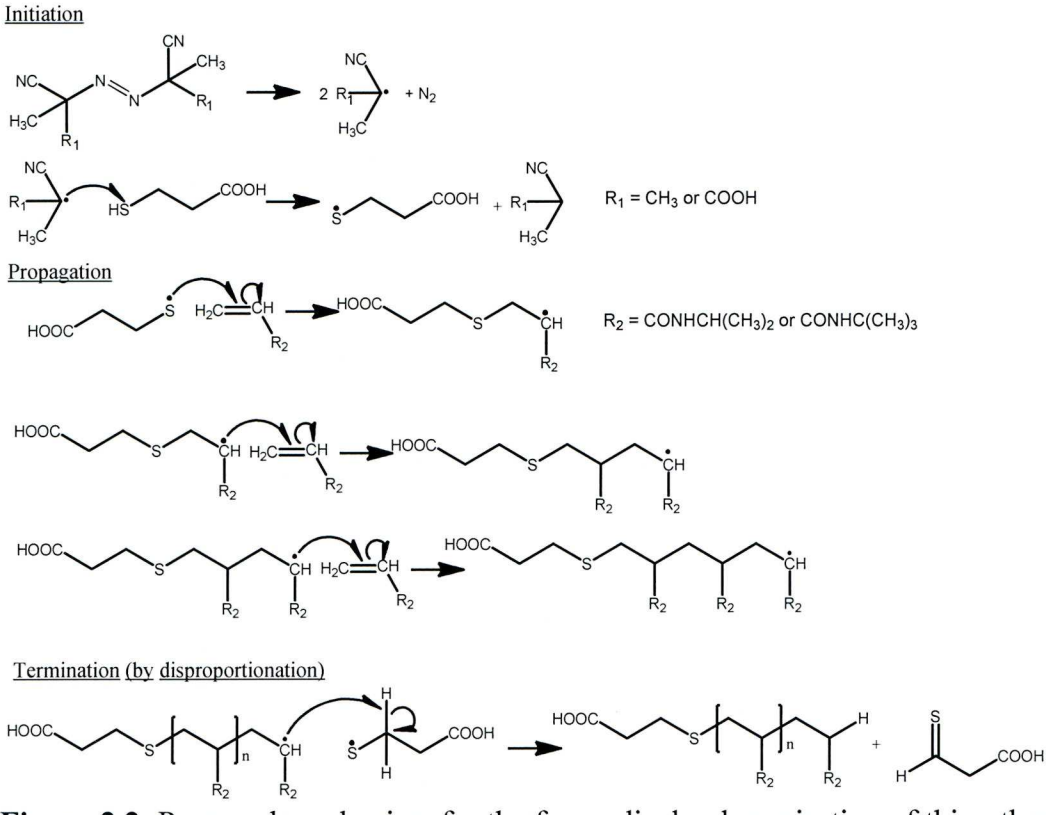

Figure 2.2. Proposed mechanism for the free radical polymerisation of thio-ether carboxylic acid terminated poly(alkylacrylamide) polymers.

2.4 Results and Discussion

2.4.1 Size of the thermo-responsive polymer coated magnetic nanoparticles

A series of polymers were synthesised and used to coat magnetic nanoparticles in an attempt to produce water stable colloidal suspensions of these nanoparticles. By varying the polymer synthesis conditions, it was possible to produce polymers with different molecular weight (Mw) and LCSTs. From this series, polymer P1 (Mw = 6800, LCST = 23.5 ^{o}C) was found to produce the most stable and monodisperse Co nanoparticles and polymer P2 (Mw = 10 000, LCST = 28 ^{o}C) was most suitable for γ-Fe_2O_3 nanoparticles (The general structure for both polymers is shown in Figure 2.1 and the synthesis of these polymers is

described in Section **6.2**). Elemental analysis of the synthesised NPs indicated that the polymers where bound their surface (Table 2.1).

Table 2.1. Results of the elemental analysis of the polymer coated Co and γ-Fe_2O_3 NPs. The remainder of the weight is assumed to be due to oxygen

Element	Polymer coated Co NPs %w/w	Polymer coated γ-Fe_2O_3 NPs % w/w
C	38.34	38.415
H	7.41	7.635
N	7.16	7.88
S	0.2	0.14
Fe	-	29.32
Co	36.28	-

From the TEM images depicted in Figure 2.3 it can be seen that the polymer coated Co and γ-Fe_2O_3 NPs have a mean diameter of 7 ± 1 nm and 8 ± 1 nm, respectively. In addition, dynamic light scattering found the hydrodynamic diameters of the polymer coated Co and γ-Fe_2O_3 NPs to be 17.4 nm and 23.7 nm,

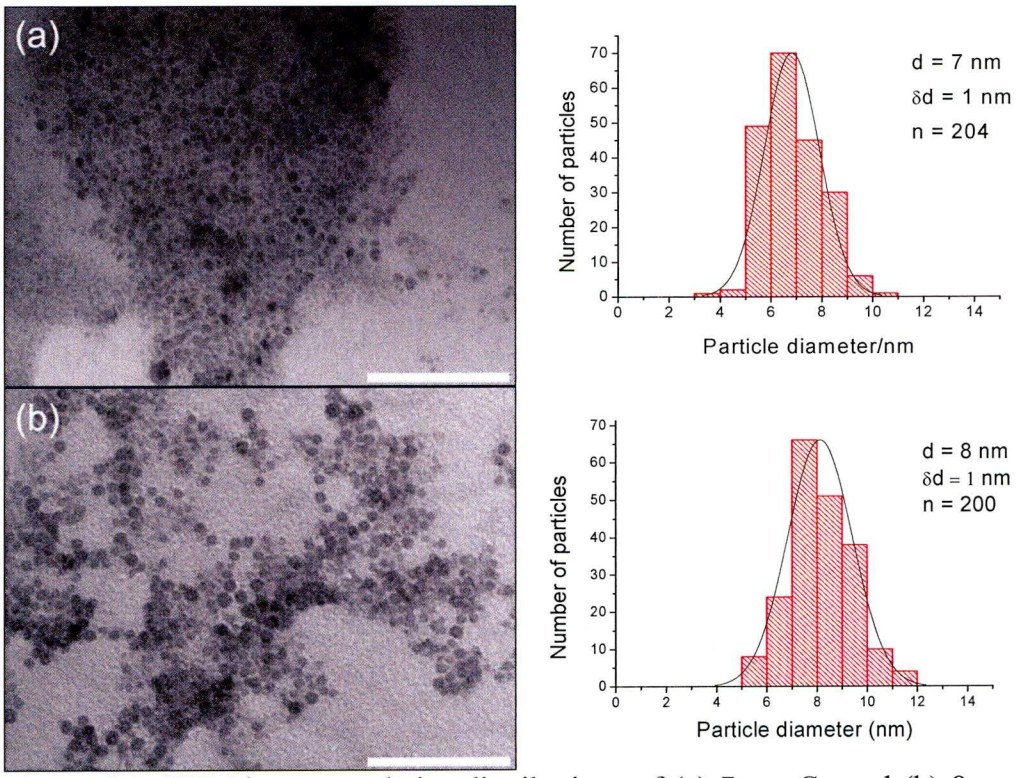

Figure 2.3. TEM images and size distributions of (a) 7 nm Co and (b) 8 nm γ-Fe_2O_3 nanoparticles coated with polymers P1 and P2, respectively. Bar 100 nm.

respectively, (Figure 2.4), supporting the elemental analysis data which suggests the presence of the polymers on the nanoparticle surface, which bind via the carboxylic acid group. Furthermore the smaller diameter of the P1 coated Co NPs is consistent with this polymer having a lower molecular weight than P2 and is therefore shorter.

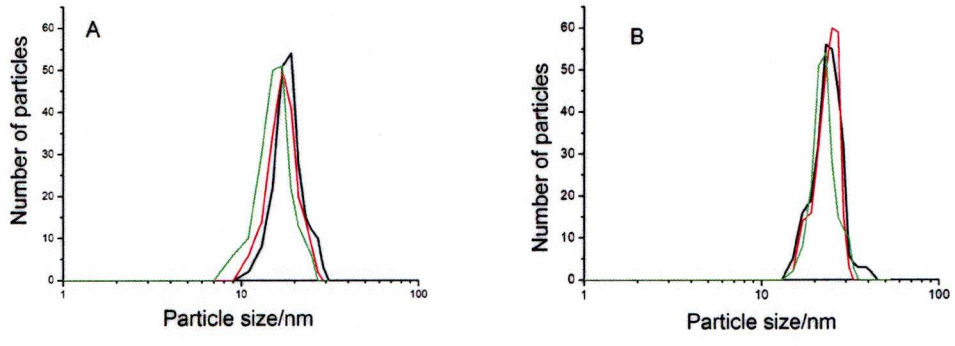

Figure 2.4 Hydrodynamic diameters of (A) P1 coated Co NPs and (B) P2 coated γ-Fe_2O_3 NPs as measured by dynamic light scattering. The smaller diameter of the P1 coated NPs (A) compared to the P2 coated γ-Fe_2O_3 NPs (B) is due to the lower molecular weight of polymer P1, which is therefore shorter (and the slightly smaller Co NPs). The three traces represent three measurements made on the same sample.

The different reaction conditions used to synthesise the polymer coated Co and γ-Fe_2O_3 NPs may account for why they are stabilised by different polymers. The Co NPs are synthesised in DCB at 180 °C, while the γ-Fe_2O_3 NPs are made in dioctyl ether at 286 °C. Two different mechanisms have been suggested to explain the formation of polymer-coated NPs. In the 'polymer capping' model[202, 203] the polymer chains adsorb onto the growing particle and form a layer that can inhibit any further growth. The other mechanism suggested by Tannenbaum *et al.*[203] involves a combination of the capping mechanism and particle formation kinetics. In this model, the formation of the particles is affected by the surface tension between the particle and the polymer solution as

well as the energy involved in the particle formation. The former is sensitive to chemical interaction between the particle and the solvent and the layer in contact with the cluster is composed of both solvent and polymer. The latter represents the energy gain associated with metal atoms aggregating into nuclei compared to their distribution in solution and is thus relatively insensitive to a specific system[204].

2.4.2 Magnetic properties of the thermo-responsive polymer coated magnetic nanoparticles

All of the synthesised particles are superparamagnetic at room temperature as indicated by the closed hysteresis loops seen in Figure 2.5b. The zero-field-cooled and field-cooled magnetisation curves of the Co and γ-Fe_2O_3 nanoparticles are shown in Figure 2.5a and indicate that the Co nanoparticles have very low blocking temperature of approximately 6 K, whereas it is approximately 92 K for the γ-Fe_2O_3 nanoparticles. The higher blocking

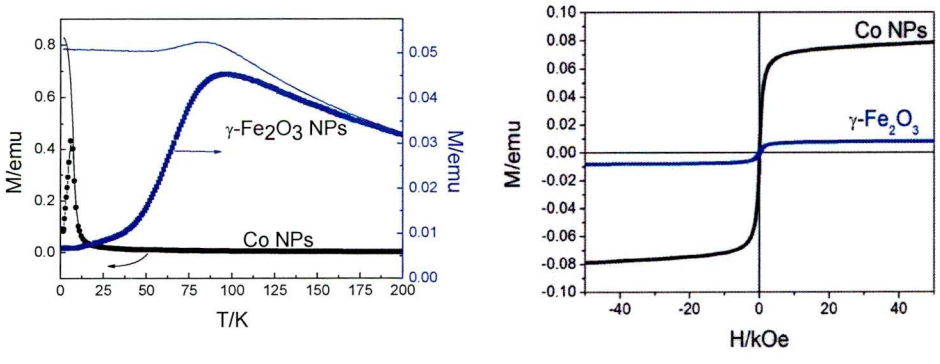

Figure 2.5. Zero-field cooled (symbols) and field cooled (lines) magnetization of the polymer coated Co and γ-Fe_2O_3 NPs as a function of temperature (a). The abscissa on the left is the magnetic moment measured for the P1 coated Co nanoparticles, and the abscissa on the right is the magnetic moment measured for the P2 coated γ-Fe_2O_3 nanoparticles. T_B for Co and γ-Fe_2O_3 nanoparticles is 6 K and 92 K respectively. The magnetization of the polymer coated Co and γ-Fe_2O_3 as a function of magnetic field at room temperature (b) show closed hysteresis loops at room temperature, indicating the NPs are superparamagentic at this temperature.

temperature observed in the γ-Fe_2O_3 nanoparticles is probably due to the contribution of different sources of anisotropy (e.g. surface anisotropy) that are not present in the Co NPs.

2.4.3 Stability of the thermo-responsive polymer coated magnetic in aqueous solution

The surface charge of nanoparticles is an important factor determining the stability of nanoparticles in a suspension. Surface charge can be measured via the ζ-potential of the nanoparticle, where a higher value for ζ-potential (and thus surface charge) indicates that the nanoparticles are more electrostatically repulsive to each other, making them more stable in a suspension. The ζ-potential of the thermo-responsive polymer coated Co and γ-Fe_2O_3 nanoparticles was measured over a wide range of pH, the results of which are shown in Table 2.2. At pH 1 the ζ-potential for the Co nanoparticles was found to be 22 mV and 14 mV for the γ-Fe_2O_3 nanoparticles. As the pH increased the ζ-potential became more negative to reach a value of -21 mV for the Co nanoparticles and -45 mV

Table 2.2. The effect of pH on the ζ-potential of the thermo-responsive polymer coated Co and γ-Fe_2O_3 NPs.

pH	ζ-potential of Co NPs (mV)	ζ-potential of γ-Fe_2O_3 NPs (mV)
1	22 ± 3	14 ± 3
4	8 ± 3	2 ± 3
6	6 ± 2	-21 ± 2
9	-11 ± 4	-31 ± 7
11	-21 ± 3	-45 ± 3

The results are the mean value and standard deviation of three separate experiments.

for the γ-Fe_2O_3 nanoparticles pH 11. At neutral pH the ζ-potential was found, by extrapolation, to be approximately -5 mV and –24 mV for the Co and γ-Fe_2O_3 nanoparticles, respectively.

The dependence of the ζ-potential upon pH may be result of surface ionisation of the nanoparticles, although the loss of protons from terminal carboxylic groups in increasingly basic conditions may have a contributory effect, resulting in an overall increase in negative charge on the outer shell of the particles. It was observed that regardless of ζ-potential, the NPs remained stable in aqueous dispersions across a wide pH range, suggesting the polymer shell has a good stabilising effect upon the nanoparticles.

The stability of the thermo-responsive coated magnetic NPs in electrolyte solution was studied by increasing the NaCl concentration of a nanoparticle dispersion in 10 mM phosphate buffer solution. The results are depicted in Figure 2.6 and it can be seen that both the Co and γ-Fe_2O_3 NPs are stable up to 0.3 M NaCl (normal physiological NaCl concentration is approximately 0.15 M). This suggests that the polymer coating had a charge stabilising effect upon the NPs. Up to 0.3 M NaCl the NPs are electrostatically repulsed from one another, however above this concentration the degree of electrostatic screening overcomes this repulsion and the NPs are 'salted out'.

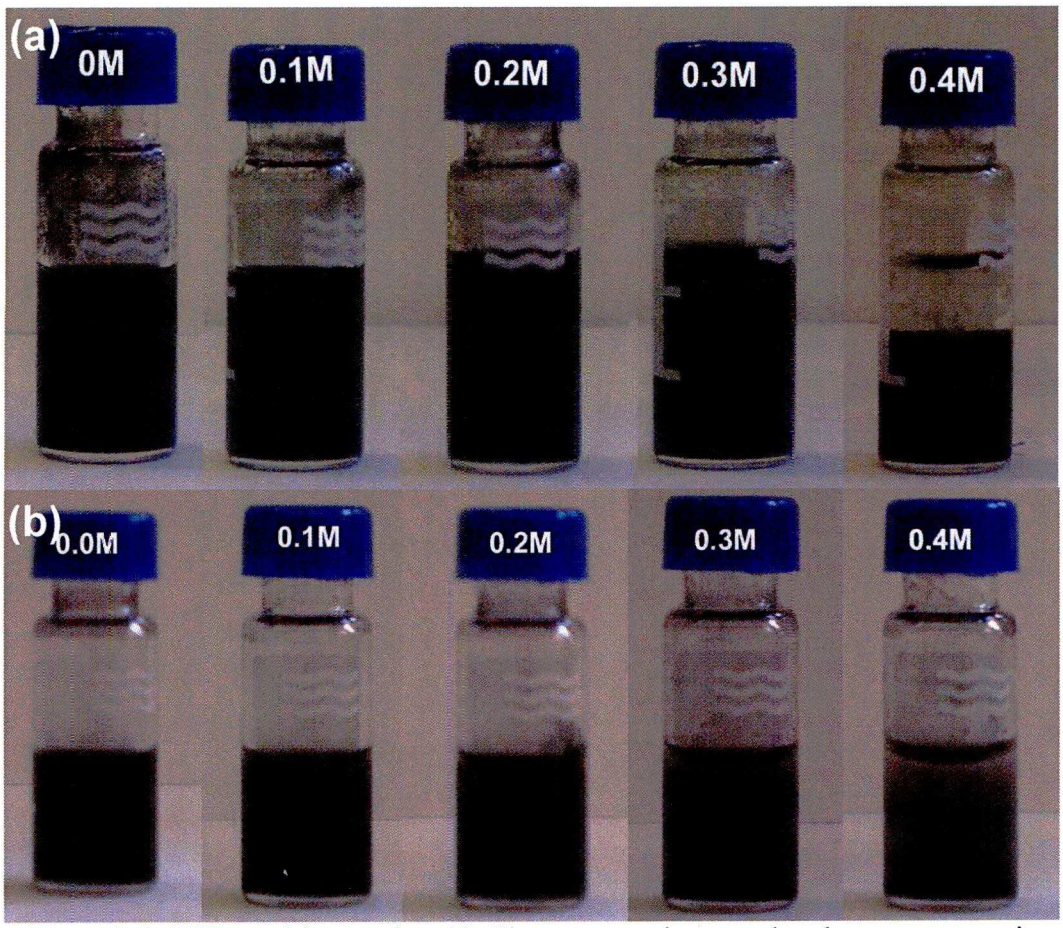

Figure 2.6. Effect of increasing NaCl concentration on the thermo-responsive polymer P1 coated Co (a) and polymer P2 coated γ-Fe_2O_3 NPs.

2.4.4 Effect of temperature on the stability of the thermo-responsive polymer coated magnetic

The stability of the nanoparticles in water and phosphate buffer solution (PBS) over a range of temperatures was studied and, as an example, the results for γ-Fe_2O_3 nanoparticles are presented in Figure 2.7. The γ-Fe_2O_3 NPs were stable up to 37 °C in both water and PBS, while the Co nanoparticles precipitated above 37 °C in PBS and 25 °C in water. The LCST of polymers P1 and P2 is 23.5 °C and 28 °C, respectively, in both water and PBS, and the differences between these and the precipitation temperatures may be due to the energy gain associated with the interactions of polymer chains adsorbing onto the nanoparticle surface compared to polymer-solution interactions. Also, at pH 7.4, both the Co and γ-Fe_2O_3 nanoparticles are negatively charged, thus the nanoparticles acquire a

degree of charge-stabilisation that will partially offset the hydrophobic polymer interactions, raising the overall aggregation temperature to above that of the polymer LCST. The adsorption of thermo-responsive polymer chains to the nanoparticle surface would be expected to lower their LCST by reducing the degrees of freedom of the polymer chain and promoting neighbouring chain interactions. However, it is likely that some of the polymer chains have been surface-entrapped, potentially with the terminal carboxyl group free. As a consequence, charge repulsion from carboxyl ions exposed in 'loops' from the surface and anionic nanoparticles would broaden and raise the LCST, as observed by Larsson *et al.*[205].

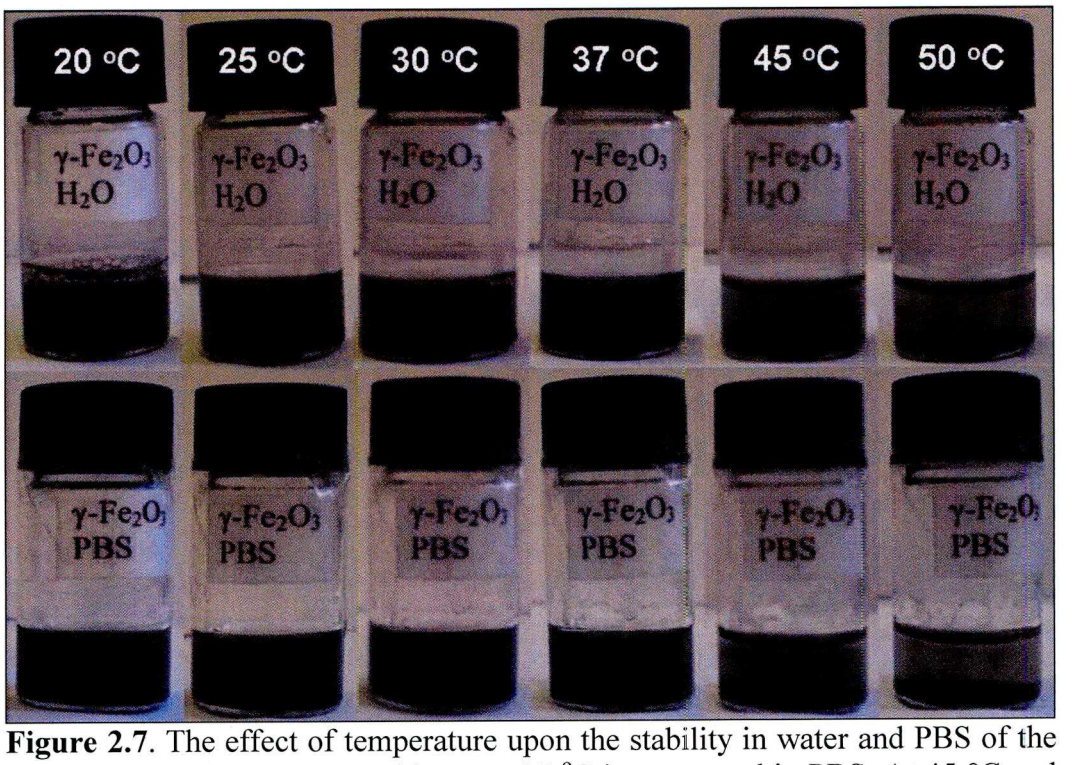

Figure 2.7. The effect of temperature upon the stability in water and PBS of the γ-Fe_2O_3 NPs. The NPs are stable up to 37 °C in water and in PBS. At 45 °C and above, precipitation of the NPs is apparent.

When compared to the poly(N-isopropylacrylamide) brushes reported by Yim *et al.*[206, 207] the polymer chains adsorbed onto the magnetic nanoparticles were likely to extend no more than a few nanometres into the solution, however,

this still represented a substantial 'corona' compared to the diameters of the nanoparticles. Therefore, at the physiological pH 7.4, it is possible that a combination of charge and steric shielding afforded by the polymer chains could increase the stability below 37 °C (or 25 °C for Co nanoparticles in water), but would not be enough to prevent particle aggregation above this temperature, due to collapse of the attached polymer chains.

In all cases the process was observed to be reversible, in that, upon cooling below these temperatures, the nanoparticles can be redispersed. The reversible aggregation of the nanoparticles is a consequence of the temperature sensitive phase transition of the polymer coating. As the temperature increases, the polymer brush changes conformation, resulting in the collapse of the polymer coil. This allows the nanoparticles to flocculate. Upon cooling the polymer coil is re-established causing the particles to disaggregate (Figure 2.8). The swelling/deswelling or 'smart' behaviour of the polymer in response to external stimuli suggests that thermal responsive coated magnetic nanoparticles would be favourable for nucleic acid adsorption[208], drug release[208] and biomolecular conjugates[209]. Furthermore, polymer coated magnetic nanoparticles can be exploited for use in a therapeutic application by binding therapeutic agents to the polymer (e.g. anionic DNA[210] or hydrophobic anti-cancer drugs[211]). The magnetic nanoparticles can then be targeted to a specific site by using a magnetic field as well as changing the temperature to control the release of the therapeutic agent.

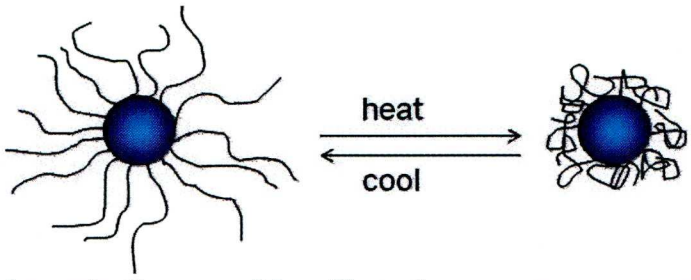

Figure 2.8. Schematic diagram of the effect of temperature upon extension and collapse of the pendant polymer chains on the nanoparticle surface. (Polymers and NPs not drawn to scale).

2.5 Conclusion

Magnetic NPs were synthesised, using a facile one-step method, which consisted of a Co or γ-Fe_2O_3 core and a shell of thermo-responsive polymer. Elemental analysis and dynamic light scattering of the NPs suggested the presence of the polymer chains on the nanoparticle surface. The synthesised NPs were found to be superparamagnetic at room temperature meaning they are not magnetically attracted to each other. This is an important consideration for biomedical applications, as agglomeration of NPs *in vivo* can lead to embolism and blood vessel damage. The polymer coating allowed the NPs to be transferred to aqueous solution where the polymer stabilised the nanoparticle dispersions. The dispersions were also found to be stable across a wide pH range and in electrolyte solution up to 0.3 M NaCl, which suggests that the polymers also impart a degree of charge stability on the NPs. The temperature dependent, reversible agglomeration of the NPs would suggest that the thermo-responsive nature of the polymers was retained after they became adsorbed onto the nanoparticle surface. The reversible responses of the polymers to external stimuli can be exploited for use as therapeutic delivery agents as well as a variety of biomedical applications.

In order to produce monodisperse NPs with a variety of size and shape using this method several parameters need to be investigated. The following chapters will look at novel synthesis methods for producing magnetic NPs with a range of sizes and ways of dispersing them in aqueous solution

Chapter 3

Magnetic nanoparticles synthesised by pulsed laser irradiation of cobalt carbonyl

3.1 Aims and objectives

The diversity of potential applications of magnetic NPs requires the production of NPs with tailored properties, such as size. The development of new synthesis techniques is therefore of great importance. In this chapter a novel synthesis method for producing Co NPs is described. The key innovation is the use of pulsed laser irradiation, at wavelengths of 266 nm and 355 nm, to decompose $Co_2(CO)_8$ in an organic solvent (DCB) containing stabilising ligands (OA and TOPO). It is important to be able to control the properties of the synthesised NPs, for example, by effect of changing the reaction conditions. Thus the effect of changing the ligand concentration and the wavelength of light used will also be investigated, which may also give an insight to the formation mechanism of the NPs.

$$Co_2(CO)_8 \xrightarrow[h\nu]{\text{OA \& TOPO}} 2Co + 8CO$$

Scheme 3.1. Synthesis of Co NPs by pulsed laser irradiation

3.2 Introduction

As discussed in Section **1.3** magnetic NPs have many potential biomedical applications. For use in these applications the magnetic NPs need to be biocompatible and biodegradable, and hence iron oxide NPs have been developed for these purposes. However, one drawback of using iron oxide is the need for relatively large NPs due to their comparatively low magnetic susceptibility[212]. The use of larger NPs can result in the increased chance causing an embolism and damage to blood vessels[70]. It is therefore desirable to use NPs with improved magnetic properties such as Co, so that smaller NPs can be used.

The main disadvantage of using Co in biomedical applications is its toxicity. However, this may be overcome by the use of NPs with a diameter of less than 8 nm. This is because NPs at this diameter are capable of glomerular filtration and can therefore be rapidly cleared from the body[195]. The renal clearance of metallic NPs is enhanced if they have a cationic or zwitterionic surface charge[195]. The surface of Co NPs can be modified post-synthesis by ligand exchange techniques that will also solubilise them for use in biological systems[199].

Several methods have been developed for the synthesis of magnetic NPs including thermal decomposition of organometallic compounds such as dicobalt octacarbonyl [$Co_2(CO)_8$] at high temperature in organic solvent and the presence of suitable stabilisers[8, 213]. Cobalt NPs have also been synthesised that are coated with hydrophilic polymers or peptides as ligands, which allows the NPs to be dispersed in aqueous solution[23, 122, 170]. Another method to synthesise Co NPs is to use a laser to induce the decomposition of $Co_2(CO)_8$ vapour produced by the evaporation of the precursor[116]. This laser evaporation method has been used to produce a variety of nanosized materials such as FeCo alloy and silica coated iron oxide NPs[117-119]. Ultra-violet irradiation of a cobalt (II) acetate solution has also been used to synthesise Co NPs which have certain morphologies depending upon the experimental parameters[120]. For any particular application there is an optimal size of NPs. For instance, biomedical applications require NPs with a size comparable to bio-molecules[37] and indeed, very small NPs are desirable for labelling cellular organelles. *In vivo*, very small NPs are also more rapidly transported across the endothelium, thereby having shorter circulation time than larger NPs[195]. It may also be easier to get a large number of smaller NPs into a

cell than a small number of larger NPs but with the overall mass of magnetic material being the same.

In a novel approach for the synthesis of the NPs less than 5 nm in diameter, laser pulses were used to stimulate the rapid decomposition of cobalt carbonyl in a solution of stabilisers. While Co NPs are very sensitive to air oxidation, especially at such a small size, this system was chosen because of their high saturation magnetisation and strong response to an external magnetic field and it may be possible that this technique can be used for the synthesis of more stable NPs, for example, those made of an FeCo alloy.

3.3 Results and Discussion

3.3.1 Size of Co nanoparticles produced by laser pyrolysis

Details of the synthesis can be found in Section **6.4**. Cobalt NPs, with a mean diameter of 2.8 ± 0.5 nm were synthesized by irradiating a solution of $Co_2(CO)_8$ and stabilizing ligands (OA, 0.04 M and TOPO, 0.02 M) in DCB with laser pulses at a wavelength of 266 nm (Figure 3.1a). Low mass-thickness contrast of Co NPs due to their small size and lower electron density compared with common Au NPs, means the Co NPs do not appear very dark in the TEM image. Reversing the concentration of the ligands (OA, 0.02 M and TOPO, 0.04 M) whilst maintaining the same precursor concentration, produced statistically significantly (t-test, P = 0.02) larger NPs with a mean diameter of 3.7 ± 0.6 nm (Figure 3.1b). The lower OA concentration means the growing NPs are encapsulated at a slower rate which results in them having a larger diameter[12]. The stabilizing ligands form a corona on the surface of the NPs, generating steric

repulsion, which can prevent aggregation of the NPs due to Van der Waals forces. The ligands can also, to a certain degree, protect the NPs from oxidation. The size of our NPs is comparable with the Co NPs synthesized using laser induced pyrolysis of $Co_2(CO)_8$ vapour by Zhao *et al.*[116], however, upon annealing in a reducing atmosphere, the latter NPs coalesced to form much larger particles.

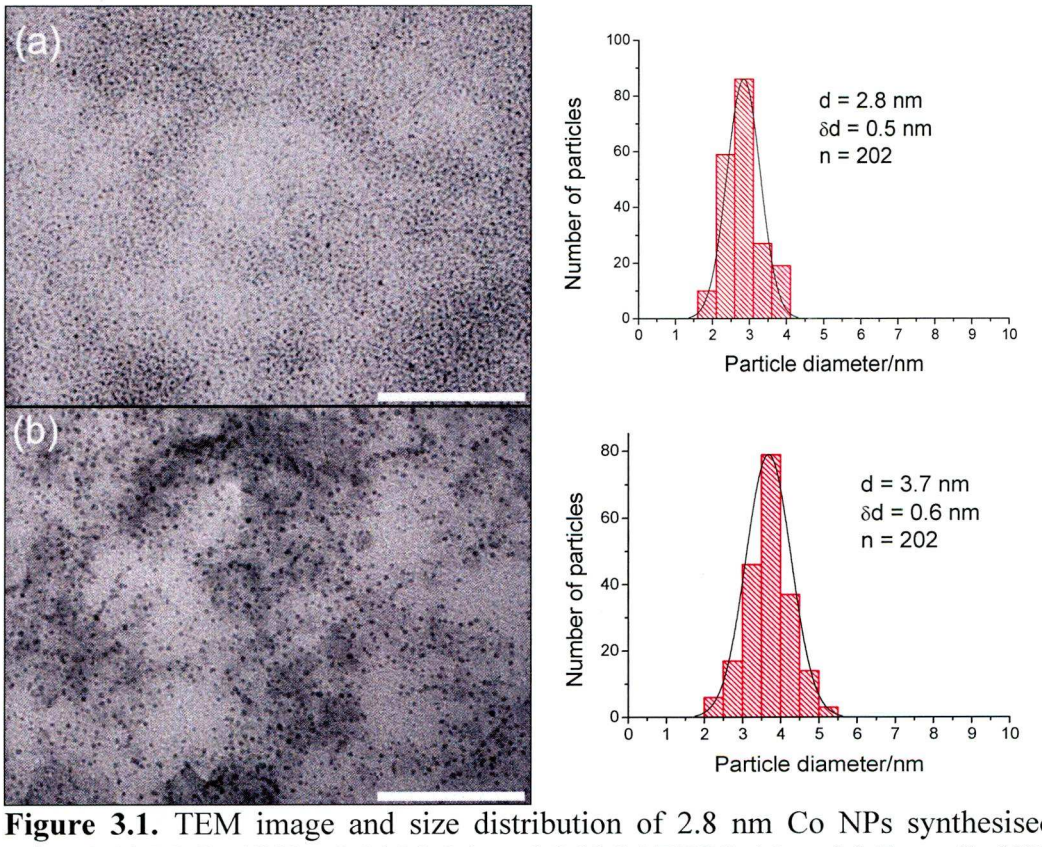

Figure 3.1. TEM image and size distribution of 2.8 nm Co NPs synthesised using 0.10 M $Co_2(CO)_8$, 0.04 M OA and 0.02 M TOPO (a) and 3.7 nm Co NPs synthesised using 0.10 M $Co_2(CO)_8$, 0.02 M OA and 0.04 M TOPO (b) in DCB by irradiation with laser pulses at 266 nm. d = mean particle diameter, δd = standard deviation, n = number of particles measured. Bar 100 nm.

Since both $Co_2(CO)_8$ and DCB absorb light at 266 nm, it is unclear if the NPs were formed by chemical photolysis of the precursor or by pyrolysis caused by localised heating of the solvent. To investigate this, the synthesis was further carried out using laser pulses at 355 nm while the other reaction conditions were kept constant. At this wavelength only $Co_2(CO)_8$ absorbs light, but not DCB.

Irradiation with laser pulses at this wavelength for 30 min consistently produced Co NPs with a bimodal distribution (Figure 3.2). These observations are discussed further in Section **3.5**.

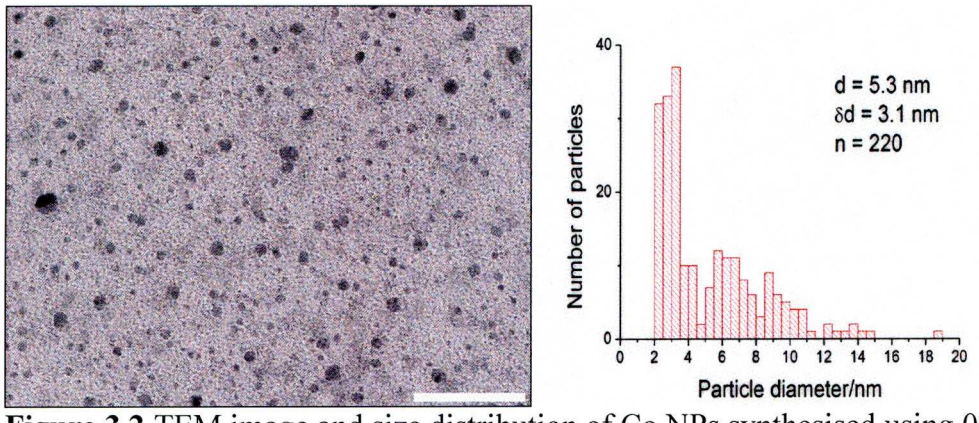

Figure 3.2 TEM image and size distribution of Co NPs synthesised using 0.10 M $Co_2(CO)_8$, 0.04 M OA and 0.02 M TOPO in DCB by irradiation with laser pulses at 355 nm. d = mean particle diameter, δd = standard deviation, n = number of particles measured. Bar 100 nm.

3.3.2 Magnetic Properties of Co nanoparticles produced by laser pyrolysis

The ZFC and FC magnetisation curves of the 2.8 nm Co NPs, synthesised as above, are plotted in Figure 3.3. These NPs have a very low T_b of approximately 6 K. The sharp peak in the ZFC curve and the splitting of the ZFC and FC curves close to T_b suggest that the Co NPs have a narrow size distribution, which is consistent with the TEM images in Figure 3.1.

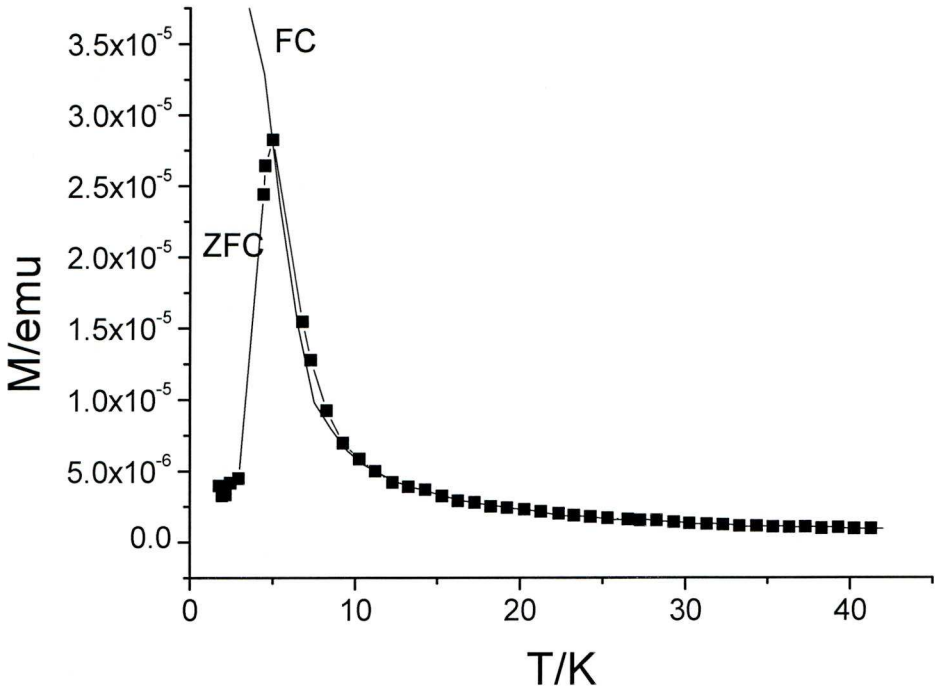

Figure 3.3. ZFC and FC magnetisation curves of the 2.8 nm Co NPs produced using light at 266 nm, showing a blocking temperature of 6 K.

The ZFC curve of the Co NPs produced at a wavelength of 355 nm has a peak at around 34 K, and also an upturn at a very low temperature which could be due to the presence of very small NPs (Figure 3.4). The splitting between the ZFC and FC data also occurs at a temperature well above the peak at 34 K because of the contribution of relatively large NPs. This is consistent with the TEM observations in Figure 3.2, were the Co NPs were found to have a bimodal distribution.

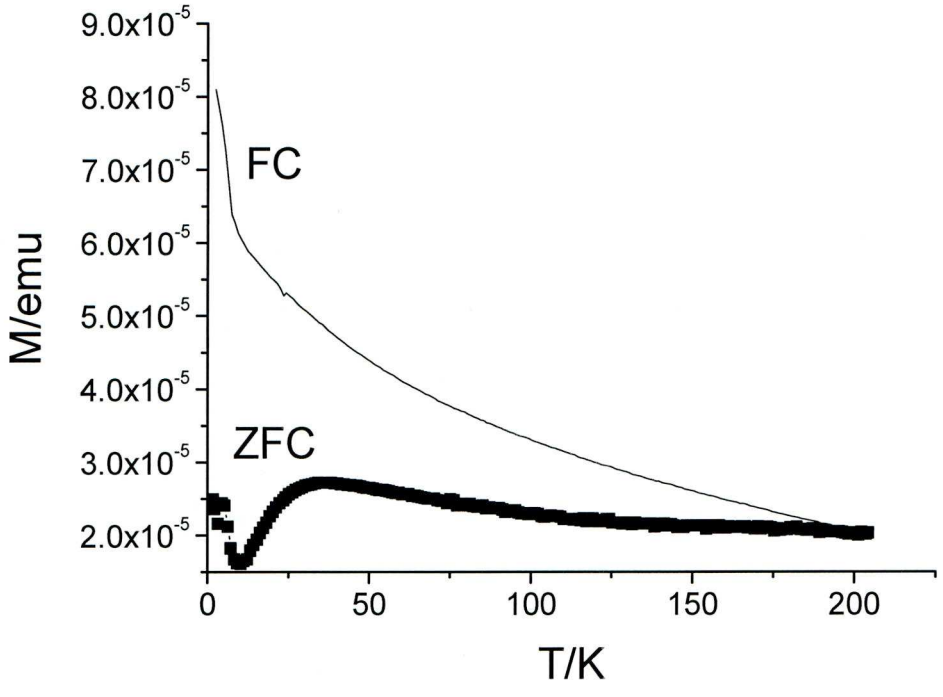

Figure 3.4. ZFC and FC magnetisation curves of Co NPs produced by irradiation of $Co_2(CO)_8$ at a wavelength of 355 nm.

3.3.3 Formation mechanism of Co nanoparticles produced by laser pyrolysis

The UV-visible spectrum of DCB (Figure 3.5) shows strong absorbance at 266 nm, resulting in a significant temperature jump following absorption of a short laser pulse, whereas DCB does not absorb light at 355 nm. In contrast, $Co_2(CO)_8$ absorbs light at both wavelengths (Figure 3.5); the peak near 266 nm can be associated with $Co_2(CO)_8$ in a bridged form and that near 355 nm with $Co_2(CO)_8$ in non-bridged form[214, 215](structures are shown in Figure 3.5). Irradiation of $Co_2(CO)_8$ at 266 nm results in the majority of the photolysed molecules undergoing cobalt-carbonyl bond dissociation producing $Co_2(CO)_7$, while at 355 nm the major process is homolysis of the cobalt-cobalt bond, resulting in two $Co(CO)_4$ radicals[216]. Both species may undergo further

decarbonylation, which ultimately may result in the formation of nuclei followed by the growth process of the NPs[217].

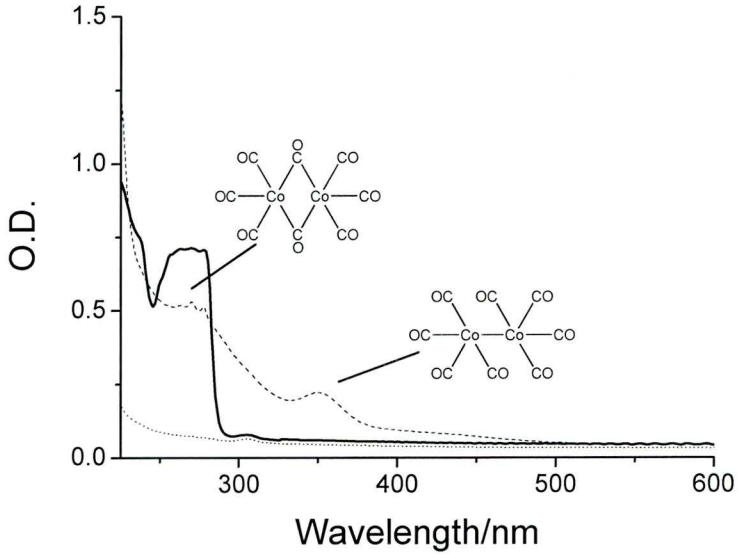

Figure 3.5. UV-visible spectrum of $Co_2(CO)_8$ (0.2 M in decane) (dashed line), DCB (solid line) and decane (dotted line) path length approximately 16 μm

From the UV-visible absorbance spectra, the approximate values of the extinction coefficients of DCB and $Co_2(CO)_8$ at the relevant wavelengths were determined. This yielded 60 M^{-1} cm^{-1} for DCB at 266 nm[218], and 1 500 M^{-1} cm^{-1} and 600 M^{-1} cm^{-1} for $Co_2(CO)_8$ at 266 and 355 nm, respectively. Using these extinction coefficients, it was possible to estimate the fraction of laser pulse energy absorbed and thus the laser pulse-induced temperature increase in the first layer of the sample. For the conditions used here, and assuming that all of the absorbed laser pulse energy was rapidly converted to heat, the estimated temperature increase was approximately 75 ± 20 K for excitation at 266 nm, whereas for excitation at 355 nm the maximum temperature increase was only in the order of 5-10 K.

For excitation at 266 nm, the temperature increase occurs to a depth of only a few μm and the heat is estimated to dissipate in less than 100 μs[219]. However, it is possible that this rapid temperature increase and decrease is sufficient to cause a short burst of nucleation, followed by a slower growth phase due to rapid diffusion of the sample. Temporal separation of the nucleation and growth phases of particle formation is known to give rise to populations of NPs with a narrow size distribution[220]. This could explain why at 266 nm, monodisperse Co NPs are formed.

The average particle size is determined by the length of the growth phase, and thus, by kinetic competition between particle growth and encapsulation of the NPs by OA and TOPO. The NPs produced by *pulsed* laser irradiation are smaller than those produced by conventional thermal decomposition (8-9 nm) using similar reactant concentrations[106], where the conditions for growth are continuous. Kinetic control of the growth phase also explains the different particle sizes obtained for different ligand concentrations.

Laser pulses at 355 nm penetrate to a larger depth, thus affecting a larger volume and yielding a smaller temperature increase, which is insufficient to contribute to the breakdown of $Co_2(CO)_8$. This means that at this wavelength formation of the NPs is a purely photolytic process. This seems to lead to a longer nucleation phase (possibly limited by the rate of further decarbonylation after formation of the initial photoproduct, see above) and less separation from the growth phase, resulting in the formation of NPs with a broader size distribution. Cobalt NPs do not have an absorption peak at 355 nm[221, 222], therefore, the broad size distribution of the NPs obtained at this wavelength is

unlikely to be a result of annealing, melting or fragmentation of the synthesised NPs. The X-ray diffraction pattern in Figure 3.6 indicates that the as synthesised Co NPs are amorphous, since the pattern is featureless. This is not unexpected, as Co NPs obtained in similar ways have also been found to be amorphous[147, 223].

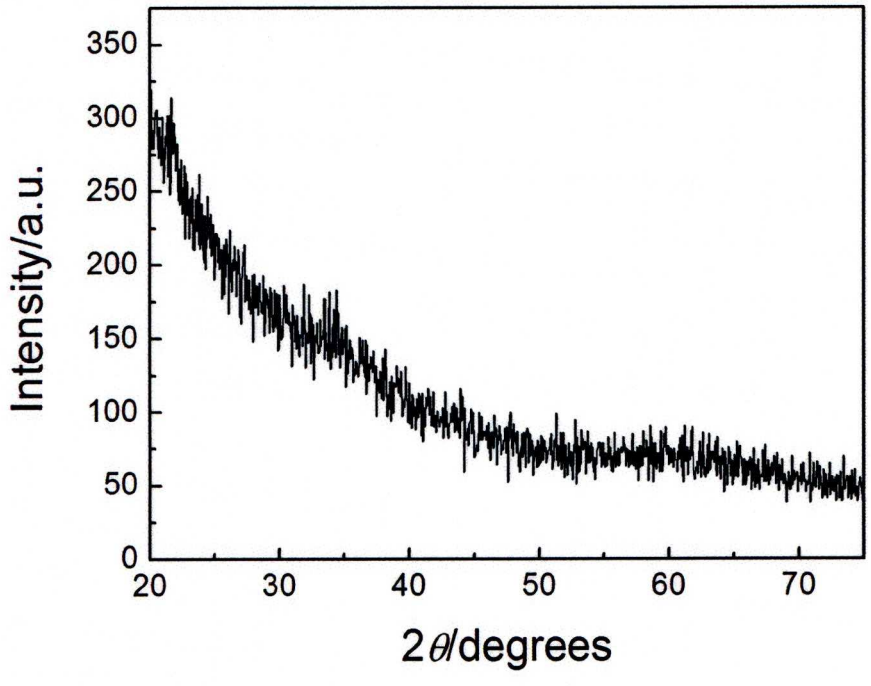

Figure 3.6. XRD pattern of Co NPs synthesised by pulsed laser irradiation of $Co_2(CO)_8$, at 355 nm, in the presence of 0.04 M OA and 0.02 M TOPO.

3.4 Conclusion

Using a novel method, namely, the decomposition $Co_2(CO)_8$, dissolved in DCB, by pulsed laser irradiation, it has been possible to synthesise small (<5 nm) Co NPs in a solution of DCB. Producing Co NPs of this size is significant for potential use in biomedical application as their size would allow the rapid renal clearance from the body, and thus, avoiding the unwanted toxic effects of prolonged exposure to Co. The size of the NPs could be controlled by adjusting certain reaction conditions, such as ligand concentration and wavelength of light.

Adjusting the wavelength of light used to irradiate the precursor also helped to understand the formation mechanism of the Co NPs using this technique. From this it was deduced that chemical photolysis of $Co_2(CO)_8$ can produce Co NPs, however, Co NPs with a narrow size distribution were only produced when the pulsed laser irradiation caused localised heating of the solvent (i.e. at 266 nm).

Using this technique, very small Co NPs can be produced, however, they are very susceptible to oxidation, which results in a diminishment of their magnetic properties. This may be overcome by synthesising alloy NPs that are resistant to oxidation, or by encasing the magnetic NPs with a layer of a noble metal such as gold. These techniques will be discussed in the next two chapters.

Chapter 4

Synthesis of magnetic nanoalloys by the thermal decomposition of bimetallic carbonyl clusters

4.1 Aims and objectives

The aim of this chapter is to synthesise a series of alloy magnetic NPs using the thermal decomposition of bimetallic carbonyl clusters. This is a novel method of producing alloy NPs, which are usually produced by the decomposition and /or reduction of two or more precursors where control of the composition of NPs can prove difficult. Using the thermal decomposition of bimetallic carbonyl clusters as single source precursors it may be possible to produce alloy magnetic nanoparticles with well controlled composition. Control of other characteristics is also very important; therefore, the effect of changes in the reaction conditions on physical properties of the synthesized nanoparticles is also explored. This method may also be applied to a wide variety of alloy compositions.

$$[FeCo_3(CO)_{12}]^- \xrightarrow[\text{heat}]{\text{OA \& TOPO}} FeCo_3 + 12CO$$

Scheme 4.1. Synthesis of alloy nanoparticles by the thermal decomposition of a bimetallic carbonyl cluster

4.2 Introduction

For use in biomedical applications, NPs need to both biocompatible and degradable. For this reason, iron oxide NPs can be used, however, these NPs have a relatively low saturation magnetisation compared to metal NPs, which requires the use of NPs that are tens of nanometres in diameter[212]. The use of larger NPs can be a problem, especially if they aggregate, because of the potential to cause an embolism and damage to blood vessels[70]. It is therefore desirable to use smaller NPs that have enhanced magnetic properties, for

example those made from pure metals such as Co or Fe and alloys that contain these metals such as FePt, FeNi or FeCo. However, Co or Fe NPs can be difficult to obtain due to the sensitivity of these metals to oxidation in the atmosphere, which diminishes their magnetic properties[224, 225]. This makes alloy magnetic NPs (or nanoalloys) of particular interest due to their magnetic properties such as high saturation magnetisation[124] and their resistance against oxidation.

Nanoalloys form when two or more metals co-aggregate to produce compositionally ordered structures, with properties that differ from those of bulk alloys or NPs of the individual components[152, 226-229]. A variety of methods have been used to synthesise nanoalloys such as co-reduction of mixed metal ions in aqueous solution[230-235] and polyol[123, 124, 197], sequential reduction[236-239] of metal ions, electrochemical methods[240-242], radiolysis[243-245], microwave plasma decomposition[246], reduction of double complexes[247, 248] and the thermal decomposition of two or more metal carbonyls[139, 225, 249, 250]. A "true" nanoalloy is formed when there is no preferential aggregation of metal atoms into monometallic areas of the nanoparticle, i.e. there is not any kinetically induced phase separation of the constituent metal atoms of the nanoalloy[139]. This can prove difficult when producing nanoalloys from separate sources, such as the decomposition of two or more carbonyl compounds, due to the different decomposition temperature of the different carbonyls[197]. Other processes, such as polyol reduction, have produced nanoalloys such as FeCo and FeNi, however, controlling the composition of the NPs remains a challenge[197].

These problems may be overcome by employing bimetallic compounds as single-source molecular precursors, in order to have the different metals

always in intimate contact. Among these, bimetallic carbonyl clusters are quite attractive, since they can be prepared with several different sizes and composition and, moreover, they are decomposed under very mild conditions[251, 252]. This approach has been well documented by the use of homo- and bi-metallic metal carbonyl clusters for the preparation of supported metal nanoparticles to be used in heterogeneous catalysis[253-258]. Conversely, very little is known on the use of metal carbonyl clusters as precursors of magnetic bimetallic nanoparticles. An interesting exception is represented by the use of the neutral $Fe_3Pt_3(CO)_{15}$ for the preparation of FePt nanoparticles having high coercitivity[259]. A larger spectrum of metals and compositions may be reached by using anionic instead of neutral bimetallic carbonyl clusters, due to the richer chemistry of the former

Thus, different types of bimetallic magnetic nanoparticles have been synthesized, starting from molecular bimetallic carbonyl cluster anions, *i.e.* $[FeCo_3(CO)_{12}]^-$ [260, 261], $[Fe_3Pt_3(CO)_{15}]^{2-}$ [262], $[FeNi_5(CO)_{13}]^{2-}$ [263] and $[Fe_4Pt(CO)_{16}]^{2-}$ [262]. In these experiments, the thermal decomposition of the anionic bimetallic carbonyl clusters systematically resulted in the formation of a series of alloy NPs, with a composition reflecting that of the precursor, i.e. $FeCo_3$, FePt, $FeNi_5$ and Fe_4Pt. Thus, this method seems to eliminate the problems of phase separation and composition control. From this series the $FeCo_3$ NPs were chosen for further investigation due to the relative size compared to the other alloy NPs. The reaction conditions used to synthesise these NPs were adjusted to investigate what effect this would have upon the size and shape of the NPs.

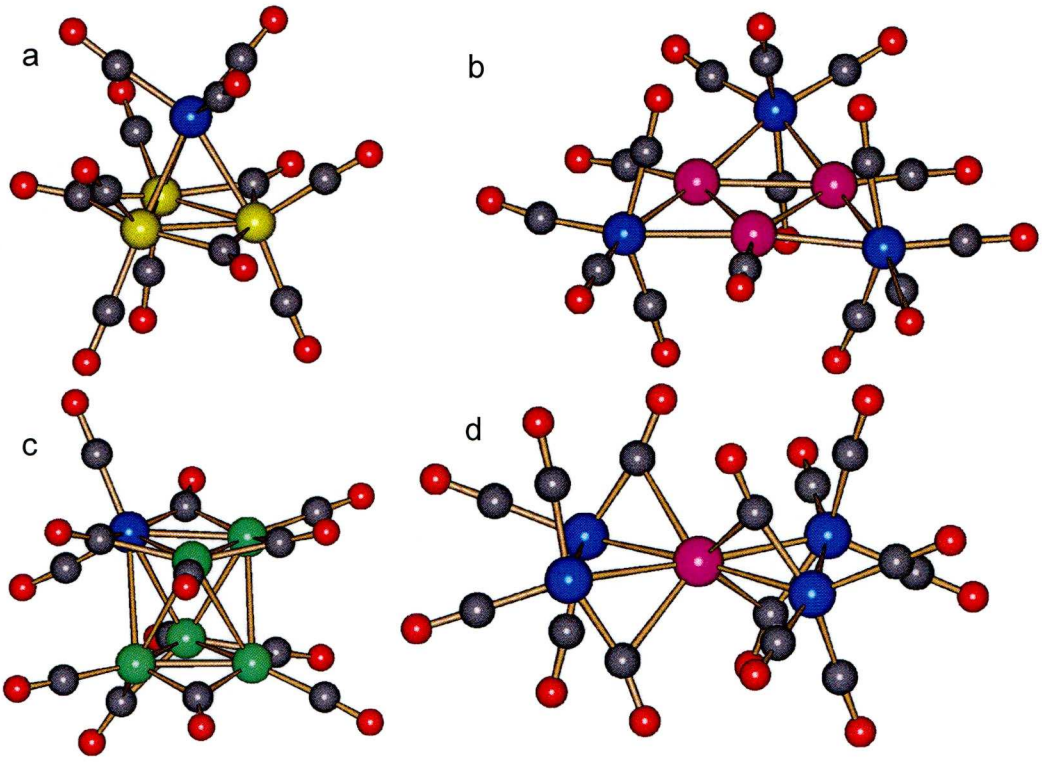

Figure 4.1. Molecular structures of (a) $[FeCo_3(CO)_{12}]^-$, (b) $[Fe_3Pt_3(CO)_{15}]^{2-}$, (c) $[FeNi_5(CO)_{13}]^{2-}$ and (d) $[Fe_4Pt(CO)_{16}]^{2-}$ (Co yellow, Fe blue, Pt purple, Ni green, C grey, O red). Structure drawings have been performed with SHAKAL99[264]

4.3 Results and discussion

The thermal decomposition of bimetallic carbonyl clusters was used to produce alloy NPs with a variety of compositions, e.g. FeCo, FePt, FeNi. For further details see Section **6.5**. The composition of the alloy NPs was controlled by the composition of the polynuclear carbonyl cluster that was used as the precursor in the synthesis. For example the Fe-Co NPs were produced from $[Net_4][FeCo_3(CO)_{12}]$ retained the 1:3 composition of the precursor. The composition of the alloy NPs was calculated from the relative mass of each metal by elemental analysis (Table 4.1). This would indicate that the decomposition of the precursor follows the classical LaMer model[265]; formation of initial metal

nuclei, their agglomeration, and/or nuclei growth via decomposition of the rest of the carbonyl on them.

Table 4.1. Results of the elemental analysis used to calculate the composition of the alloy nanoparticles synthesised from the thermal decomposition of bimetallic carbonyl clusters

Precursor	Fe (%)	Co (%)	Ni (%)	Pt (%)	relative molar amount Fe[a]	relative molar amount Co	relative molar amount Ni	relative molar amount Pt	nanoparticle composition
$[FeCo_3(CO)_{12}]^-$	8.35	25.97	-	-	0.15	0.44	-	-	$FeCo_3$
$[FeNi_5(CO)_{13}]^{2-}$	10.94	-	44.83	-	0.20	-	0.76	-	$FeNi_4$
$[Fe_3Pt_3(CO)_{15}]^{2-}$	11.58	-	-	37.47	0.21	-	-	0.19	FePt
$[Fe_4Pt(CO)_{16}]^{2-}$	16.02	-	-	14.60	0.29	-	-	0.07	Fe_4Pt

[a] Relative molar amounts for each element were calculated by dividing the percentage weight by the atomic mass of that element.

4.3.1 Size of the Magnetic Nanoalloys

All the NPs produced were spherical and the average diameter of the NPs varied depending on their metal composition. Figure 4.2a, for example, shows a TEM image of $FeCo_3$ NPs with an average diameter of 6.8 ± 0.8 nm, while Figures 4.2b, 4.2c and 4.2d show TEM images of $FeNi_4$, FePt and Fe_4Pt NPs, produced under the same conditions (reactant concentrations, etc.), with average diameters of 4.1 ± 0.7 nm, 2.6 ± 0.4 nm and 3.7 ± 0.6 nm. However, varying the reaction conditions, such as ligand concentration (Figure 4.3) and temperature, had no statistically significant effect (student t-test, $P = 0.02$) upon the size or composition of the alloy NPs. This suggests that the dominating factor that controls the size and shape of the magnetic alloys is the configuration of the bimetallic carbonyl precursor they were synthesized from.

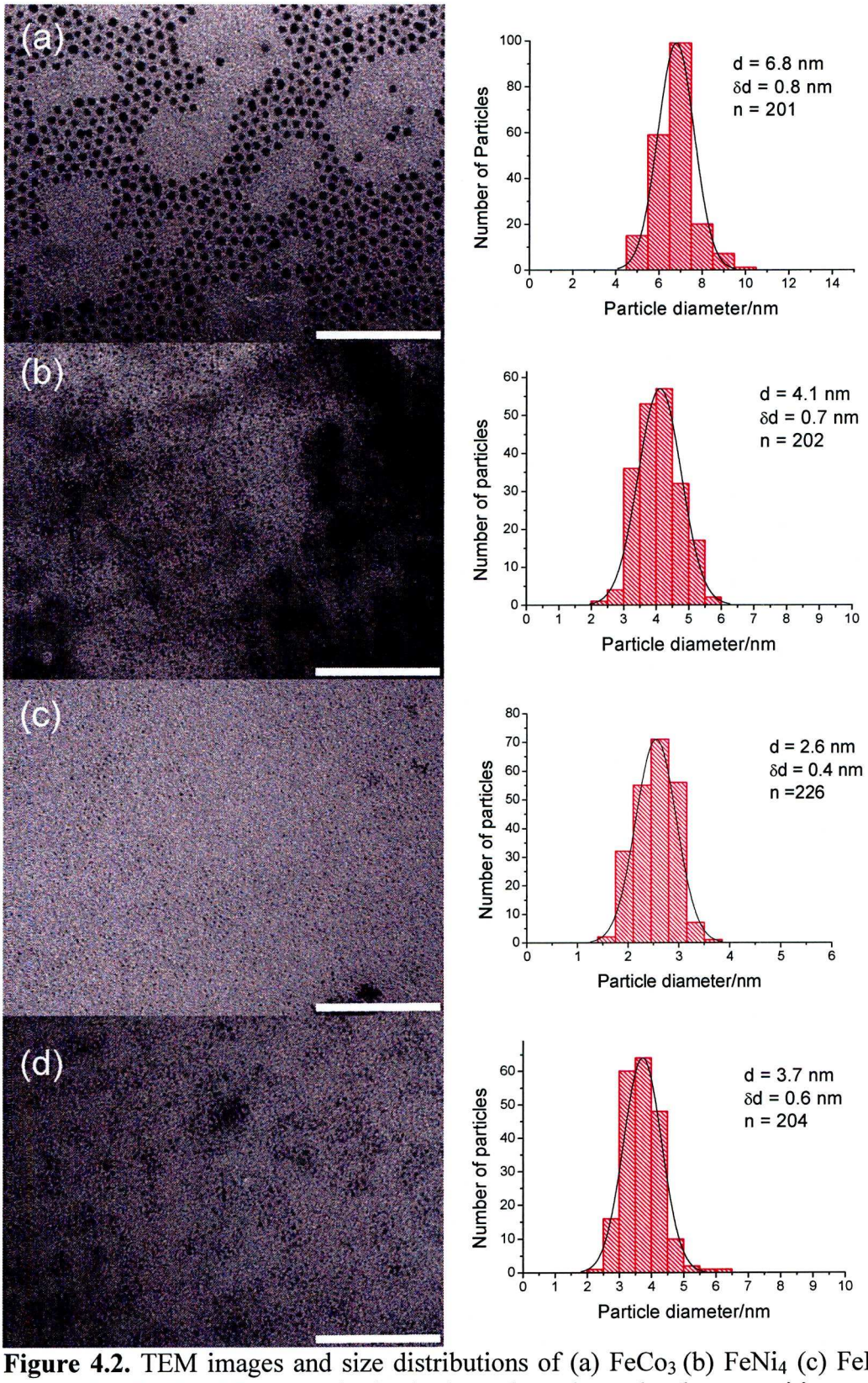

Figure 4.2. TEM images and size distributions of (a) $FeCo_3$ (b) $FeNi_4$ (c) FePt and (d) Fe_4Pt NPs synthesised by the thermal decomposition of $[NEt_4][FeCo_3(CO)_{12}]$, $[NMe_4]_2[FeNi_5(CO)_{13}]$, $[NMe_3CH_2Ph]_2[Fe_3Pt_3(CO)_{15}]$ and $[NMe_3CH_2Ph]_2[Fe_4Pt(CO)_{16}]$ and coated with OA and TOPO.

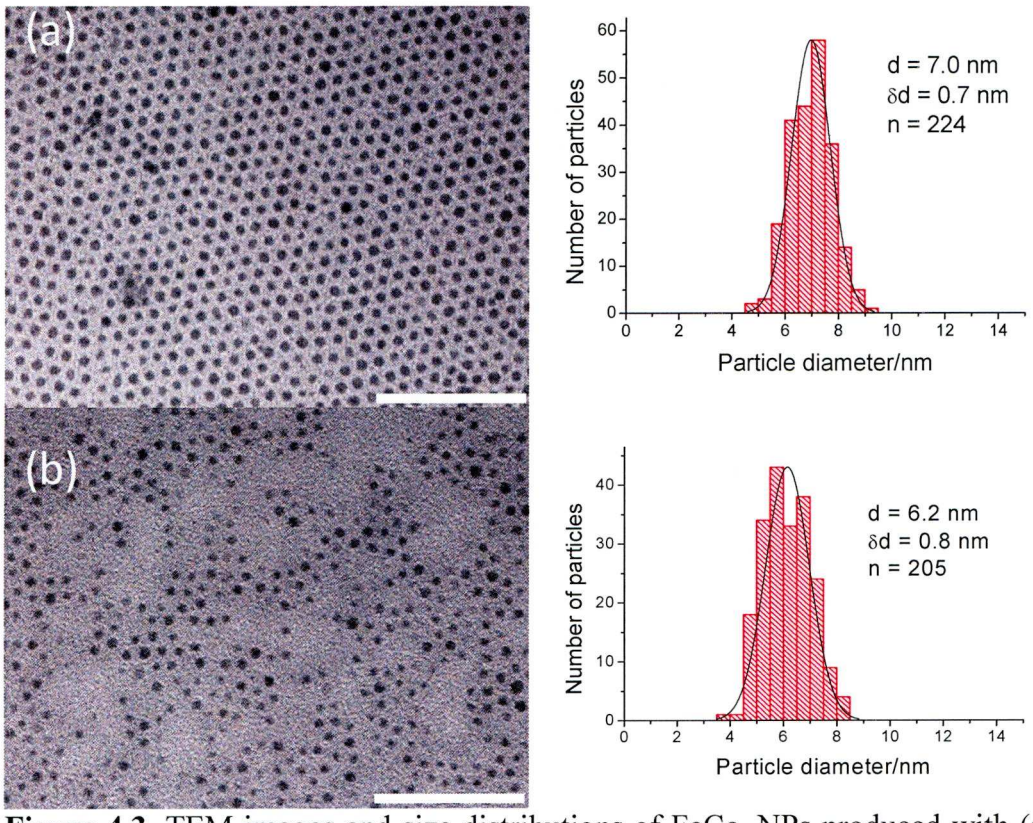

Figure 4.3. TEM images and size distributions of $FeCo_3$ NPs produced with (a) 0.055 mmol OA or (b) 0.22 mmol OA. Varying the concentration of OA had no significant effect upon the average diameter of the NPs.

4.3.2 Magnetic properties of the Nanoalloys

The ZFC and FC magnetization curves of the magnetic alloy NPs are shown in Figure 4.4 and indicate that the NPs are superparamagnetic at room temperature. The sharp peaks in the ZFC curves and the splitting of the curves near to the blocking temperatures indicate that the NPs have a narrow size distribution, which is consistent with the TEM images in Figure 4.1. Changing the ligand oleic acid (OA) for myristic acid (MA) and trioctylphosphine oxide (TOPO) for hexadecylamine (HDA) in the synthesis of the $FeCo_3$ NPs had no significant effect upon the magnetic properties of the synthesized NPs (Figure 4.5). This suggests that the crystal structure of the NPs is not affected by the nature of the ligand used in their synthesis.

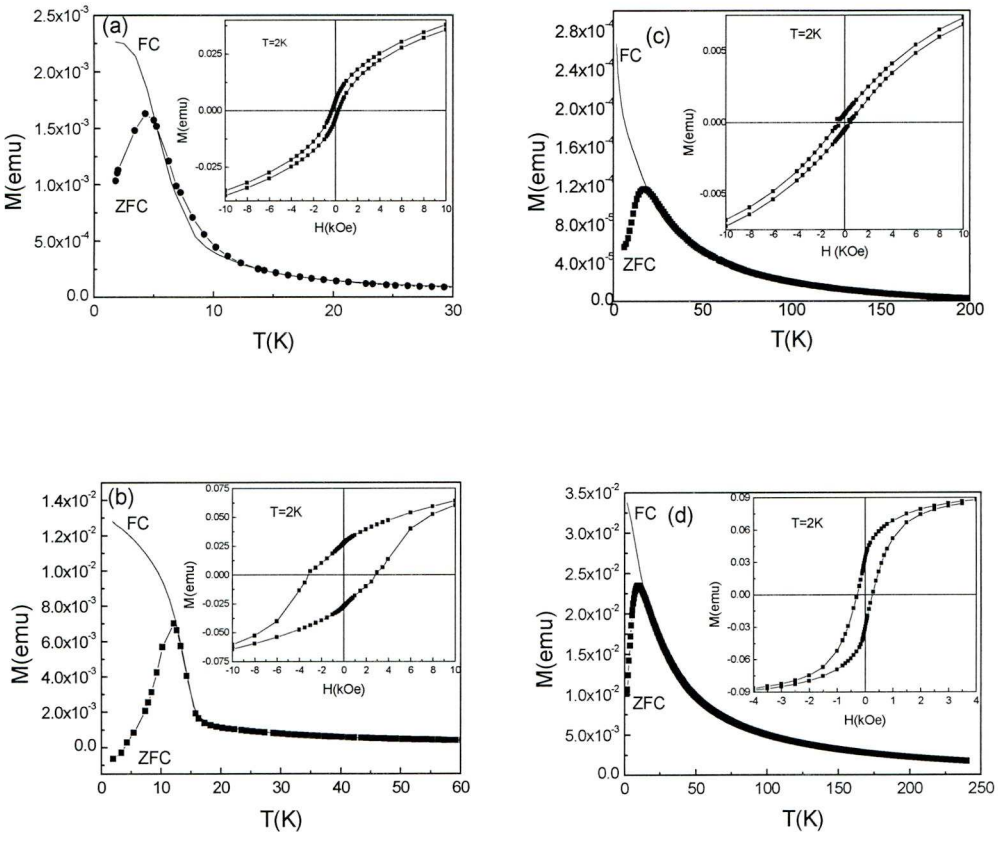

Figure 4.4. Zero-field cooled and field cooled magnetization curves of (a) $FeCo_3$ (b) $FeNi_4$ (c) FePt and (d) $FePt_4$ NPs coated with OA and TOPO. The insets show the hysteresis curves at 2 K for each sample.

Some of the physical properties of the magnetic alloy NPs are summarized in Table 4.2. An interesting point of note is the difference in value for the anisotropy constant between the Fe-Pt alloy NPs. The XRD patterns in Figure 4.7 reveal that both FePt and Fe_4Pt NPs are fcc in structure (JCPDF No. 00-002-1167). This would suggest that the differences in the magnetic properties of the FePt and Fe_4Pt NPs are due to differences in their composition rather differences in their crystal structure (e.g. fct Fe-Pt alloys have a typical anisotropy constant of 7000 kJ/m^3). This indicates that subtle differences in the composition of the NPs can be achieved by the use of the appropriate precursor. The XRD patterns of the synthesised alloy NPs are discussed further in Section **4.3.3**.

Table 4.2. Summary of the magnetic properties of the nanoalloys produced by thermal decomposition of a range of bimetallic carbonyl clusters and coated with OA and TOPO.

NP Composition	Diameter (nm)	T_b (K)	H_c at 2 K (Oe)	K (kJ/m^3)	M_s (Am^2/kg)
$FeCo_3$	7.0	4	300	8	123
$FeNi_4$	4.4	12	3000	115	187
FePt	2.6	17	400	638	128
Fe_4Pt	3.2	10	250	130	209

The ZFC and FC magnetisation curves of $FeCo_3$ alloy NPs synthesised in the presence of either OA and TOPO or MA and HDA are shown in Figure 4.4 and reveal the NPs have blocking temperatures of approximately 4 K and 6 K, respectively. It is interesting to note that the magnetic properties of the $FeCo_3$ NPs were not affected by changes to the reaction conditions, in this case, the type of ligand used to stabilise the NPs. The effects of changing the type of ligand used to stabilise the alloy NPs during synthesis are discussed further in Section **4.3.4**.

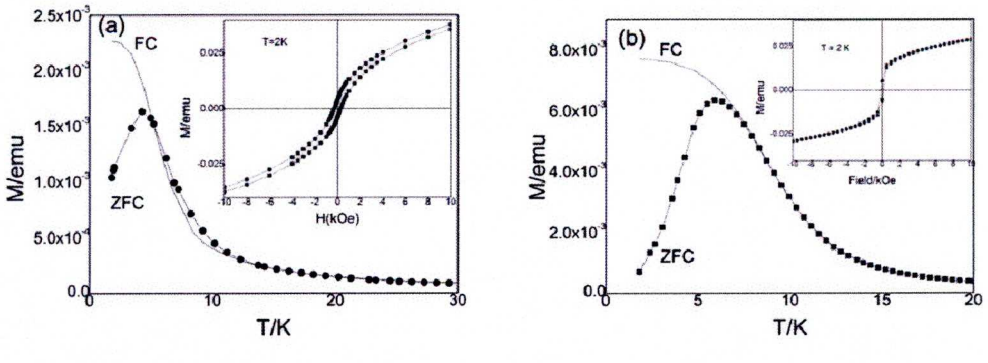

Figure 4.5. ZFC and FC magnetisation curves of $FeCo_3$ alloy NPs stabilised with (a) OA and TOPO or (b) MA and HDA. The inset shows the hysteresis curves at 2 K.

4.3.3 X-Ray diffractometry of the magnetic alloy NPs

The XRD pattern of the OA -TOPO coated $FeCo_3$ NPs shown in Figure 4.5 indicates the presence of bcc structure typical of Fe-Co alloys (JCPDF No. 03-065-4131) and ε-Co (JCPDF No. 03-065-9722). Moreover, the pattern suggests that the $FeCo_3$ NPs have not become oxidised as it does not match the XRD patterns for any iron oxides or cobalt oxides.

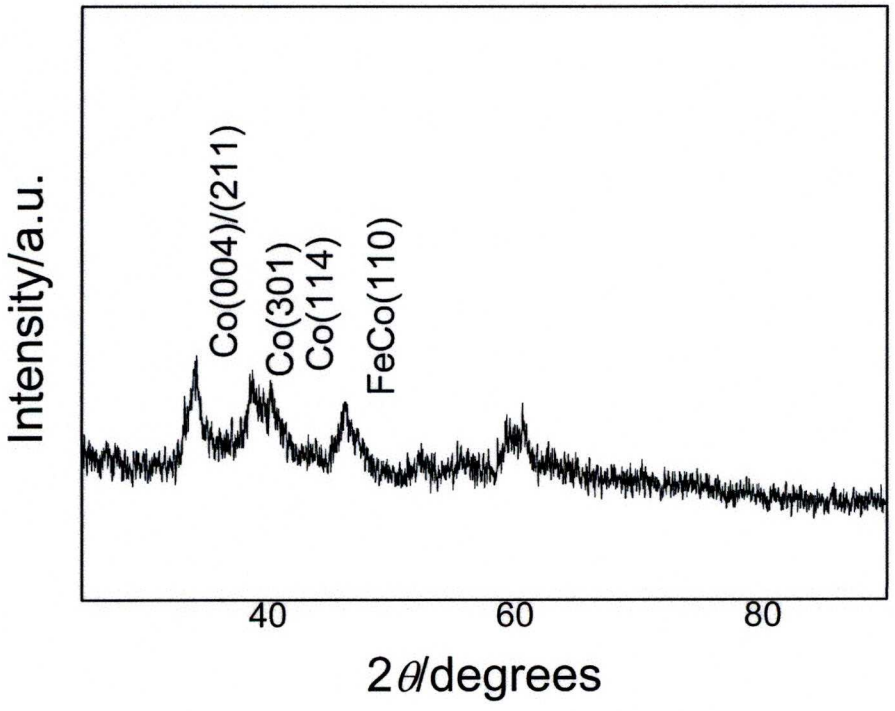

Figure 4.6. XRD pattern of the $FeCo_3$ alloy NPs synthesised by the thermal decomposition of $[NEt_4][FeCo_3(CO)_{12}]$.

The XRD patterns of the Fe-Pt alloy NPs are shown in Figure 4.7 reveal that both FePt and Fe_4Pt NPs are fcc in structure (JCPDF No. 00-002-1167). This contradicts the findings of Inomata *et al.*[266], who suggested that FePt alloy had a tetragonal structure and Fe_4Pt was cubic. Nevertheless, no peaks were observed

that indicated the presence of iron oxide, suggesting the Fe-Pt alloy NPs are resistant to oxidation thus maintaining their magnetic properties.

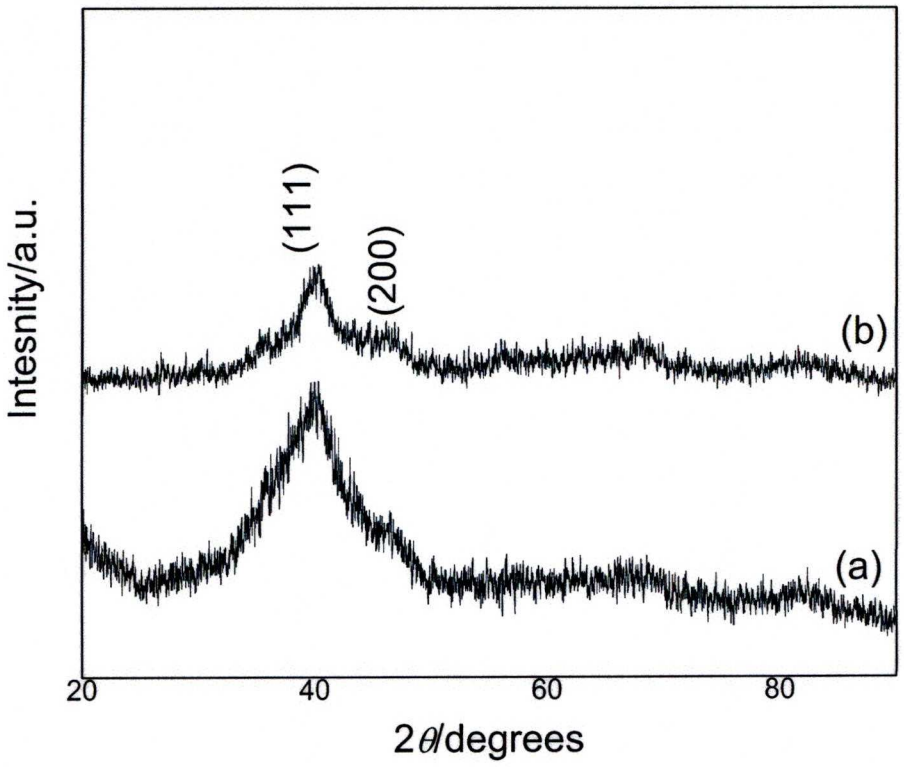

Figure 4.7. XRD patterns of (a) FePt and (b) Fe_4Pt alloy NPs, synthesised by the thermal decomposition of $[NMe_4CH_2Ph][Fe_3Pt_3(CO)_{15}]$ and $[NMe_4CH_2Ph][Fe_4Pt(CO)_{16}]$, respectively.

4.3.4 Effect of ligand type on nanoalloy particle size

The effect upon the size and shape of the magnetic nanoalloys by changing the hydrocarbon tail of the ligands was investigated. Combinations of ligands with "kinked" (e.g. oleic acid, oleylamine), "straight" (e.g. myristic acid, hexadecylamine) or "bulky" e.g. trioctylphosphine oxide, adamantane carboxylic acid) hydrocarbon chains were used to stabilize $FeCo_3$ alloy NPs (Figures 4.8 to 4.10). These ligands have previously been shown to affect both the size and the shape of alloy NPs that were produced by the concurrent thermal

Table 4.3. Effect of changing the hydrocarbon tail and/or the head group of the stabilizing ligand on the diameter of $FeCo_3$ NPs.

	Size of $FeCo_3$ NPs (nm)		
	hexadecylamine	oleylamine	TOPO
myristic acid	7.6 ± 1.4	6.8 ± 0.7	6.8 ± 1.0
oleic acid	8.1 ± 1.0	7.6 ± 1.8	6.0 ± 0.7
adamantane carboxylic acid	6.8 ± 0.8	7.1 ± 1.5	5.3 ± 0.7

decomposition/reduction of two or more precursors[141]. However, as summarized in Table 4.3, changing the nature of the surfactant had no statistically significant ($P = 0.02$) effect upon the size, shape or composition of the $FeCo_3$ alloy NPs produced by the decomposition of $[NEt_4][FeCo_3(CO)_{12}]$. Again this suggests the composition of the precursor determines the physical characteristics of the synthesized magnetic nanoalloys. Moreover, it is expected that several other compositions might be obtained by simply changing the nature of the carbonyl cluster precursor.

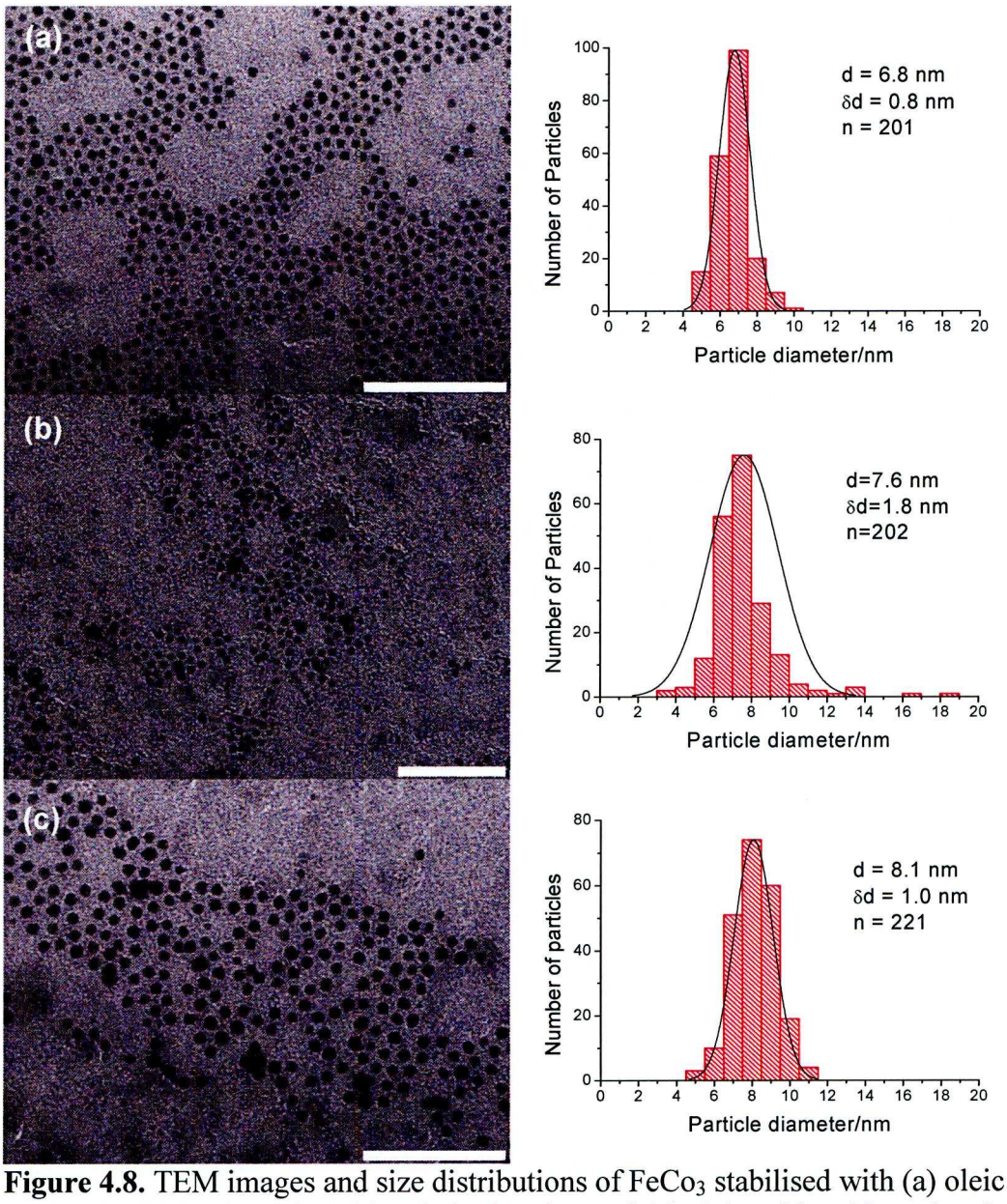

Figure 4.8. TEM images and size distributions of $FeCo_3$ stabilised with (a) oleic acid and TOPO, (b) oleic acid and oleyl amine and (c) oleic acid and hexadecyl amine. Bar 100 nm.

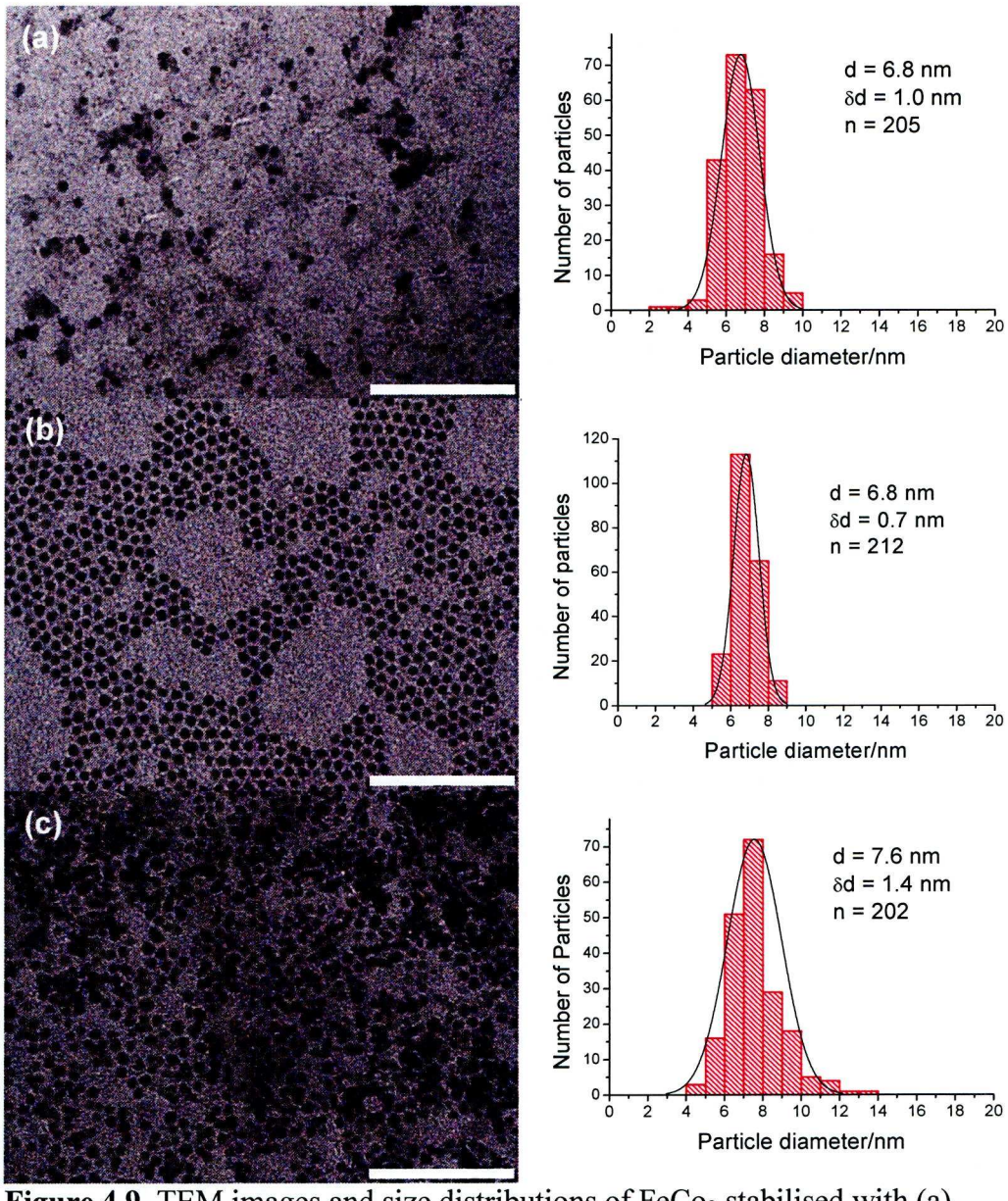

Figure 4.9. TEM images and size distributions of $FeCo_3$ stabilised with (a) myristic acid and TOPO, (b) myristic acid and oleyl amine and (c) myristic acid and hexadecyl amine. Bar 100 nm.

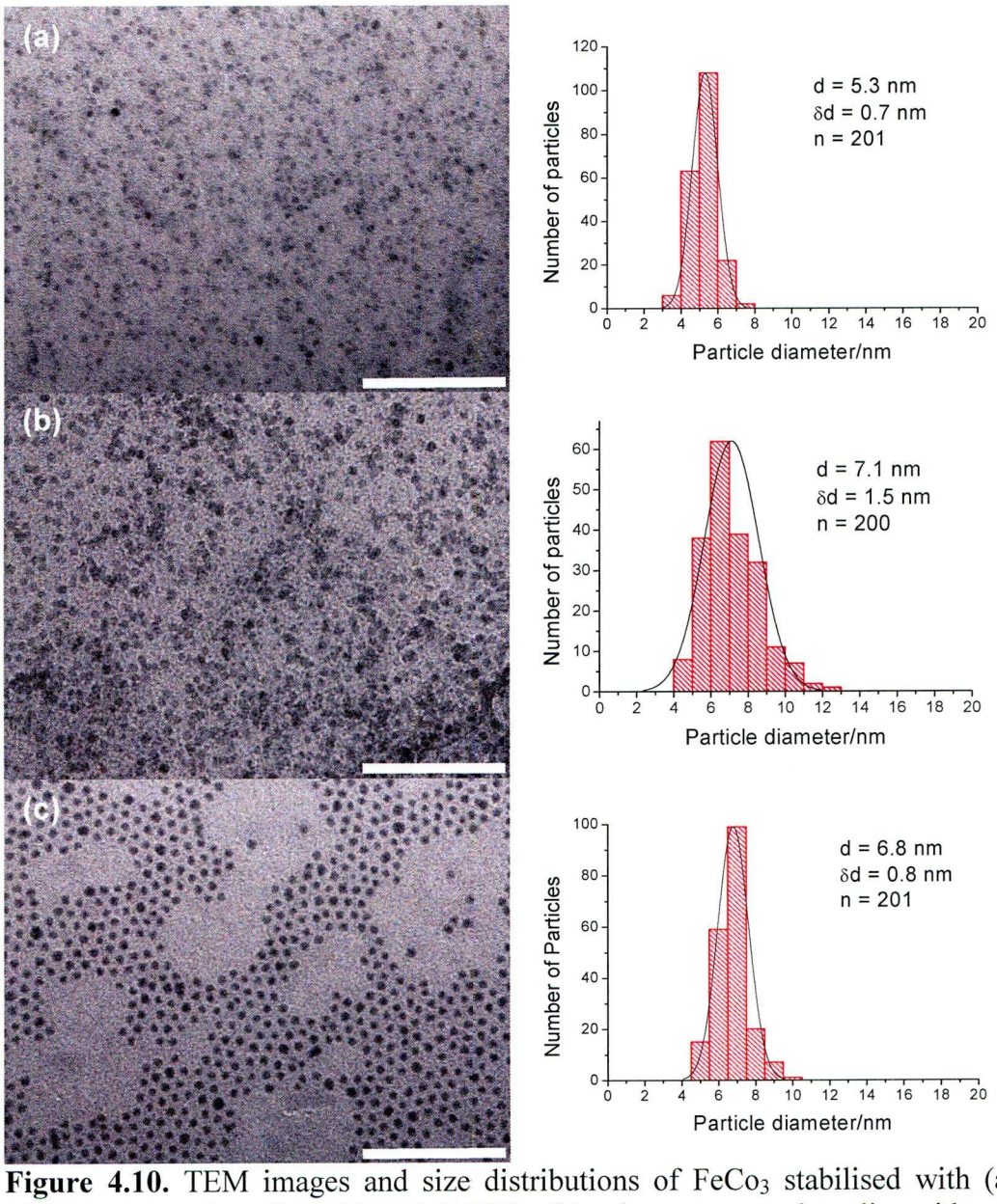

Figure 4.10. TEM images and size distributions of $FeCo_3$ stabilised with (a) adamantane carboxylic acid and TOPO, (b) adamantane carboxylic acid and oleyl amine and (c) adamantane carboxylic acid and hexadecyl amine. Bar 100 nm.

4.4 Conclusion

A series of alloy NPs was synthesized by the thermal decomposition of the respective bimetallic carbonyl cluster. The physical and chemical properties of the alloy NPs were determined by the metal atom content of the cluster. Changing the synthesis conditions, such as ligand concentration and ligand type had no significant effect upon the size of the NPs. This may be a result of the

stability of the metal-metal bond already present in the nucleus of the cluster that promote the development of new metal-metal bonds between the two elements in the forming NPs. The alloy NPs obtained have a narrow size distribution and, in most cases, they retain the composition of the molecular precursors. This work demonstrates that anionic bimetallic carbonyl clusters are perfect precursors for the preparation of alloy NPs with controlled composition and containing different types of metals (i.e. Fe-Co, Fe-Ni, Fe-Pt). This may be a general procedure and the scope of this work can be extended to several other elements (e.g. Fe-Rh, Fe-Pd, Fe-Ag, Fe-Au, Fe-Cd, Ni-Co, Ni-Rh, Ni-Pd, Ni-Pt, Ni-Cd, Ni-Au, Co-Pt; in different ratios), due to the fact that the chemistry of anionic bimetallic carbonyl clusters is well established and rather rich[267-269].

Chapter 5

(Bio)Functionalisation of magnetic nanoparticles

5.1 Aims and objectives

To be useful in biomedical applications magnetic NPs need to be dispersed in aqueous solution. Fine control over the physical properties of the NPs can easily be achieved when they are synthesised in organic solvent, however this usually produces NPs with a hydrophobic coating which needs to be modified to make it more hydrophilic. In this chapter, the transfer of magnetic NPs to aqueous solution by functionalising the nanoparticle surface will be studied. The surface of the hydrophobic NPs will be modified to make them more hydrophilic, firstly by exchanging the capping ligand used in the nanoparticle synthesis (OA) with a thermo-responsive polymer or a phosphine oxide functionalised polyethylene glycol. In a second method, Pluronic F127 is added to the hydrophobic ligand layer to try and give the NPs an overall hydrophilic coating the addition of a stabilising molecule or the addition of a gold layer. The third method involves the reduction of a gold salt at the surface of pre-synthesised magnetic NPs to add a layer of gold and form a core-shell structure. The gold coated NPs can be further functionalised by the addition of thiolated biomolecules. Once the NPs are dispersed in aqueous solution it is vital that they are stable in physiological conditions, Therefore, the stability of the NPs in aqueous solution to external stimuli such as changes in pH, temperature or increases in electrolyte concentration will also be studied.

5.2. Introduction

The previous two chapters discussed novel synthesis methods to produce magnetic NPs, however, the syntheses were carried out in organic solvent in the

presence of hydrophobic ligands such as OA, TOPO OLA etc, which produced NPs that are not water-soluble. To be useful in biomedical applications, the NPs need to be transferred to an aqueous phase. One method to overcome this is post-synthesis modification of the surface of the NPs to produce a core-shell system. The versatility of core-shell NPs compared to those fabricated from a single species also makes them particularly useful. Core-shell magnetic NPs usually consist of a magnetic core (e.g. cobalt, iron oxide) and a shell that can not only provide a hydrophilic layer to the NPs, but also a platform for functionalisation of the NPs. The surface modification can be achieved by adding an additional metal such as gold[25], or replacing the hydrophobic ligand with macromolecules such as peptides[23, 142] and hydrophilic polymers[122, 170, 270, 271], or other substances such as DMSA (2,3-dimercaptosuccinic acid)[272], betaine hydrochloride[273] and silanes[274]. Alternatively, an amphiphilic polymer can be added to the hydrophobic layer without replacing it, but has the overall effect of creating a hydrophilic shell on the NPs[275].

A series of polymers was used in the surface modification process of Co and iron oxide NPs. For the ligand-exchange type modification, thermo-responsive polymers (see Section **2.2**, page 43, for the properties of these polymers) and phosphine oxide-poly(ethylene glycol) (PO-PEG) were used. The phosphine oxide moiety of this polymer is known to bind very strongly to iron oxide. For the ligand-addition type modification Pluronic F127 was used. Pluronic F127 is a co-polymer made from two A-chains of polyethylene oxide (PEO) and one B-chain of polypropylene (PPO) in an ABA configuration. The coating procedure is driven by the hydrophobic-hydrophobic interactions between the PPO chain and the oleic acid on the as synthesised NPs (Figure 5.1).

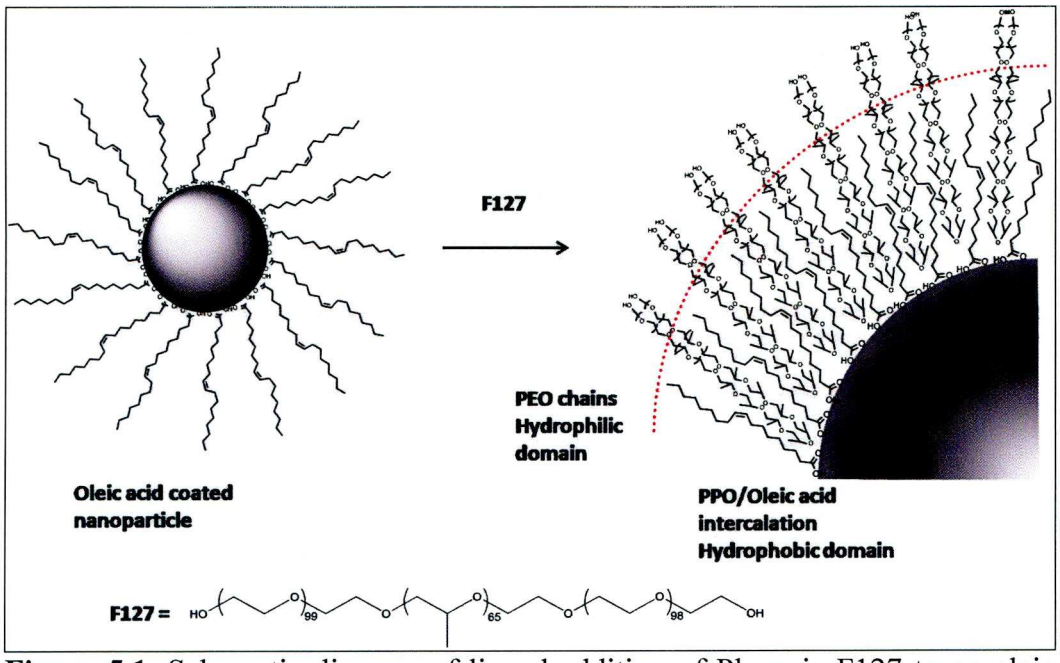

Figure 5.1. Schematic diagram of ligand addition of Pluronic F127 to an oleic acid coated magnetic nanoparticle (adapted from Qin et al[275]).

The modified NPs can then be further functionalised by the conjugation of functional groups, such as biotin, to the polymers. Alternatively, the surface of Co and iron oxide NPs had been coated with a layer of gold. This is achieved by reducing a gold salt on the surface of the NPs to form an additional metal layer. The gold surface can be functionalised using well known thiol chemistry[25].

5.3 Results and discussion

5.3.1 Thermo-responsive polymer stabilised Co and iron oxide nanoparticles

A series of thermo-responsive polymers were used to enhance the hydrophilicity of hydrophobic magnetic NPs (synthesised as per Section **6.6**) by a process of ligand exchange. The technique is described in further detail in Section **6.7**. Of these polymers, it was found that polymer P3 (LCST = 36 °C, Mw = 4500) was most suitable to stabilise Co NPs in aqueous solution, and

polymer P4 (LSCT = 42 °C, Mw = 6000) was most suitable for use with iron oxide NPs in aqueous solution. Polymer P3 was designed to have an increased number of carboxylic acid groups present, which would enhance the binding to the nanoparticle surface. The proposed structure of these polymers is shown in Figure 5.2, while their synthesis and physical properties are described in Section **6.2**.

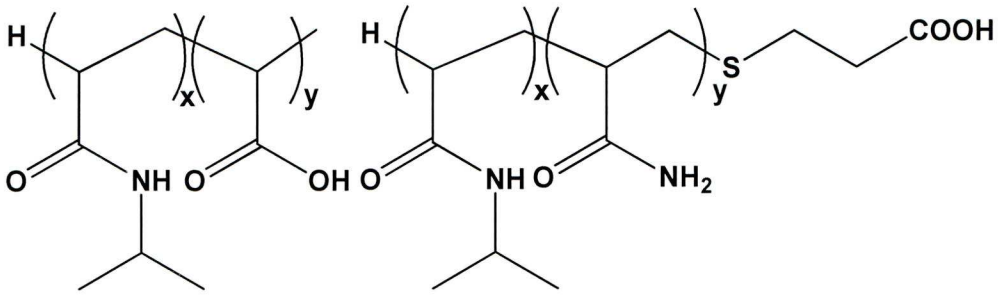

(P3) (P4)

Figure 5.2. Proposed structure of poly(isopropylacrylamide-co-acrylic acid) (polymer P3) and poly(isopropylacrylamide-co-amide) (polymer P4).

5.3.1.1 Size of the Co and iron oxide nanoparticles ligand exchanged with thermo-responsive polymers

The TEM images of the Co and iron oxide NPs before and after ligand-exchange with thermo-responsive polymers are presented in Figure 5.3. For Co, prior to ligand-exchange, discrete NPs were dispersed in organic solution. However, after ligand-exchange using polymer P3, the NPs formed larger 'spherical aggregates' in aqueous solution having relatively large diameter of about 100 nm (Figure 5.3b). When only polymer P3 is heated in a solvent solution, the formation of similar sized polymer spheres was observed. The discrete Co NPs were observed within the aggregates, indicating that the NPs became embedded in the polymer spheres as they formed. Similar results were

seen when this polymer was used with iron oxide. On the other hand, when polymer P4 was used to stabilise iron oxide NPs, discrete NPs can be seen in the TEM images both before and after ligand-exchange process (Figures. 5.3c and 5.3d, respectively), thus indicating that the ligand-exchange process did not result in an aggregation of these NPs.

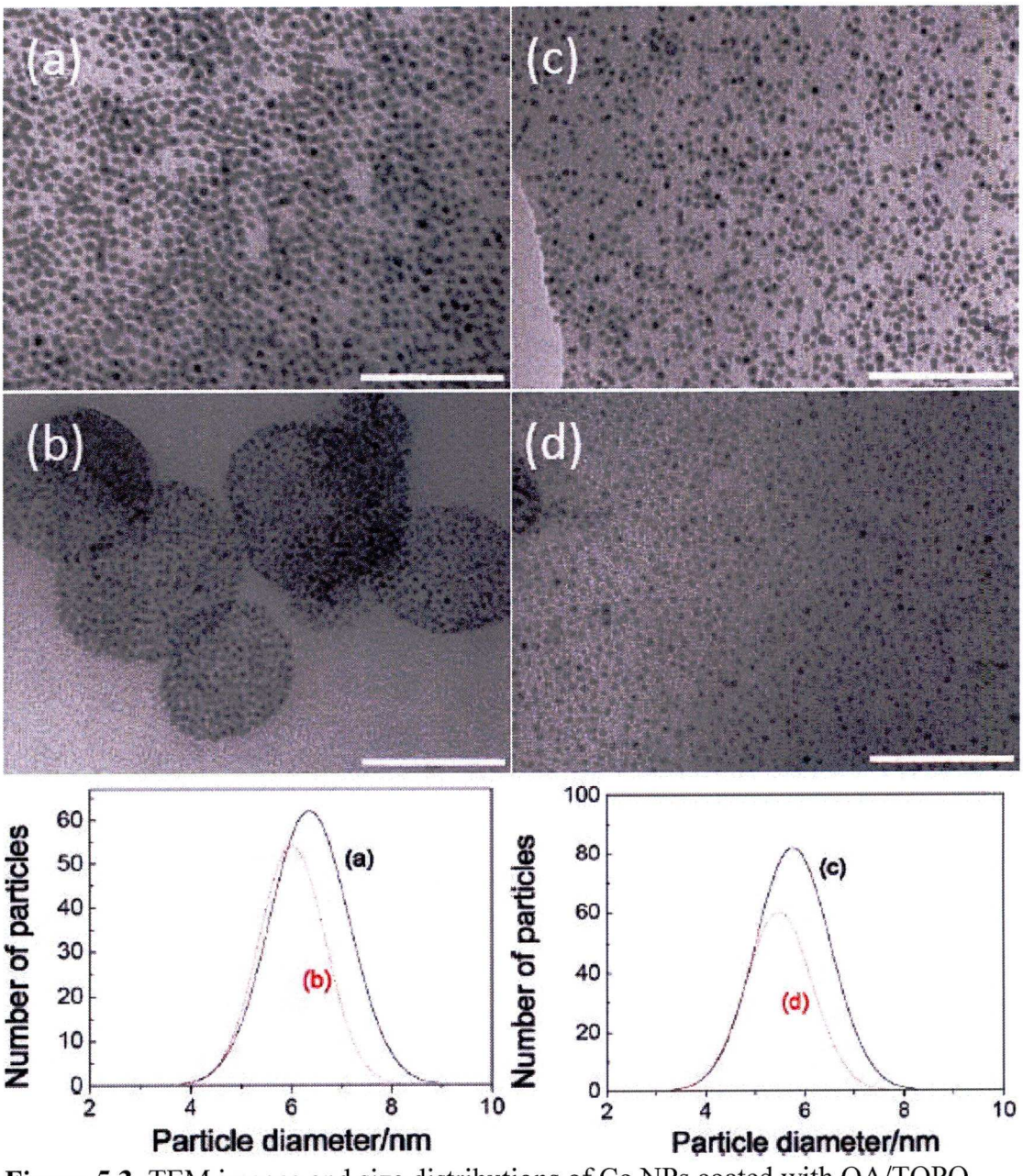

Figure 5.3. TEM images and size distributions of Co NPs coated with OA/TOPO (a), Co NPs coated with P3 polymer after the ligand-exchange (b), iron oxide NPs coated with OA (c) and iron oxide NPs coated with P4 polymer after the ligand-exchange (d). Bar 100 nm.

5.3.1.2 Magnetic properties of thermo-responsive polymer stabilised magnetic nanoparticles

The results of the ZFC and FC magnetization of the thermo-responsive polymer coated Co and iron oxide NPs are presented in Figure 5.4. For Co NPs in the 'spherical aggregates', a broad peak in the ZFC curve and blocking temperature of about 190 K was observed. This blocking temperature is expected for relatively large NPs and is therefore consistent with the TEM image in Figure 5.3b. On the other hand, for iron oxide NPs, the blocking temperature is much smaller at about 12 K, supporting the suggestion that these NPs are discrete in aqueous solution. The coercivity measured at 5 K for Co and iron oxide NPs is about 1.3 and 0.1 kOe, respectively. The higher coercivity observed for the

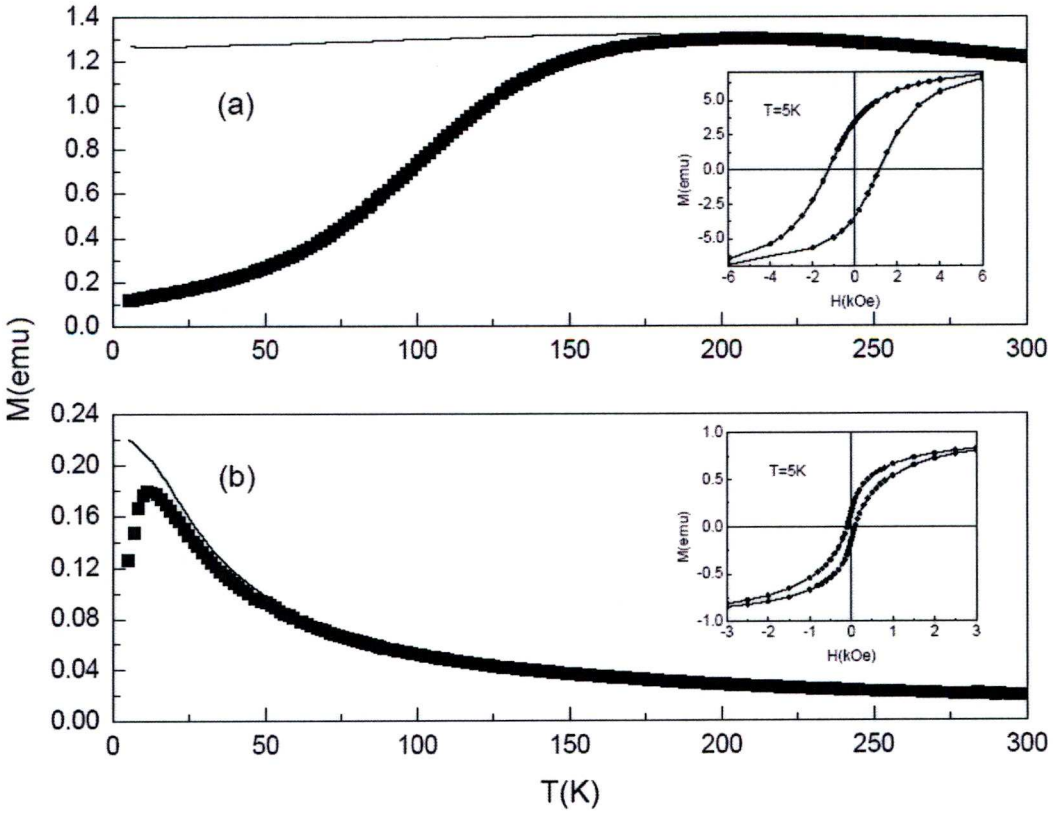

Figure 5.4. ZFC (symbols) and FC (lines) magnetization of the thermo-responsive Co (a) and iron oxide (b) NPs as a function of temperature. The insets shows hysteresis loops measured at 5 K.

polymer embedded Co NPs again suggests that they have the magnetic properties of much larger NPs since the coercivity is related to nanoparticle size[276].

5.3.1.3 Effect of temperature on the stability of the thermo-responsive polymer coated nanoparticles

The response of the polymers P3 and P4 to changes in temperature were maintained when they were bound to the Co and iron oxide NPs, respectively as depicted in Figure 5.5, where the NPs aggregated above the LCST of the parent coating polymers in solution. This phenomenon was previously observed when using thermo-responsive polymers in a one-step synthesis procedure and is discussed further in Section **2.7**. Briefly, as the temperature increased, the polymers changed conformation and the chains collapsed, creating a more hydrophobic surface that destabilized the dispersion and resulted in flocculation of the NPs. This process was reversible in that upon cooling to a temperature below LCST the NPs were redispersed into the solution as the polymer coils were re-established.

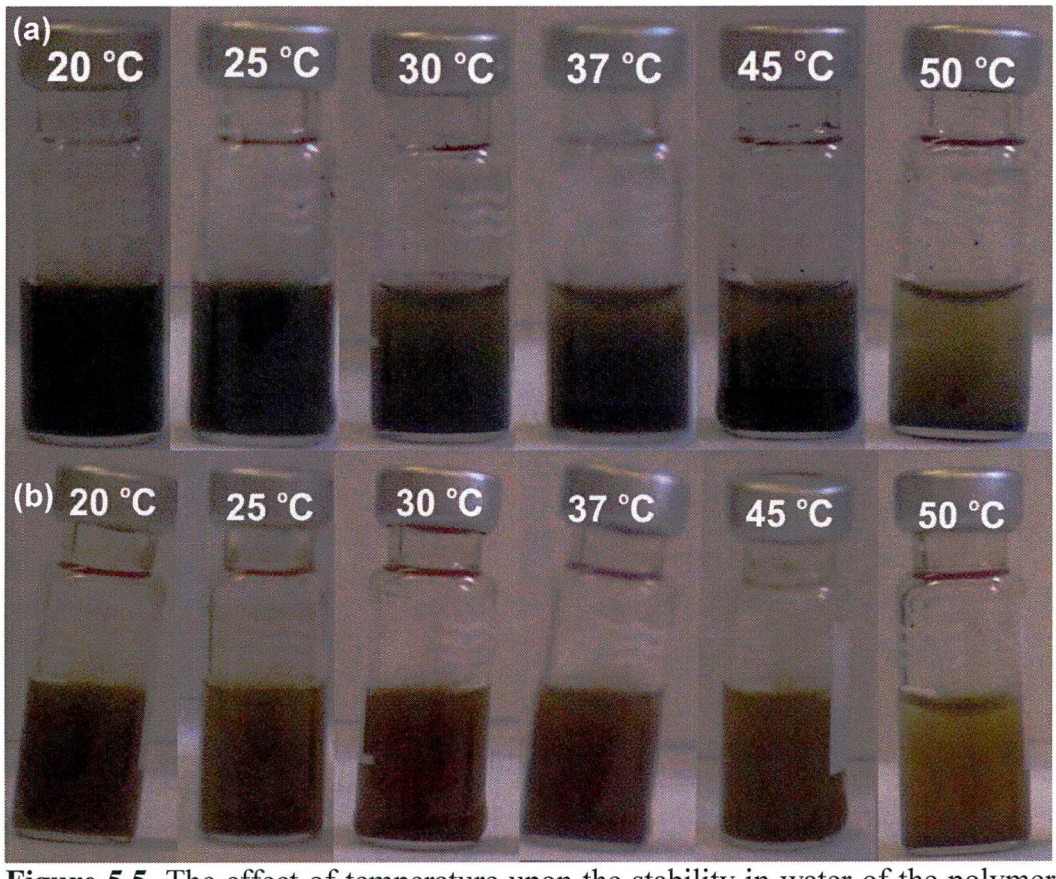

Figure 5.5. The effect of temperature upon the stability in water of the polymer coated Co (a) and iron oxide (b) NPs.

5.3.1.4 Stability of thermo-responsive polymer coated magnetic nanoparticles in aqueous solution

The stability of the NPs in different electrolyte conditions and pH was investigated (for further details see Section **6.11**). The spherical-like aggregates of Co NPs are not as stable in electrolyte solution as the discrete iron oxide NPs. The Co NPs were stable up to 0.2 M NaCl, while the iron oxide NPs were stable up to 0.5 M (Figure 5.6). This is probably due to the iron oxide NPs not forming aggregates similar to those observed for Co NPs.

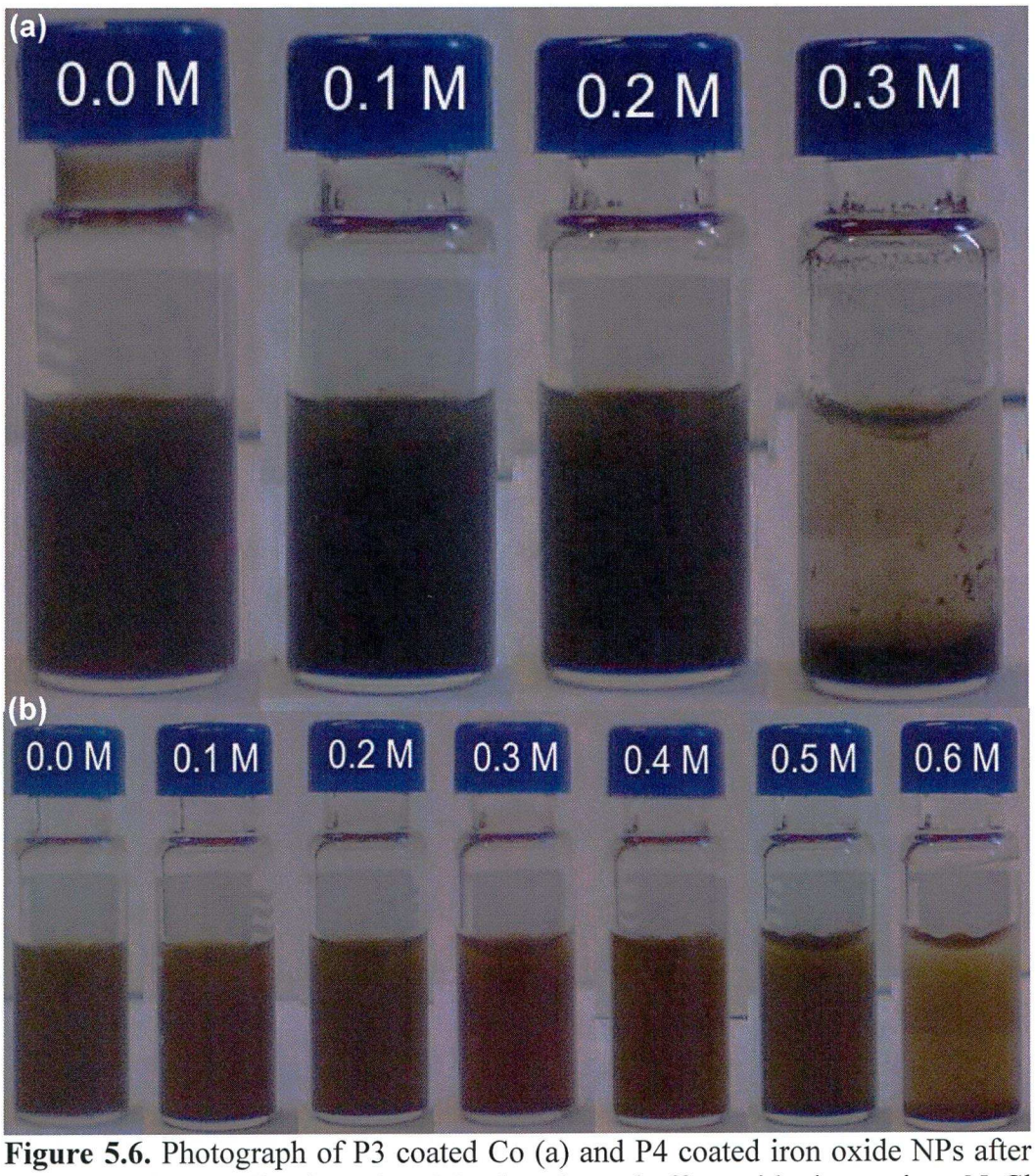

Figure 5.6. Photograph of P3 coated Co (a) and P4 coated iron oxide NPs after ligand exchange (b) in 10 mM phosphate buffer with increasing NaCl concentrations.

Both types of NPs had similar responses to changes in pH. Both the ligand-exchanged Co and iron oxide NPs were found to be stable from pH = 7 to pH = 12 (Figure 5.7). In basic conditions the carboxylic acid groups of the surface entrapped polymer chains can lose a proton, resulting in an overall negative charge that can help stabilize the NPs through increased electrostatic screening.

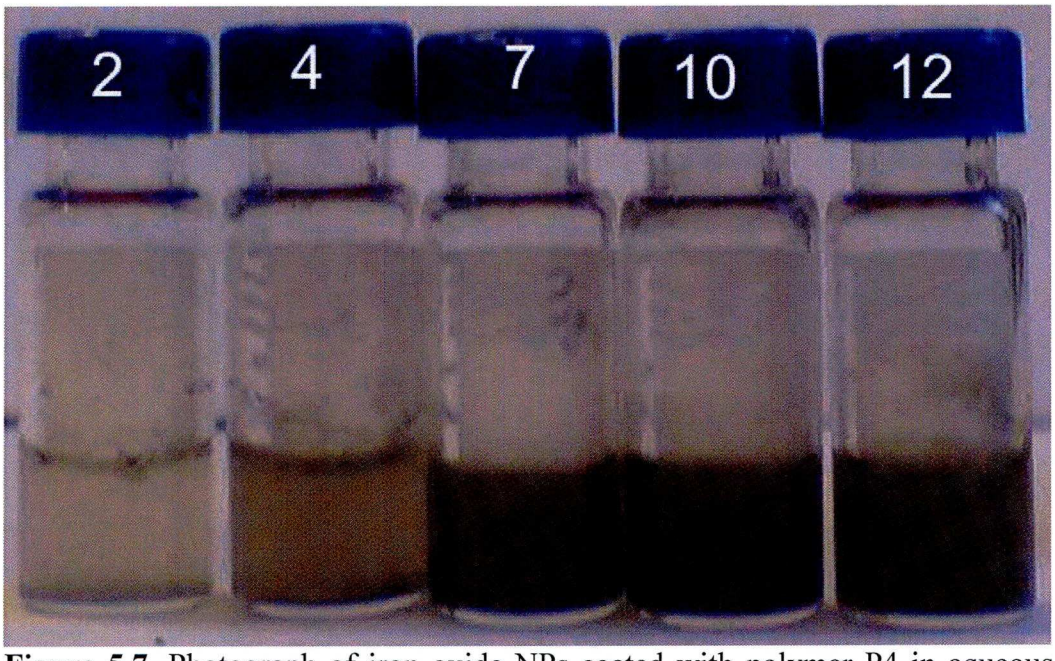

Figure 5.7. Photograph of iron oxide NPs coated with polymer P4 in aqueous solutions from pH = 2 to pH = 12.

5.3.2 PO-PEG stabilised magnetic nanoparticles

The thermo-responsive polymers P3 and P4 were found to facilitate the dispersion of Co and iron oxide NPs in aqueous solution. However, to achieve improved stability in electrolyte solution, a different polymer was used in a ligand exchange process (as described in Section **6.9**). This polymer was phosphine oxide-polyethylene glycol (PO-PEG) with a molecular weight of approximately 5000 g/mol. The phosphine oxide moiety is known to bind well to iron oxide[277] and was therefore used to functionalise PEG. The proposed structure is shown in Figure 5.8 and the details of the synthesis can be found in section **6.8**. Matrix assisted laser desorption ionization time-of-flight (MALDI-TOF) mass spectrometric and ^{31}P NMR analysis revealed the formation of the PO-PEG.

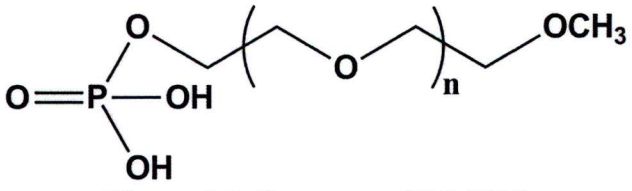

Figure 5.8. Structure of PO-PEG

5.3.2.2 Size of the PO-PEG coated magnetic nanoparticles

The TEM images in Figure 5.9 show iron oxide NPs before and after the oleic acid ligand was exchanged for PO-PEG. No aggregation of the PO-PEG stabilised iron oxide NPs was observed (Figure 5.9b) suggesting these NPs were discrete in aqueous solution prior to drying on the TEM grid. When PO-PEG was used to stabilise Co NPs in aqueous solution, the NPs agglomerated and precipitated out of solution. This may be because the phosphine-oxide group does not bind strongly to the Co NP surface.

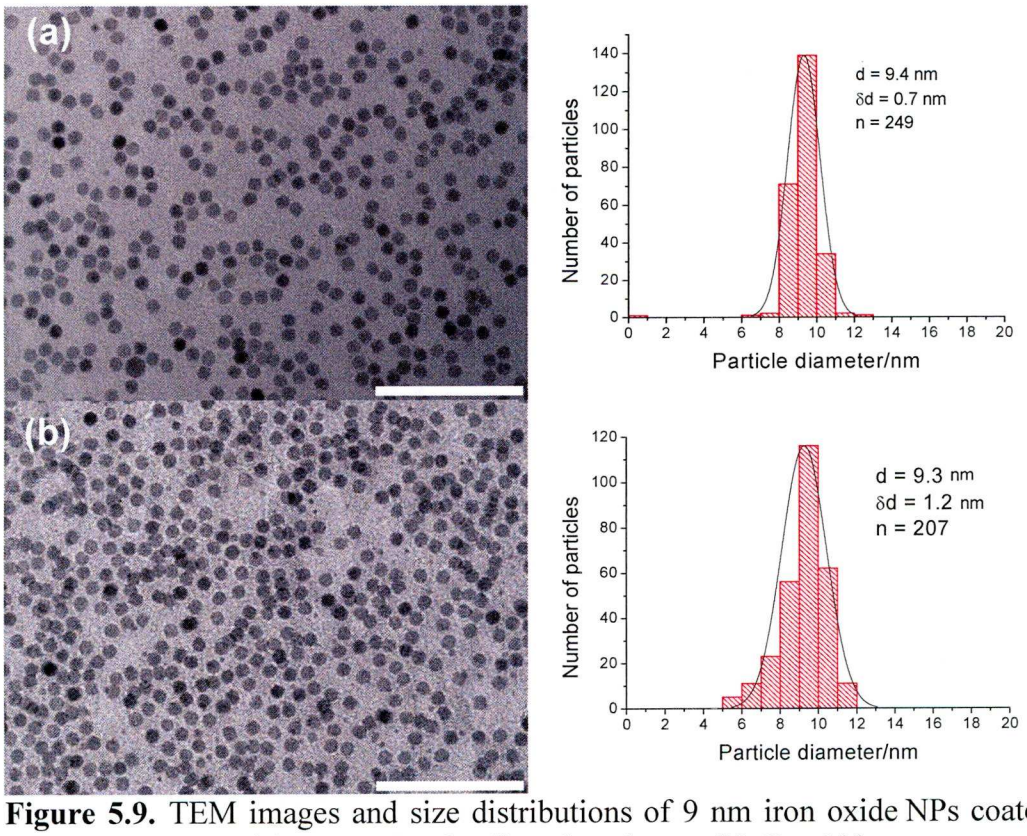

Figure 5.9. TEM images and size distributions of 9 nm iron oxide NPs coated with OA (a), and with PO-PEG, after ligand-exchange (b). Bar 100 nm.

5.3.2.3 Stability of the PO-PEG coated magnetic nanoparticles

The stability of PO-PEG coated magnetic NPs in aqueous solution was studied and they were found to be stable from pH = 4 to pH = 10 for four months (Figure 5.10). These NPs were also stable in 1 M NaCl for up to 7 days. This would suggest that the PEG portion of the polymer has a very strong stabilising effect upon the iron oxide NPs that is not affected by changes in ionic strength of the solution in which they are dispersed.

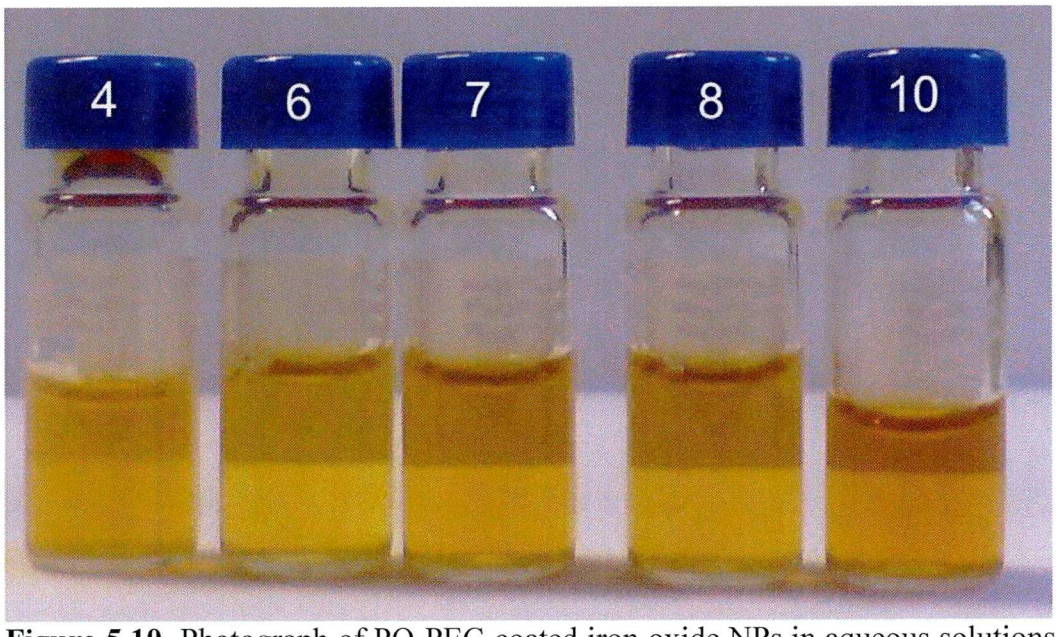

Figure 5.10. Photograph of PO-PEG coated iron oxide NPs in aqueous solutions from pH = 4 to pH = 10.

5.3.3 F127 stabilised magnetic nanoparticles

The use of PO-PEG was found to provide better stability of iron oxide NPs in electrolyte solutions than the poly(isopropylacrylamide) based polymers P3 and P4. However, PO-PEG was not very suitable for use with Co NPs, with little or no ligand exchange taking place, therefore rather than using a ligand exchange process, the polymer Pluronic F127 (Figure 5.11) was used in a ligand

addition type reaction, as described in Section **6.10**. The amphiphilic nature of this polymer can be exploited, where the hydrophobic PPO chain can interact with the hydrophobic oleic acid on the nanoparticle surface and the hydrophilic PEO chains extending outward to give an overall hydrophilic coating to the NPs.

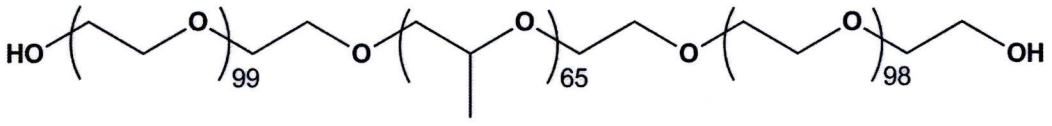

Figure 5.11. Structure of Pluronic F127

5.3.3.1 Size of the Pluronic F127 coated magnetic nanoparticles

Figure 5.12 shows TEM images of iron oxide NPs before and after the addition of Pluronic F127 to the oleic acid layer. The iron oxide NPs remained discrete particles in aqueous solution after the addition of Pluronic F127 (Figure 5.12b). The addition of Pluronic F127 to Co NPs did not produce hydrophilic NPs. This may be due to the presence of TOPO as a co-ligand with oleic acid in the surface of these NPs. TOPO, which is not present on iron oxide NPs, may prevent the hydrophobic-hydrophobic interactions between the oleic acid and the PPO chain of Pluronic F127, resulting in little or no coating of the NPs.

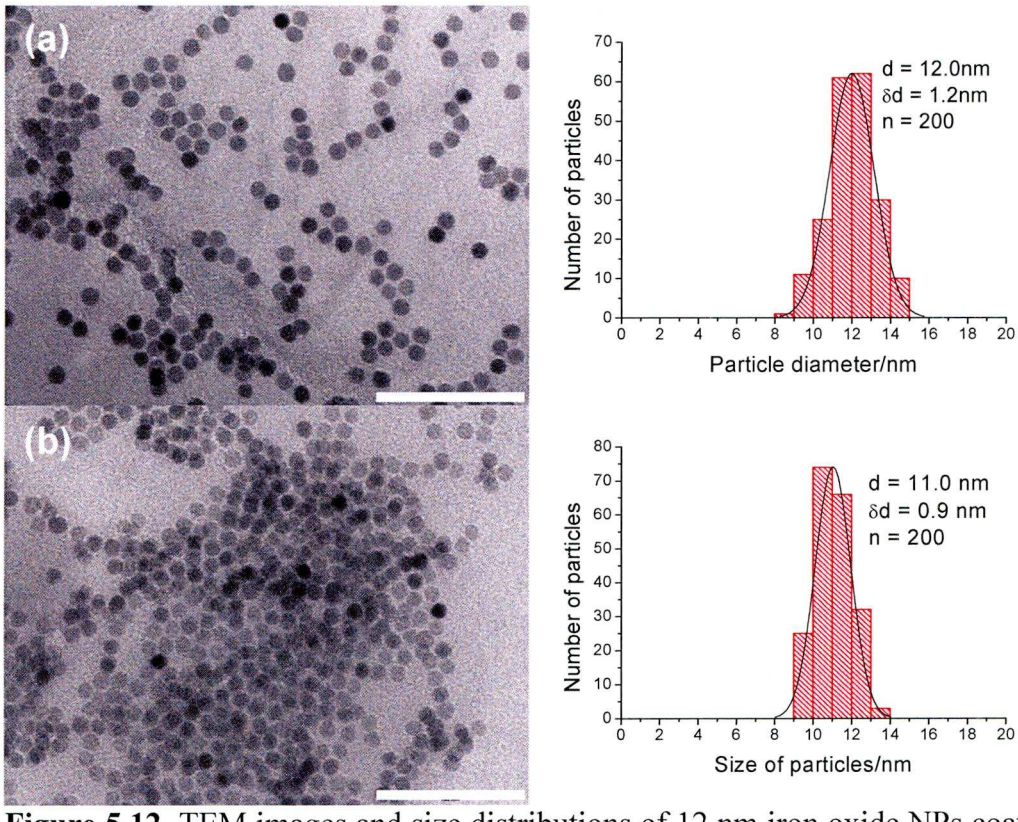

Figure 5.12. TEM images and size distributions of 12 nm iron oxide NPs coated with OA (a), and after the addition of F127 (b). Bar 100 nm.

5.3.3.2 Stability of F127 coated magnetic nanoparticles

F127 provided a hydrophilic coating to iron oxide NPs that facilitated their phase transfer into aqueous solution. Once in the aqueous solution these NPs were stable from pH = 4 to pH = 10 for four months (Figure 5.13) and in 1 M NaCl for three weeks. This would suggest this polymer also has a strong stabilising effect upon the NPs regardless of the ionic strength of the solution.

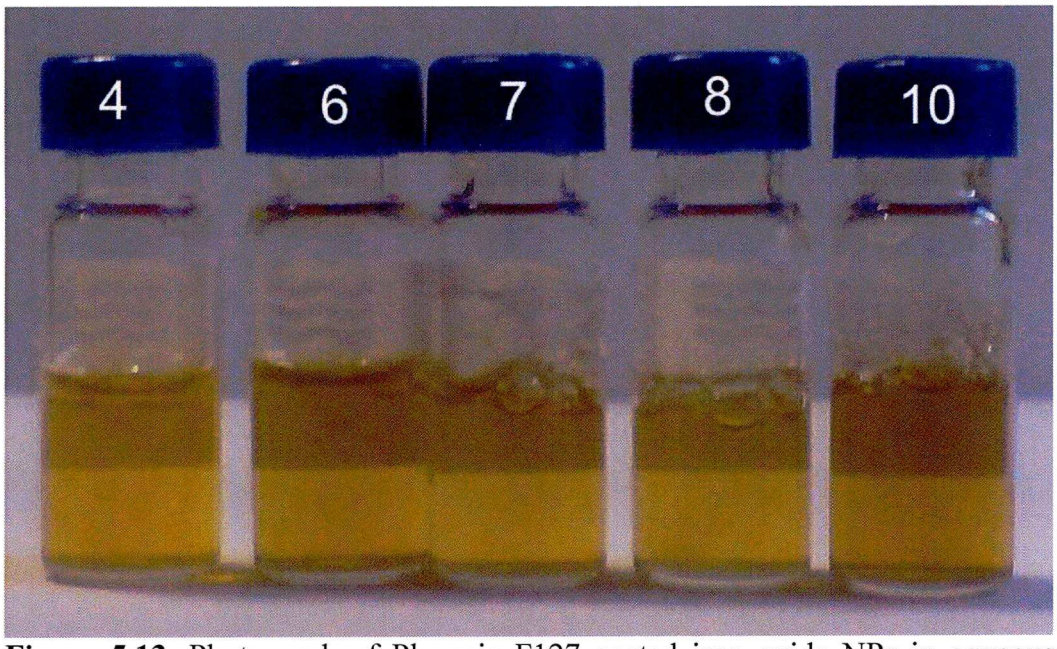

Figure 5.13. Photograph of Pluronic F127 coated iron oxide NPs in aqueous solutions from pH = 4 to pH = 10.

5.3.4 Bimetallic magnetic nanoparticles

Cobalt and iron oxide NPs were synthesised in organic solvent using standard methods and coated with NaAOT and oleic acid, respectively. The reduction of a gold salt was then used to coat the synthesised NPs with a layer of gold (Figure 5.14). More details of the synthesis methods can be found in Sections **6.12** and **6.13**. The addition of a Au layer can protect the magnetic nanoparticle from oxidation and provide a stage for functionalisation of the NPs.

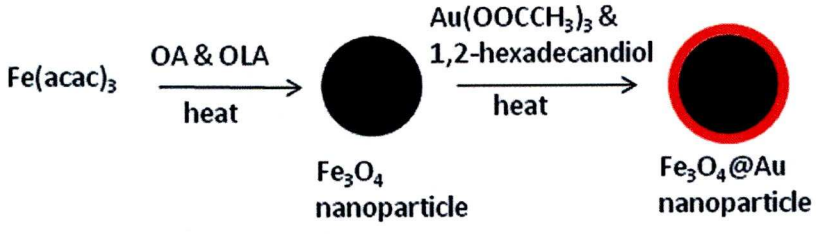

Figure 5.14. Schematic diagram of the formation of Fe_3O_4@Au NPs

5.3.4.1 Size of the bimetallic magnetic nanoparticles

It can be seen from the TEM images in Figure 5.15 that both the NaAOT coated Co and Co-Au bimetallic NPs have a narrow size distribution (standard deviation of 0.8 nm for both types of NPs). Both the Co and the Co-Au NPs have similar average diameters as would be expected for an atom exchange process, where for each Au atom reduced a Co atom is oxidised, resulting in no overall change in nanoparticle diameter[25]. This suggests that the bimetallic NPs have formed by a redox transmetallation process and not by another means such as galvanisation. In the redox transmetallation process, the Au^{3+} ions are reduced on the surface of the Co NPs with the simultaneous oxidation of neutral Co^{0} atoms to Co^{2+} ions.

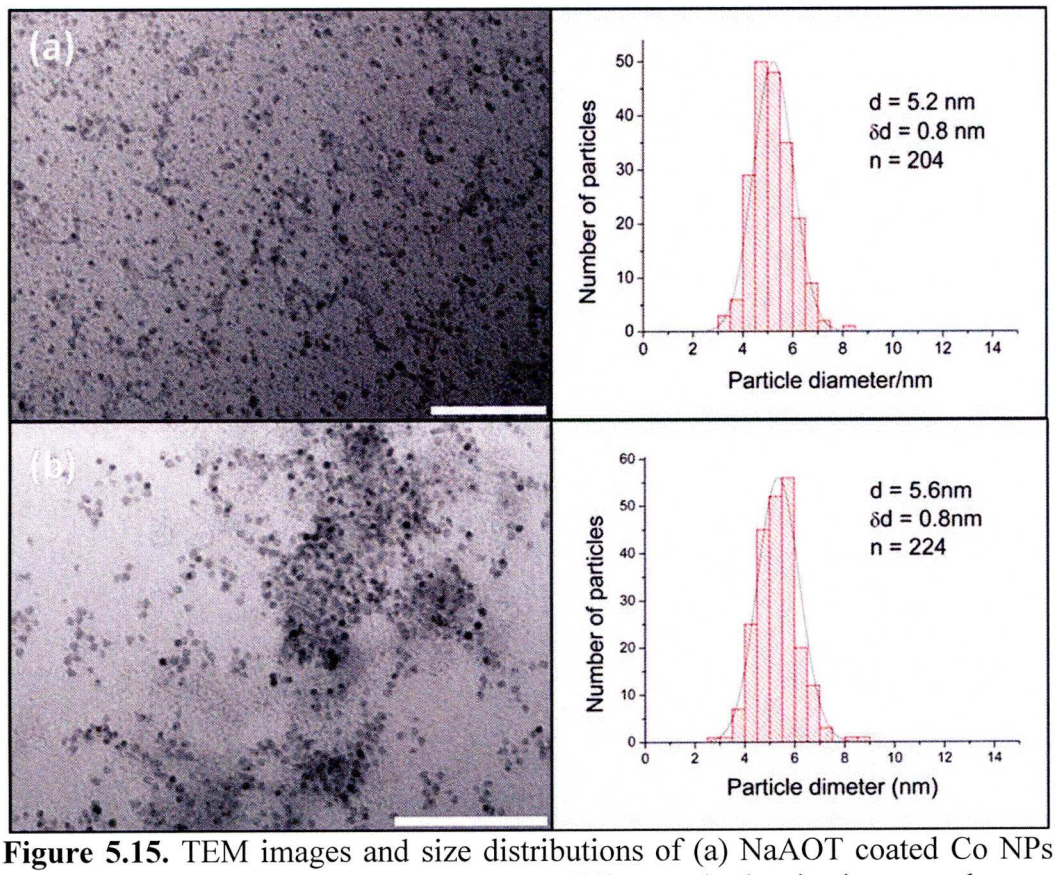

Figure 5.15. TEM images and size distributions of (a) NaAOT coated Co NPs and (b) Co-Au NPs. There is no significant difference in the size between the two types of NPs. Bar 100 nm

In contrast, the average nanoparticles diameter of the Fe_3O_4-Au NPs increased to 9.2 ± 1.3 nm from 6.7 ± 0.7 nm for the Fe_3O_4 seeds (Figure 5.16a and b). This would indicate that the Au layer with an average thickness of ~1.2 nm was added to the surface of the Fe_3O_4 NPs, resulting in an increase in diameter. Figure 5.15c shows a TEM image of the Fe_3O_4-Au NPs taken from an aqueous solution of thiolated DNA. It can be seen that there is no aggregation of however, they do the NPs (the average nanoparticles diameter remains at ~9 nm),

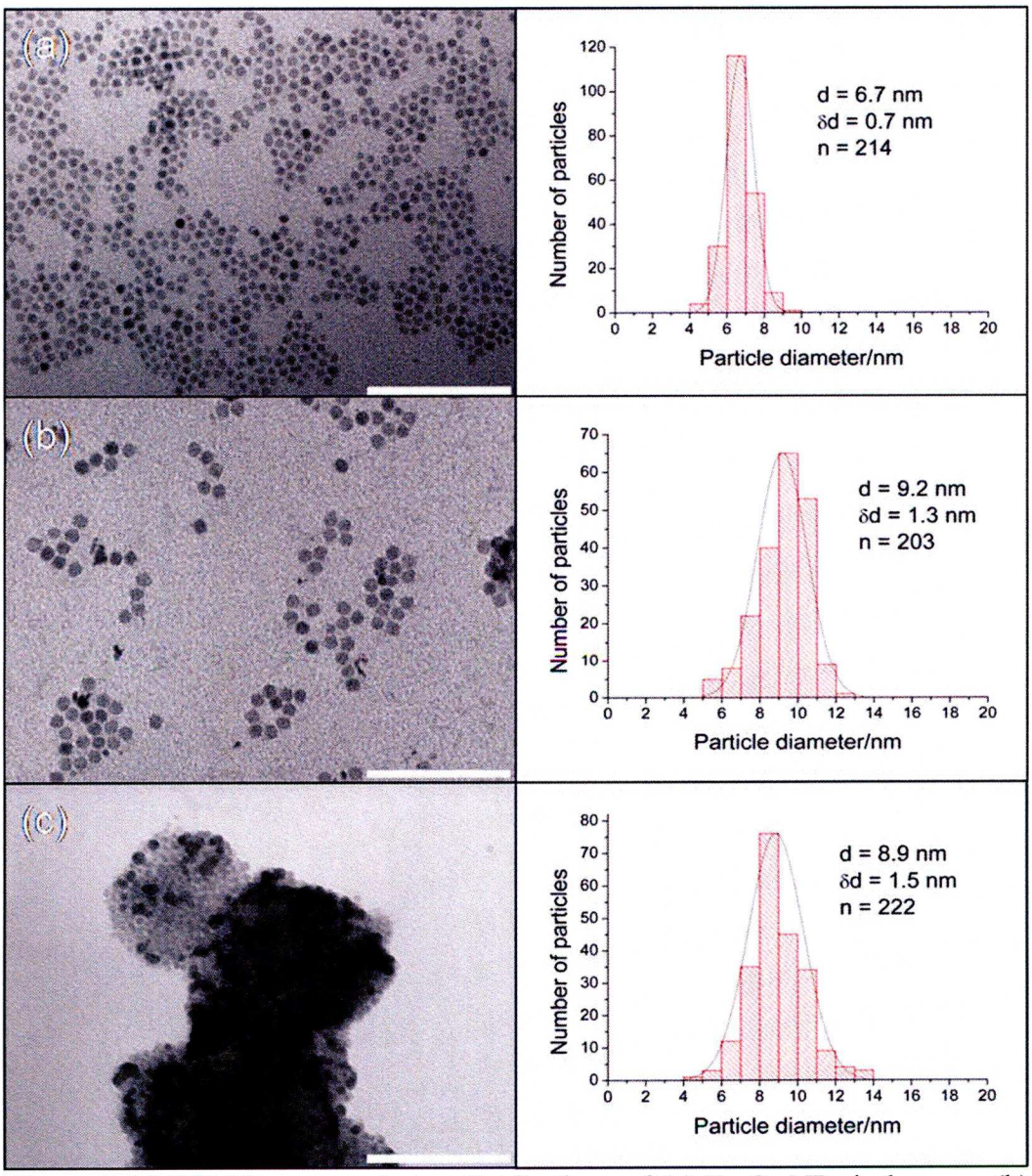

Figure 5.16 TEM images and size distributions of (a) Fe_3O_4 NPs in hexane, (b) Fe_3O_4-Au NPs in water and (c) Fe_3O_4-Au NPs in water with thiolated DNA. The Fe_3O_4-Au NPs are approximately 2.5 nm larger than the Fe_3O_4 NPs. Bar 100 nm

however, they do appear to be embedded in a matrix. This is probably a result of the DNA drying on the TEM grid.

5.4.3.2 X-Ray diffraction of the bimetallic NPs

Figure 5.17 shows the XRD pattern of Co-Au NPs and shows diffraction peaks at $2\theta = 38.2^{\circ}$, 44.4°, 65.6° and 77.5°, which can be indexed to (111), (200), (220) and (311) planes of Au in the cubic phase. The absence of any diffraction peaks for Co is probably due to the heavy atom effect of the Au[278] as it combines with the Co NPs. This effect has been previously observed in similar NPs[24, 130, 131].

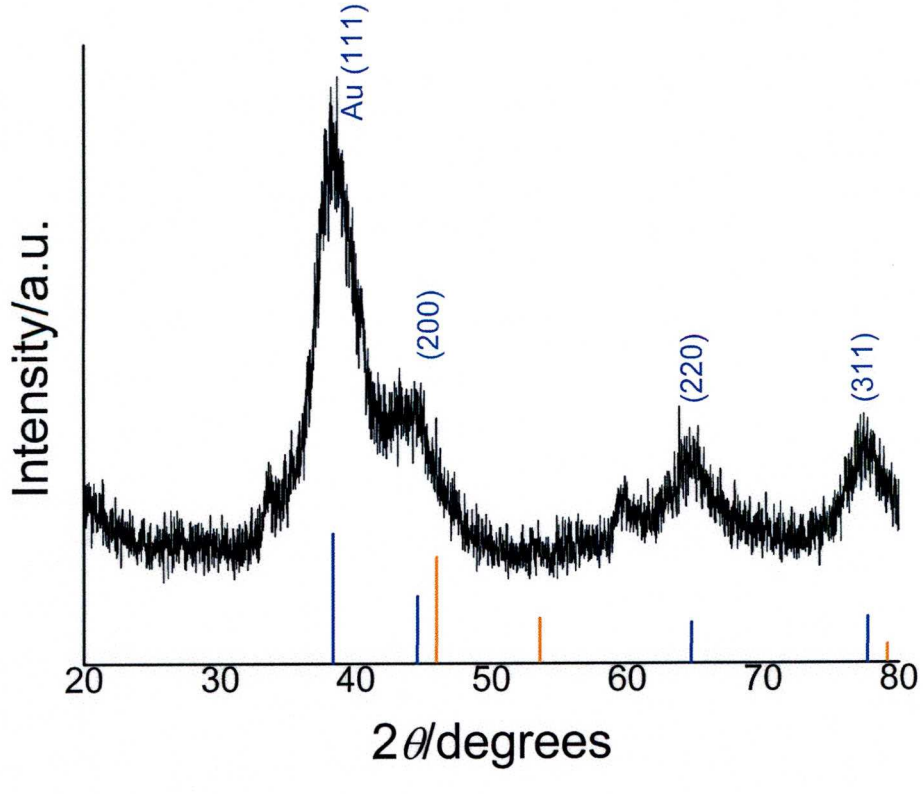

Figure 5.17. XRD pattern of Co-Au NPs. Reference peaks for Co and Au are shown in orange and blue, respectively.

The XRD patterns of Fe_3O_4 and Fe_3O_4@Au NPs are compared in Figure 5.18. The XRD pattern of Fe_3O_4@Au NPs (curve b) displays peaks for both Fe_3O_4 and Au, however the peaks for the magnetite are subdued when compared to the XRD pattern of Fe_3O_4 alone (curve a). This is most likely caused by the heavy atom effect from Au[278] as a result of the formation of Au-coating on the Fe_3O_4 NPs. This effect has been observed previously and[24, 130, 131] provide further evidence for complete coverage of the iron oxide core by an Au shell and supporting the TEM images in Figure 5.16.

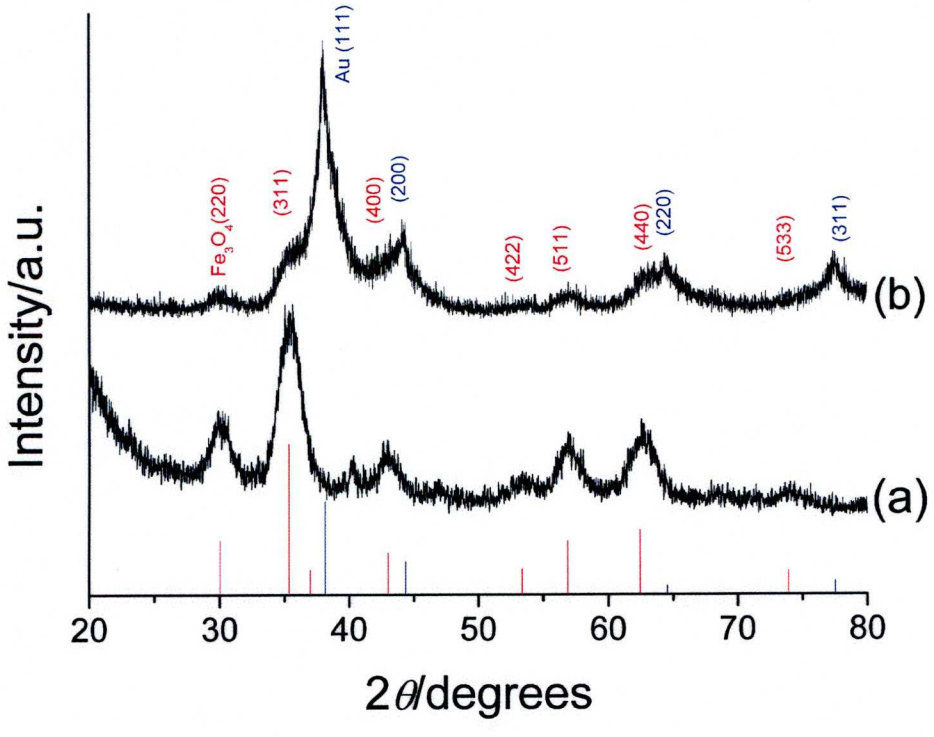

Figure 5.18. XRD patterns of (a) Fe_3O_4 and (b) Fe_3O_4@Au NPs. Reference peaks for Fe_3O_4 and Au are shown in red and blue respectively.

5.4.3.3. UV/Visible spectra of the bimetallic magnetic nanoparticles

The UV/visible absorption spectra for Co, Au and Co@Au bimetallic NPs are shown in curves a-c in Figure 5.19. The Co NPs show mostly silent feature in the visible region, while the Au NPs display surface plasmon resonance band at 520 nm. The surface plasmon resonance band of the Co@Au bimetallic NPs show a red-shift covering a range from 500 to 650 nm in spectrum, which is commonly observed in other Au bimetallic systems.[279, 280]

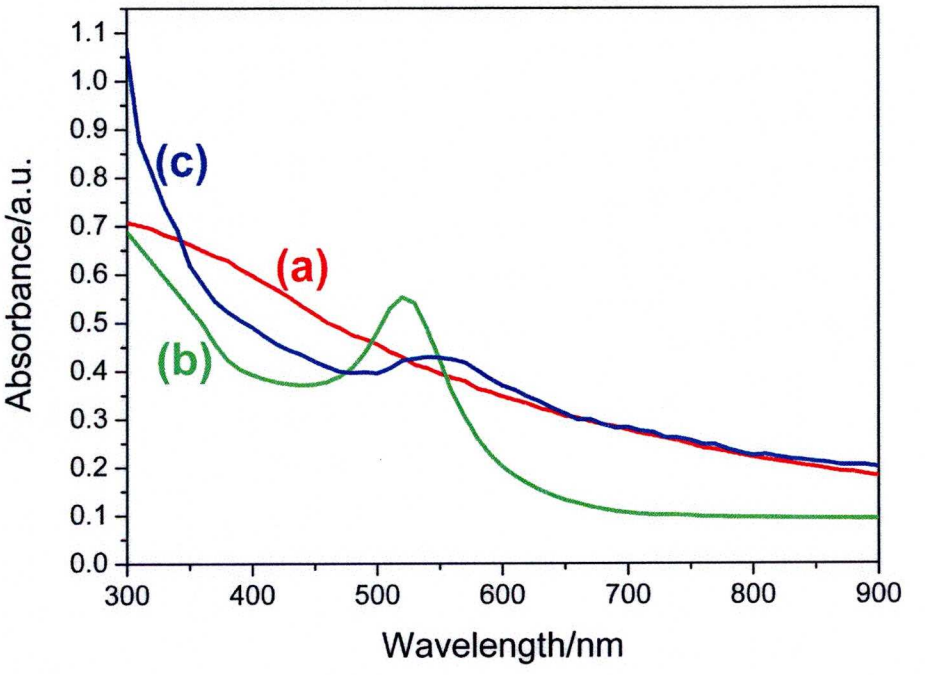

Figure 5.19. UV-visible spectra in toluene of (a) NaAOT coated Co NPs, (b) Au NPs and (c) Co@Au NPs. A sharp absorption peak can be observed for the Au NPs at 520 nm whereas for the Co@Au NPs, the absorption peak broadens, covering a range from 500 to 650 nm in spectrum of the indicating the presence of Au.

Similar shifts in the surface plasmon resonance band seen in Figure 5.19 were observed in the spectra of the Fe_3O_4-Au NPs (Figure 5.20, curves b and c), while the spectrum of Fe_3O_4 NPs was largely silent (Figure 5.20 curve a), indicating the presence of Au in the former sample. No increase in the shift was observed for the Fe_3O_4-Au NPs in the aqueous thiolated DNA solution, indicating that the NPs have not aggregated.

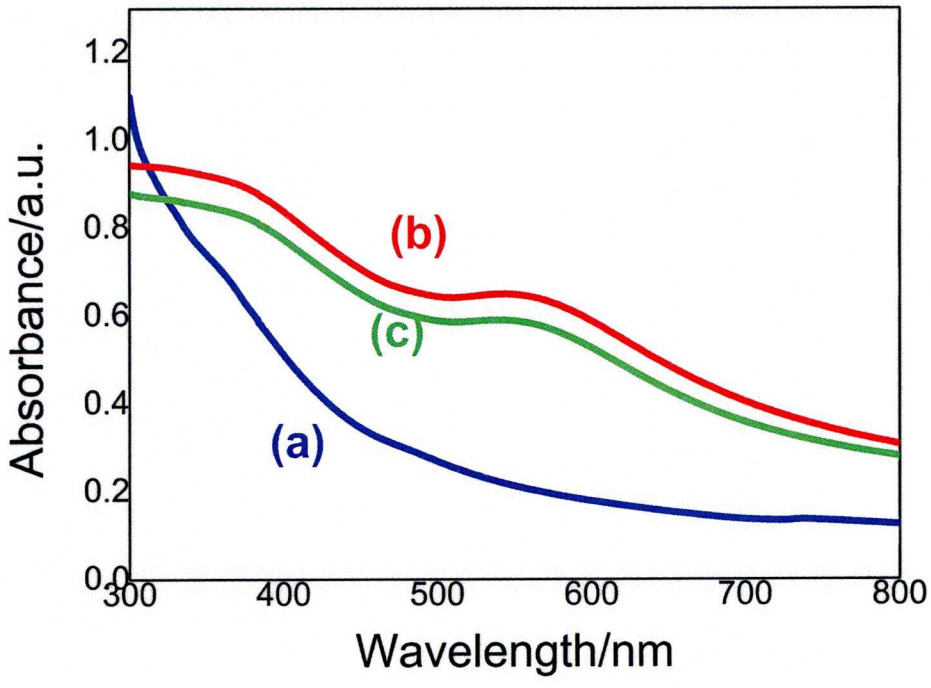

Figure 5.20. UV-visible spectra of (a) Fe_3O_4 NPs in hexane, (b) Fe_3O_4-Au NPs in water and (c) Fe_3O_4-Au NPs in water with thiolated DNA. The broad absorption peaks in the 500 to 650 nm range indicate the presence of Au in the samples.

5.4.3.4 Magnetic properties of the bimetallic magnetic nanoparticles

The ZFC and FC magnetisation curves, as a function of temperature, of the NaAOT coated Co and Co-Au bimetallic NPs are shown in Figure 5.21 and indicates a blocking temperature (T_b) of 40 K and 6 K, respectively. The fact there is a sharp peak in the ZFC curve and the ZFC-FC splitting is close to the peak position suggests a narrow size distribution for both the Co and Co-Au NPs, which is consistent with the TEM images in Figure 5.15. The maximum magnetic susceptibility can be observed in the ZFC curve and show 2.0 emu/g for NaAOT coated NPs and 0.8 emu/g for Co-Au NPs. The different magnetic properties observed between the Co and Co-Au NPs could be due to changes in the crystalline structure of the Co NPs as the gold atoms are added[280, 281]. It is also noted that Au metal itself does not contribute to the magnetism, but only adds mass to the NPs It can be seen from the hysteresis curve's measured at 2 K, in the insets of Figure 5.21 that the Co and Co-Au NPs show ferromagnetic behaviour at below T_b, with a coercivities of 650 Oe and 500 Oe, respectively. On the other hand above the T_b, the hysteresis curves above are closed indicating that the particles are superparamagnetic. For both NaAOT coated Co and Au-Co NPs, the magnetisation measured at 2 K does not become saturated at the maximum applied magnetic field of 50 kOe which could be due to either the canting moments of the surface atoms or the presence of very small particles which are paramagnetic even at very low temperature of 2 K. In addition, for the NaAOT coated Co NPs, the Co core itself is not very well protected and as a result the oxidation might occur to form a thin antiferromagnetic CoO layer on the surface. This antiferromagnetic CoO layer also contributes to the observed

unsaturated feature of the magnetisation of the NaAOT coated Co NPs at high magnetic field.

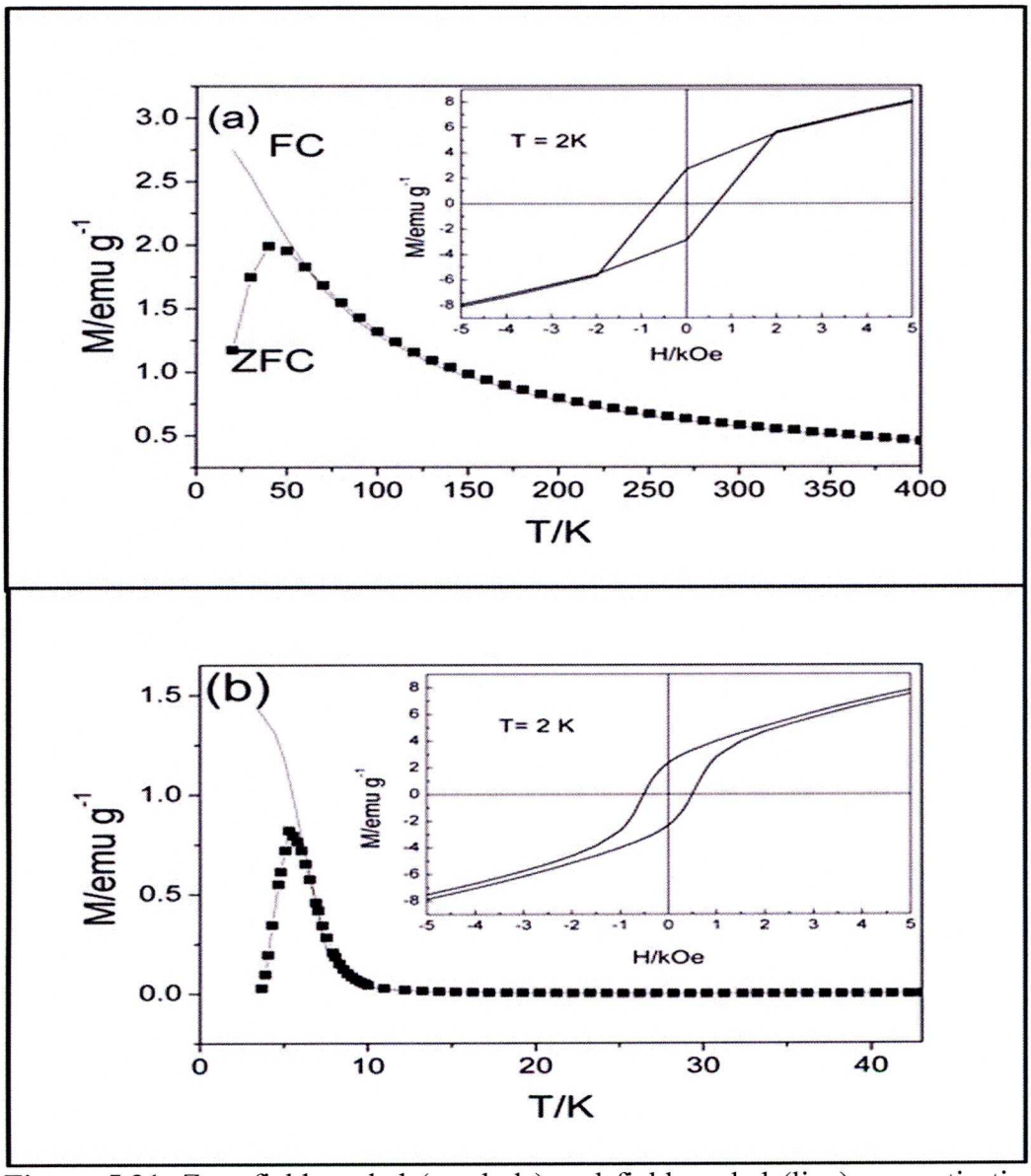

Figure 5.21. Zero-field cooled (symbols) and field cooled (line) magnetisation curves of NaAOT coated Co and Co@Au NPs as a function of temperature. The hysteresis curves measured at 2 K are shown in the insets.

Figure 5.22 shows the ZFC and FC magnetisation curves, as a function of temperature, of the Fe_3O_4 and Fe_3O_4-Au NPs. The ZFC curves have peaks at the blocking temperature, T_b, of 15 K and 29 K for the Fe_3O_4 and Fe_3O_4-Au NPs, respectively. Narrow size distributions are indicated by the sharp peak in the ZFC curve and the splitting of the ZFC and FC curves close to the peak position.

This is consistent with the TEM images in Figure 5.16. The maximum magnetic susceptibility observed from the ZFC curves decreases from 2.8 emu/g for the Fe_3O_4 NPs to 2.1 emu/g for the Fe_3O_4-Au NPs and 1.7 emu/g for the Fe_3O_4-Au NPs in thiolated DNA solution. The initial change in the magnetic susceptibility is probably due to the addition of the diamagnetic Au layer to the Fe_3O_4 NPs and the lower value for the Fe_3O_4-Au NPs in the DNA solution could indicate that DNA is binding to the nanoparticles surface and therefore increasing the mass without contributing to magnetism. Both the Fe_3O_4 and Fe_3O_4-Au NPs display ferromagnetic behaviour below T_b and have coercivities of 90 Oe and 260 Oe, respectively. The increases in T_b and coercivity observed for the Fe_3O_4-Au NPs could arise from the increase in their average diameter, which leads to less effective coupling of the magnetic dipole moments of the core[276]. The Fe_3O_4 NPs have more efficient coupling of the magnetic cores and therefore have a lower coercivity. Above T_b both types of nanoparticle are superparamagnetic as indicated by the closed hysteresis curves. Similar magnetic properties were observed for the Fe_3O_4-Au NPs in both water and thiolated DNA solution (Figure 5.22b and c). This, along with the TEM and UV/vis spectra, indicates that the Fe_3O_4-Au NPs are stable in the presence of thiolated DNA.

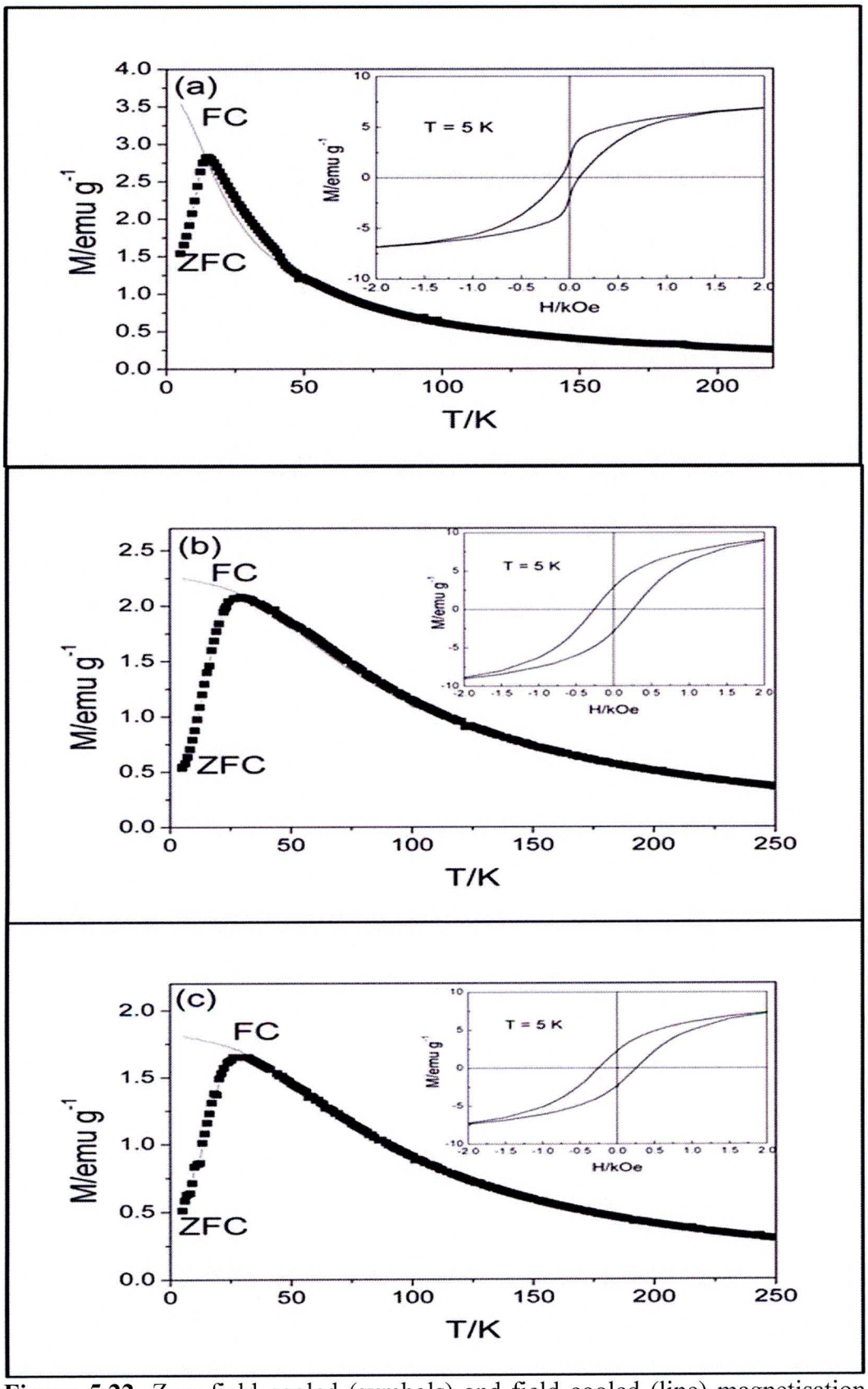

Figure 5.22. Zero-field cooled (symbols) and field cooled (line) magnetisation curves of (a) Fe_3O_4 NPs in hexane, (b) Fe_3O_4@Au NPs in water and (c) Fe_3O_4@Au NPs in water with thiolated DNA, as a function of temperature. The hysteresis curves measures at 5 K are shown in the insets.

5.4.3.5 High resolution transmission electron microscopy

A high resolution TEM (HRTEM) image and energy dispersion X-ray (EDX) spectrum of a Co-Au bimetallic nanoparticles are depicted in Figure 5.23. The spectrum displays peaks at 2.5 and 9.5 MeV that correspond to Au and a peak at 7.0 MeV which corresponds to Co, suggesting that the NPs have a Co@Au bimetallic structure. However, it can be seen in the HRTEM that the Co-Au NPs do not have a core shell structure. It has been suggested that NPs produced by a similar method have slightly more complicated structure than a simple core-shell. Cheng et al.[280] suggest that Au not only grows on the surface of the NPs, but will also diffuse into the Co cores, to produce metastable Co-Au NPs.

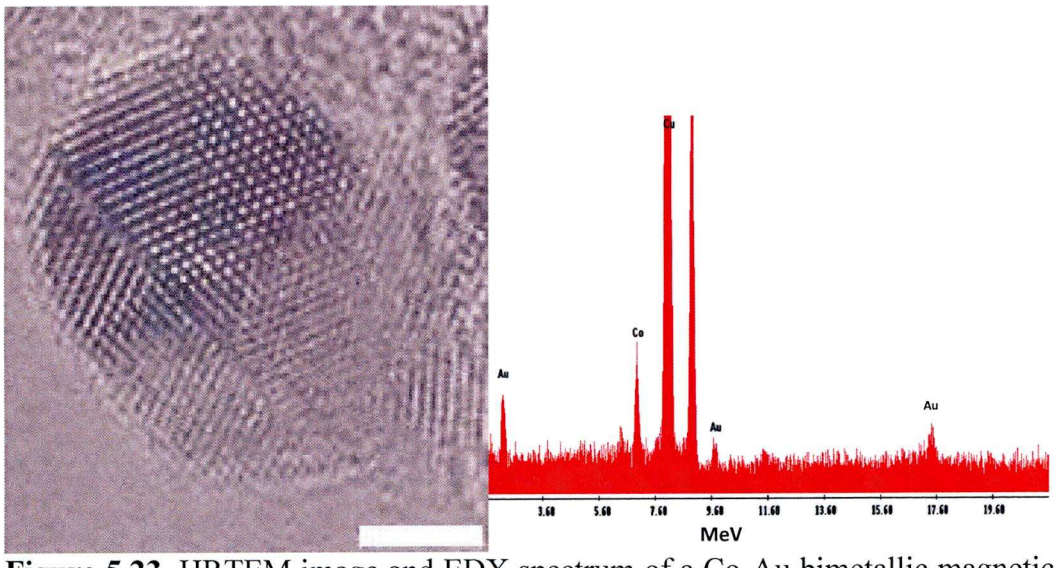

Figure 5.23. HRTEM image and EDX spectrum of a Co-Au bimetallic magnetic nanoparticle. Bar 2 nm

Attempts to transfer these NPs to aqueous solution using 11-mercaptoundecanoic acid as a stabilising ligand resulted in agglomeration and precipitation of the NPs. This is because the ligand could not bind strongly to the nanoparticle surface due to the low gold content.

Figure 5.24 shows the HRTEM image and EDX spectrum of a single Fe_3O_4-Au nanoparticle. The spectrum has peaks at 0.75 MeV, 6.5 MeV and 7 MeV that correspond to metallic Fe and peaks at 2 MeV, 9.5 MeV and 11.5 MeV for Au. Furthermore the HRTEM image shows variation in contrast between the dark Fe_3O_4 core and the lighter Au shell. The core appears darker on this image as mass contrast appears to dominate over diffraction contrast, rendering the shell lighter even though Au has a higher electron density than Fe_3O_4. The lattice distances measured for the shell correspond to the known Au lattice parameters for the (111) phase and those measured for the core match well with the Fe_3O_4 lattice parameters for the (311) phase.

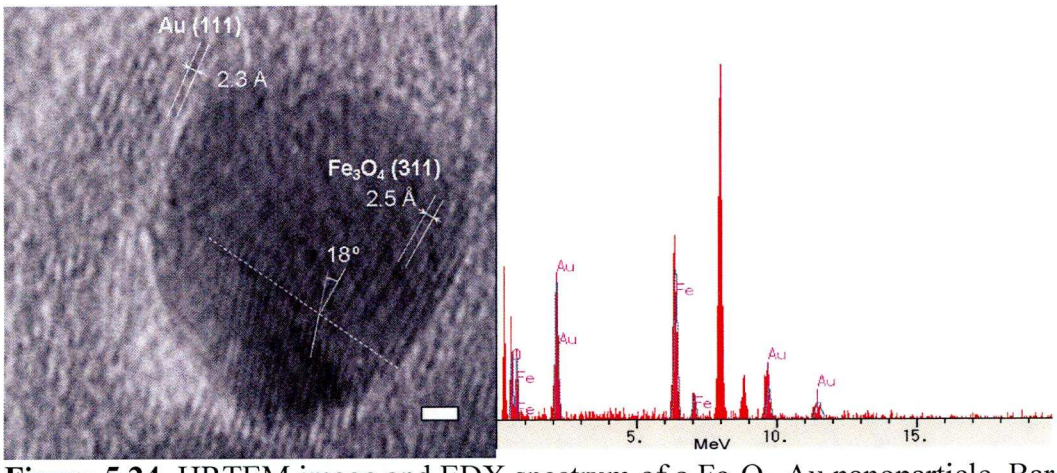

Figure 5.24. HRTEM image and EDX spectrum of a Fe_3O_4-Au nanoparticle. Bar 1 nm.

5.4 Conclusion

The modification of the surface of magnetic NPs is one approach to improve the solubility and stability of these particles in aqueous solution. This is the first step required to use magnetic NPs in biomedical applications. To this end, Co and iron oxide NPs were synthesised then functionalised with one of four polymers and latterly a layer of gold. The initial method for functionalising the magnetic NPs was to exchange the hydrophobic ligand with a hydrophilic or

amphiphilic polymer. Thermo-responsive polymers were found to successfully stabilise magnetic NPs of various sizes, however, the polymer used to stabilise the Co NPs resulted in the formation of spherical aggregates that were not particularly stable in electrolyte solution. The thermo-responsive polymer coated iron oxide NPs were much better dispersed in aqueous solution and this was reflected in the improved stability in electrolyte solution. Using PO-PEG as a ligand gave the iron oxide NPs even better stability, however, this polymer was not suitable for use with Co NPs due to the relatively poor binding of the phosphine oxide to the Co nanoparticle surface.

The second surface modification method was the addition of Pluronic F127 to the hydrophobic layer of the NPs. The iron oxide NPs stabilised by this method were found to be the most stable in electrolyte solution (up to seven days). This improvement in stability is likely to be a result of the terminal hydroxyl groups of the hydrophilic PEO chains substituting sodium ions to produce stable a sodium salt. However, like PO-PEG, this polymer did not facilitate the phase transfer of Co NPs. This probably arose because the F127 did not intercalate properly with the oleic acid layer on the Co NPs due to the presence of TOPO as a co-ligand in that layer.

While both the ligand exchange and ligand addition techniques worked very well for iron oxide NPs, stable dispersions of discrete Co NPs in aqueous solution still proved difficult to achieve. Consequently, Co and iron oxide NPs were coated with a layer of Au by the reduction of a Au salt on the nanoparticle surface. As well as providing a platform for functionalisation of the NPs Au can be used to protect easily oxidised cobalt NPs. The initial data acquired (UV-

visible spectra, EDX, etc) indicated that the Co-Au particles produced had a bimetallic structure. However, further examination of the morphology by the use of high resolution TEM could not discern the presence of a core-shell structure. The absence of a Au shell on the surface of the NPs would also explain why attempts to stabilise these NPs using 11-mercaptoundecanoic acid resulted in agglomeration and precipitation of the NPs. On the other hand, the larger size of the Fe_3O_4-Au NPs compared to the Fe_3O_4 seeds suggested that a gold layer had successfully been added to the latter. The presence of a Fe_3O_4-Au core-shell structure was further supported by HRTEM, where two distinct layers with different lattice distances could be observed.

Chapter 6

Methods and materials

6.1 General methods

All the synthesis was carried out using standard airless techniques. The $Co_2(CO)_8$ was weighed out under air free conditions using a glove box. The TEM samples were prepared by adding 10 μL of sample in water or organic solvent to a carbon-coated copper TEM grid at room temperature, covered with a watch glass, and allowed to evaporate slowly. Images were obtained using an FEI Tecnai G^2 120 kV TEM at the Department of Physiology, University of Liverpool, operated at 100 kV and visualised using analySIS software. The diameter (d) of the NPs was taken as the mean of a minimum of 200 (n) NPs measured using Bersoft Image Measurement 5.2 software. The hysteresis and ZFC-FC response curves were obtained in the Department of Physics, University of Liverpool, using an RF Quantum Design Magnetic Property Measurement System (MPMS) XL SQUID magnetometer. The UV/visible spectra were obtained using a Molecular Devices Spectromax 384 spectrometer. Chemicals and reagents were purchased from Sigma-Aldrich Chemical Company, Dorset, UK. The anhydrous solvents were used without further purification.

To establish the response of the polymer coated NPs to changes in pH, the NPs were diluted 10 to 1 in water and the pH adjusted with either 0.1 M HCl or 0.1 M NaOH to give a pH range from 1 to 12. The measurements were taken using a Brookhaven Instruments Corp. ZetaPlus Zeta Potential Analyser running ZetaPALS software. Elemental analysis was carried out using a Spectro CirosCCD ICP-AES. X-ray diffraction (XRD) patterns were obtained using a Rigaku RINT-2500 diffractometer (CuK_α radiation line λ=1.5408Å; 40 kV/100 mA).

6.2 Synthesis of thermo-responsive polymers

The polymers were synthesised as follows, *N*-isopropylacrylamide and *N*-tert-butylacrylamide, (or acrylic acid or acrylamide) were dissolved in propane-2-ol (40 ml) with 3-mercaptopropanoic acid and 4,4'-azo-bis(4-cyanovaleric acid) or α,α'-azobis(isobuytronitrile) (for exact amounts see Table 6.1). The solution was degassed by freeze-thaw cycles under vacuum at least three times. The tube was then placed in an oil bath at 65 °C for 24 hrs. After cooling to room temperature, the mixture was concentrated under reduced pressure and the residue added to diethyl ether (250 ml). The precipitated polymer was filtered and the residue was redissolved in the minimum amount of tetrahydrofuran and reprecipitated into diethyl ether (250 ml) another three times. The purified polymer was dried *in vacuo* at 20 °C for 16 hrs.

The molecular weight (Mw) of the polymers was determined by titration of the dissolved polymer (approx. 0.1 g) in water (50 ml) with freshly prepared sodium hydroxide solution (10 mM). The end point was determined by using phenolphthalein solution (1 % w/v in ethanol) as an indicator. The LCST was determined by dissolving the polymers in water at a concentration of 10 mg/l and cooled to 5 °C then heated to 50 °C at 0.5 °C/min in a heating block of a UV spectrometer.

Table 6.1. The amounts of monomers and free radical initiators to make the thermo-responsive polymers, with varying lowest critical solubility temperature (LCST) and molecular weight, used to coat Co and γ-Fe_2O_3 nanoparticles.

	Polymer P1	Polymer P2	Polymer P3	Polymer P4
N-iPAm (g)	8.4	9.0	6.3	9.0
N-t-BAm(g)	1.8	1.1	-	-
Acrylic acid	-	-	0.1	-
Acrylamide	-	-	-	1.0
3-MPA (ml)	0.19	0.19	-	0.19
ACVA (g)	-	0.33	-	-
AIBN (g)	0.19	-	0.06	0.19
LCST (^{o}C)	23.5	28.0	36	42
Mw	6800	10000	4500	6000

The LCST was taken at the onset of a sharp increase in absorption at 500 nm which is indicative of an increase in the turbidity of the solution due to the phase transition of the polymer. To study the effect of temperature upon the stability of the NPs in solution, 0.5 ml aliquots of aqueous nanoparticle suspension was mixed with either water (2 ml) or phosphate buffer solution (PBS) (2 ml; 10 mM). PBS was made using NaH_2PO_4 (0.84 ml; 0.2 M) and Na_2HPO_4 (2.16ml; 0.2 M) made up to 60 ml using deionised water to give a pH of 7.2. The diluted suspensions were then exposed to a range of temperatures from 5 ^{o}C to 50 ^{o}C.

6.3. Single step preparation of thermo-responsive polymer coated magnetic nanoparticles

The thermal decomposition of dicobalt octacarbonyl or iron pentacarbonyl, in the presence of the thermo-responsive polymer was used to synthesise NPs consisting of Co and γ-Fe_2O_3, respectively. In a typical Co nanoparticle synthesis, the polymer (0.04 mmol) was dissolved in DCB (8 ml) and heated to 186 °C with vigorous stirring, under N_2, before a solution of $Co_2(CO)_8$ (3.56 mmol) in DCB (2 ml) was rapidly injected into the solution. The solution was heated at this temperature for 10 min then cooled to room temperature. For the γ-Fe_2O_3 NPs, the polymer (0.04 mmol) was dissolved in dioctyl ether (10 ml) at 100 °C, under N_2 and $Fe(CO)_5$ (3.56 mmol) was added with vigorous stirring. The solution was heated to 286 °C and heated at that temperature for 30 min, then cooled to room temperature. To remove excess polymer from the solution and the NPs were concentrated by using a permanent magnet. The solvent was removed and the particles redispersed in hexane. This process was repeated three times before NPs were dried *in vacuo* at 20 °C for 30 min. The residue was redispersed in water and sonicated for 15 min. A permanent magnet was again used to concentrate the particles and the water was removed. This process was repeated three times before the particles were suspended in water.

6.4 Synthesis of Co nanoparticles by laser irradiation of $Co_2(CO)_8$

To synthesise Co NPs, a Q-switched Nd:YAG laser (Quantel Brilliant, Ltd) was used, which produces pulses with a width of 5 ns at a repetition rate of

10 Hz and a wavelength of either 355 nm or 266 nm. For both wavelengths, the pulse energy was adjusted to 15 ± 3 mJ and the beam diameter to 5 mm. In a typical synthesis, using standard airless conditions, OA (0.02 M or 0.04 M) and TOPO (0.02 M or 0.04 M) were dissolved in DCB (2 ml) in a 10 mm path length quartz absorption cell (Hellma UK, Ltd.). A solution of $Co_2(CO)_8$ (0.52 M) in DCB (0.5 ml) was added to the OA/TOPO solution which was then irradiated under vigorous stirring for 30 min. All syntheses were repeated three times and produced consistent results (Table 6.2).

Table 6.2. Results of the repeat synthesis of Co NPs by pulsed laser irradiation of $Co_2(CO)_8$

Wavelength (nm)	OA:TOPO ratio	Nanoparticle diameter (nm)		
		Synthesis 1	Synthesis 2	Synthesis 3
266	2.5:1.0	2.8 ± 0.5	2.5 ± 0.4	2.6 ± 0.4
266	1.0:2.5	3.7 ± 0.6	3.5 ± 0.5	3.5 ± 0.4
355	2.5:1.0	5.1 ± 3.1	5.3 ± 3.3	4.6 ± 2.7

6.5 Synthesis of alloy magnetic nanoparticles from bimetallic carbonyl clusters

The bimetallic carbonyl clusters were kindly provided by Dr Stefano Zacchini. OA (0.11 mmol) and TOPO (0.044 mmol) were dissolved in anhydrous DCB (4 mL), under N_2, and heated to 186 °C. A solution of the bimetallic carbonyl (0.26 mmol) in DCB (1 mL) was rapidly injected into the OA/TOPO solution with vigorous stirring. The mixture was heated at this temperature for 10 min then cooled to room temperature. All analysis and characterisation was carried out on the as prepared NPs.

6.6 Preparation hydrophobic magnetic nanoparticles

Nanoparticles for use in ligand exchange/addition experiments were first prepared in organic solvent and coated with a hydrophobic coating. In a typical Co nanoparticle synthesis, trioctylphosphine oxide (0.26 mmol) was added to a two neck flask with a condenser fitted and flushed with nitrogen for 20 min. Oleic acid (0.63 mmol) and (DCB) (15 ml) was added and the solution was heated to 186 °C with vigorous stirring. A solution of dicobalt octacarbonyl (1.58 mmol) in DCB (3 ml) was rapidly injected into the solution. The solution was heated at 186 °C for 10 min then cooled to room temperature. For the γ-Fe_2O_3 NPs, iron pentacarbonyl (6.08 mmol) was added to a solution of oleic acid (3.04 mmol) in dioctyl ether (20 ml) at 100 °C with vigorous stirring under nitrogen. The resulting mixture was heated to 286 °C and held at that temperature for 1 h. The solution was then cooled to 80 °C and allowed to air oxidise over a period of 16 h. After oxidation the solution was again heated to 286 °C for 1 h then cooled to room temperature. The diameter of the NPs was controlled by varying the concentration of oleic acid added to the solution.

6.7 Ligand exchange of hydrophobic magnetic nanoparticles with thermo-responsive polymers

The oleic acid coating of the magnetic NPs was replaced with a thermo-responsive polymer as follows: the synthesised NPs (5 ml) were precipitated by the addition of ethanol (20 ml). The NPs were washed a further two times with ethanol (20 ml) and resuspended in 1,4 dioxane (5 ml). This solution was then added to a solution of the thermo-responsive polymer (0.5 g) in 1,4-dioxane (15 ml). The mixture was then heated to 60 °C for 48 h. After this period the 1,4-

dioxane was removed *in vacuo* and the residue was washed twice with n-hexane. Once all trace of solvent was removed, the ligand exchanged NPs were suspended in water, sonicated for 15 min, then dialysed against water for 48 h, using dialysis membrane with a Mw cut off of 10 000. The solution was then freeze dried.

6.8 Synthesis of phosphine oxide-poly(ethylene glycol) (PO-PEG)

The phosphine oxide-poly(ethylene glycol) was prepared as previously published[277]. Breifly, poly(ethylene glycol) methyl ether (3 mmol) was dissolved in anhydrous THF (5 mL) and phosphorous oxychloride (3 mmol) was added. The solution was stirred at room temperature for 24 h after which the solvent was removed *in vacou*. The resulting gel was incubated at 100 °C, under vacuum, for a further 12 h.

6.9 Ligand exchange of hydrophobic magnetic nanoparticles with PO-PEG

Oleic acid coated magnetic NPs in an organic solvent suspension (5 mL) were precipitated and washed with ethanol (20 mL). The NPs were resuspended in THF (5 mL), into which PO-PEG was added (100 mg) and the solution was agitated by sonic bath for 10 min. The solvent was removed, *in vacou*, and the resulting residue was incubated at 150 °C, under vacuum, for 1 h. Water (5 mL) was added and the solution was dialysed against water against water for 48 h, using dialysis membrane with a Mw cut off of 10 000.

6.10 Ligand addition to hydrophobic magnetic nanoparticles with Pluronic F127

Oleic acid coated magnetic NPs in an organic solvent suspension (5 mL) were precipitated and washed with ethanol. The NPs were resuspended in hexane (5 mL). The phase transfer from organic solution to aqueous solution was achieved by mixing the hexane solution of NPs with and aqueous solution of Pluronic F127 (5 ml, 10 mg/mL). The mixture was sonicated for 30 min, and then lightly covered to allow the organic phase to slowly evaporate over 48 h. The aqueous solution of NPs was dialysed against water for 48 h using dialysis membrane with a Mw cut off of 10 000.

6.11 Stability of magnetic nanoparticles in electrolyte solution

Either Co or iron oxide NPs were dispersed in phosphate buffer (10 mM, 1 mL) and NaCl solution (5 M, 21 μL) was added to give a salt concentration of 0.1 M. This solution was left for 30 min to observe any aggregation, after which the process was repeated to produce a salt concentration of 0.2 M. Volumes of 5 M NaCl were added until either aggregation was observed or a salt concentration of 1 M was obtained.

6.12 Synthesis of Co-Au magnetic nanoparticles

A solution of $Co_2(CO)_8$ (0.49 g, 1.43 mmol) in anhydrous toluene (3 ml) was rapidly injected into a solution of NaAOT (0.067 g, 0.151 mmol) in toluene (27 ml) under reflux. The solution was vigorously stirred for 6 hrs at this temperature, under nitrogen and then cooled to room temperature. An aliquot (5

ml) of this solution was then diluted with toluene (20 ml) and heated to 85 °C. A solution of $HAuCl_4 \cdot 3H_2O$ (0.05 g) and oleylamine (1.25 ml) in toluene (5 ml) was injected into the Co solution and the temperature was maintained at 85 °C for 1 hr before the dark purple solution was cooled to room temperature.

A permanent magnet was placed on the outside of a glass vial containing synthesised NPs to attract the magnetic material to the side of the vial. The supernatant was removed and the remaining magnetic fraction was resuspended in toluene. This magnetic separation procedure was repeated a further two times and all analyses were carried out on this fraction.

6.13 Synthesis of gold coated iron oxide nanoparticles

6.13.1 Synthesis of Fe_3O_4 nanoparticles

$Fe(acac)_3$ (0.71 g, 2 mmol) was dissolved in phenyl ether (20 mL) with oleic acid (2 mL, 6 mmol) and oleylamine (2 mL, 4 mmol) under N_2 with vigorous stirring. 1,2-Hexadecanediol (2.58 g, 10 mmol) was added into the solution and it was heated to 210 °C and heated under reflux for 2 h, then cooled to room temperature. The solution was used as prepared without any further separation.

6.13.2 Synthesis of Fe_3O_4-Au nanoparticles

The phenyl ether reaction solution of Fe_3O_4 nanoparticles (10 mL, approx 0.33 mmol Fe_3O_4), $Au(OOCCH_3)_3$ (0.83 g, 2.2 mmol), 1,2-hexadecanediol (3.1 g, 12 mmol), oleic acid (0.5 mL, 1.5 mmol) and oleylamine (3 mL, 6 mmol) were

added to phenyl ether (30 mL) under N_2 with vigorous stirring. The reaction solution was heated to 180-190 °C and held at this temperature for 1.5 h

After cooling to room temperature, ethanol was added into the solution and the magnetic material collected using a permanent magnet. The precipitated product was washed with ethanol, and redispersed in hexane (10 mL) in the presence of oleic acid and oleylamine (approx 75 mM of each). The nanoparticle solution appeared dark purple.

6.13.3 Phase transfer of Fe_3O_4@Au NPs into aqueous solution

The Fe_3O_4-Au NPs (5ml of hexane solution) were precipitated ethanol (approx 15ml) and a permanent magnet. The precipitate was washed 2 more times then redispered in 3ml of 1M TMAOH solution. Tri-sodium citrate (0.04g) was added and the pH of the resulting solution adjusted to approx. pH6.5. The solution was the sonicated for 15 min, after which the Fe_3O_4@Au NP were collected using a magnet and redispered in pure water (5 mL) and sonicated for a further 5 min. An aliquot of this solution (100 μL) was then added to 100 μL of and solution of thiolated DNA (100 μM, kindly provided by Dr Christoph Walti, University of Leeds) and the solution was observed for any indication of aggregation.

References

1. Murray, C. B.; Kagan, C. R.; Bawendi, M. G., Synthesis and characterization of monodisperse nanocrystals and close-packed nanocrystal assemblies. *Annual Review of Materials Science* **2000**, 30, 545-610.

2. Efros, A. L.; Rosen, M., The electronic structure of semiconductor nanocrystals. *Annual Review of Materials Science* **2000**, 30, 475-521.

3. Klein, D. L.; Roth, R.; Lim, A. K. L.; Alivisatos, A. P.; McEuen, P. L., A single-electron transistor made from a cadmium selenide nanocrystal. *Nature* **1997**, 389, (6652), 699-701.

4. Joshi, H. M.; Bhumkar, D. R.; Joshi, K.; Pokharkar, V.; Sastry, M., Gold Nanoparticles as Carriers for Efficient Transmucosal Insulin Delivery. *Langmuir* **2006**, 22, (1), 300-305.

5. Elghanian, R.; Storhoff, J. J.; Mucic, R. C.; Letsinger, R. L.; Mirkin, C. A., Selective Colorimetric Detection of Polynucleotides Based on the Distance-Dependent Optical Properties of Gold Nanoparticles. *Science* **1997**, 277, (5329), 1078-1081.

6. Ohmori, M.; Matijevic, E., Preparation and Properties of Uniform Coated Inorganic Colloidal Particles .8. Silica on Iron. *Journal of Colloid and Interface Science* **1993**, 160, (2), 288-292.

7. Tartaj, P.; Gonzalez-Carreno, T.; Bomati-Miguel, O.; Serna, C. J.; Bonville, P., Magnetic behavior of superparamagnetic Fe nanocrystals confined inside submicron-sized spherical silica particles. *Physical Review B* **2004**, 69, (9), 094401 1 - 8.

8. Giersig, M.; Hilgendorff, M., The preparation of ordered colloidal magnetic particles by magnetophoretic deposition. *Journal Physics D: Applied Physics* **1999**, 32, (22), L111-L113.

9. Jung, J. S.; Choi, K. H.; Chae, W. S.; Kim, Y. R.; Jun, J. H.; Malkinski, L.; Kodenkandath, T.; Zhou, W. L.; Wiley, J. B.; O'Connor, C. J., Synthesis and characterization of Ni magnetic nanoparticles in AlMCM41 host. *Journal of Physics and Chemistry of Solids* **2003**, 64, (3), 385-390.

10. Sui, Y.; Yue, L.; Skomski, R.; Li, X. Z.; Zhou, J.; Sellmyer, D. J., CoPt hard magnetic nanoparticle films synthesized by high temperature chemical reduction. *Journal of Applied Physics* **2003**, 93, (10), 7571-7573.

11. Chinnasamy, C. N.; Jeyadevan, B.; Shinoda, K.; Tohji, K., Polyol-process-derived CoPt nanoparticles: Structural and magnetic properties. *Journal of Applied Physics* **2003**, 93, (10), 7583-7585.

12. Ban, Z. H.; Golub, V. O.; Kolesnichenko, V.; O'Connor, C. J., Novel synthesis of FeCo alloy nanoparticles and chracterization. *Abstracts of Papers of the American Chemical Society* **2004**, 227, U1454-U1454.

13. Pankhurst, Q. A.; Connolly, J.; Jones, S. K.; Dobson, J., Applications of magnetic nanoparticles in biomedicine. *Journal of Physics D: Applied Physics* **2003**, 36, (13), R167-R181.

14. Goia, D. V.; Matijevic, E., Preparation of monodispersed metal particles. *New Journal of Chemistry* **1998**, 22, (11), 1203-1215.

15. Parkes, L. M.; Hodgson, R.; Lu, L. T.; Tung, L. D.; Robinson, I.; Fernig, D. G.; Thanh, N. T. K., Cobalt nanoparticles as a novel magnetic resonance contrast agent-relaxivities at 1.5 and 3 Tesla. *Contrast Media & Molecular Imaging* **2008**, 3, (4), 150-156.

16. Schutt, W.; Gruttner, C.; Hafeli, U.; Zborowski, M.; Teller, J.; Putzar, H.; Schumichen, C., Applications of magnetic targeting in diagnosis and therapy - Possibilities and limitations: A mini-review. *Hybridoma* **1997**, 16, (1), 109-117.

17. Bonnemain, B., Superparamagnetic agents in magnetic resonance imaging: Physicochemical characteristics and clinical applications - A review. *Journal of Drug Targeting* **1998**, 6, (3), 167-174.

18. Wang, Y. X. J.; Hussain, S. M.; Krestin, G. P., Superparamagnetic iron oxide contrast agents: physicochemical characteristics and applications in MR imaging. *European Radiology* **2001**, 11, (11), 2319-2331.

19. Thanh, N. T. K.; Robinson, I.; Tung, L. D., Magnetic Nanoparticles for Biomedical Applications: Synthesis, Characterization and Uses. *Dekker Encyclopedia of Nanoscience and Nanotechnology* **2007**, 1, (1), 1 - 10.

20. Partch, R.; Brown, S., Aerosol and solution modification of particle-polymer interfaces. *Journal of Adhesion* **1998**, 67, (1-4), 259-276.

21. Stevenson, J. P.; Rutnakornpituk, M.; Vadala, M.; Esker, A. R.; Charles, S. W.; Wells, S.; Dailey, J. P.; Riffle, J. S., Magnetic cobalt dispersions in poly(dimethylsiloxane) fluids. *Journal of Magnetism and Magnetic Materials* **2001**, 225, (1-2), 47-58.

22. Levy, R.; Thanh, N. T. K.; Doty, R. C.; Hussain, I.; Nichols, R. J.; Schiffrin, D. J.; Brust, M.; Fernig, D. G., Rational and combinatorial design of peptide capping Ligands for gold nanoparticles. *Journal of the American Chemical Society* **2004**, 126, (32), 10076-10084.

23. Thanh, N. T. K.; Puntes, V. F.; Tung, L. D.; Fernig, D. G., Peptides as capping ligands for *in situ* synthesis of water soluble Co nanoparticles for bioapplications. *Journal of Physics: Conference Series* **2005**, 17, 70 - 76.

24. Wang, L. Y.; Luo, J.; Fan, Q.; Suzuki, M.; Suzuki, I. S.; Engelhard, M. H.; Lin, Y. H.; Kim, N.; Wang, J. Q.; Zhong, C. J., Monodispersed core-shell Fe3O4@Au nanoparticles. *Journal of Physical Chemistry B* **2005**, 109, (46), 21593-21601.

25. Lee, W. R.; Kim, M. G.; Choi, J. R.; Park, J. I.; Ko, S. J.; Oh, S. J.; Cheon, J., Redox-transmetalation process as a generalized synthetic strategy for core-shell magnetic nanoparticles. *Journal of the American Chemical Society* **2005**, 127, (46), 16090-16097.

26. Gaur, U.; Sahoo, S. K.; De, T. K.; Ghosh, P. C.; Maitra, A.; Ghosh, P. K., Biodistribution of fluoresceinated dextran using novel nanoparticles

evading reticuloendothelial system. *International Journal of Pharmaceutics* **2000**, 202, (1-2), 1-10.

27. Lacava, L. M.; Lacava, Z. G. M.; Da Silva, M. F.; Silva, O.; Chaves, S. B.; Azevedo, R. B.; Pelegrini, F.; Gansau, C.; Buske, N.; Sabolovic, D.; Morais, P. C., Magnetic resonance of a dextran-coated magnetic fluid intravenously administered in mice. *Biophysical Journal* **2001**, 80, (5), 2483-2486.

28. Jiles, D., *Introduction to Magnetism and Magnetic Materials*. Chapman and Hall: London, 1998.

29. Kuznetsov, A. A.; Harutyunyan, A. R.; Dobrinsky, E. K.; Filippov, V. I.; Malenkov, A. G.; Vanin, A. F.; Kuznetsov, O. A., *Scientific and Clinical Applications of Magnetic Carriers.* . Plenum: New York, 1996.

30. Kuznetsov, A. A.; Filippov, V. I.; Kuznetsov, O. A.; Gerlivanov, V. G.; Dobrinsky, E. K.; Malashin, S. I., New ferro-carbon adsorbents for magnetically guided transport of anti-cancer drugs. *Journal of Magnetism and Magnetic Materials* **1999**, 194, (1-3), 22-30.

31. Sieben, S.; Bergemann, C.; Lubbe, A.; Brockmann, B.; Rescheleit, D., Comparison of different particles and methods for magnetic isolation of circulating tumor cells. *Journal of Magnetism and Magnetic Materials* **2001**, 225, (1-2), 175-179.

32. Sincai, M.; Ganga, D.; Bica, D.; Vekas, L., The antitumor effect of locoregional magnetic cobalt ferrite in dog mammary adenocarcinoma. *Journal of Magnetism and Magnetic Materials* **2001**, 225, (1-2), 235-240.

33. Hilger, I.; Hiergeist, R.; Hergt, R.; Winnefeld, K.; Schubert, H.; Kaiser, W. A., Thermal ablation of tumors using magnetic nanoparticles - An in vivo feasibility study. *Investigative Radiology* **2002**, 37, (10), 580-586.

34. Maenosono, S.; Saita, S., Theoretical assessment of FePt nanoparticles as heating elements for magnetic hyperthermia. *Ieee Transactions on Magnetics* **2006**, 42, (6), 1638-1642.

35. Gupta, A. K.; Gupta, M., Synthesis and surface engineering of iron oxide nanoparticles for biomedical applications. *Biomaterials* **2005**, 26, (18), 3995-4021.

36. Berry, C. C.; Curtis, A. S. G., Functionalisation of magnetic nanoparticles for applications in biomedicine. *Journal of Physics D: Applied Physics* **2003**, 36, (13), R198-R206.

37. Mornet, S.; Vasseur, S.; Grasset, F.; Duguet, E., Magnetic nanoparticle design for medical diagnosis and therapy. *Journal of Materials Chemistry* **2004**, 14, (14), 2161-2175.

38. Mornet, S.; Vasseur, S.; Grasset, F.; Veverka, P.; Goglio, G.; Demourgues, A.; Portier, J.; Pollert, E.; Duguet, E., Magnetic nanoparticle design for medical applications. *Progress in Solid State Chemistry* **2006**, 34, (2-4), 237-247.

39. Hiergeist, R.; Andra, W.; Buske, N.; Hergt, R.; Hilger, I.; Richter, U.; Kaiser, W., Application of magnetite ferrofluids for hyperthermia. *Journal of Magnetism and Magnetic Materials* **1999**, 201, (1-3), 420-422.

40. Skumiel, A., Suitability of water based magnetic fluid with CoFe2O4 particles in hyperthermia. *Journal of Magnetism and Magnetic Materials* **2006**, 307, (1), 85-90.

41. Habib, A. H.; Ondeck, C. L.; Chaudhary, P.; Bockstaller, M. R.; McHenry, M. E., Evaluation of iron-cobalt/ferrite core-shell nanoparticles for cancer thermotherapy. *Journal of Applied Physics* **2008**, 103, (7), 07A307 1-3.

42. Pradhan, P.; Giri, J.; Banerjee, R.; Bellare, J.; Bahadur, D., Preparation and characterization of manganese ferrite-based magnetic liposomes for hyperthermia treatment of cancer. *Journal of Magnetism and Magnetic Materials* **2007**, 311, (1), 208-215.

43. Bulte, J. W. M.; Brooks, R. A.; Moskowitz, B. M.; Bryant, L. H.; Frank, J. A., Relaxometry and magnetometry of the MR contrast agent MION-46L. *Magnetic Resonance in Medicine* **1999**, 42, (2), 379-384.

44. Gillis, P.; Koenig, S. H., Transverse Relaxation of Solvent Protons Induced by Magnetized Spheres - Application to Ferritin, Erythrocytes, and Magnetite. *Magnetic Resonance in Medicine* **1987**, 5, (4), 323-345.

45. Muller, R. N.; Gillis, P.; Moiny, F.; Roch, A., Transverse Relaxivity of Particulate Mri Contrast-Media - from Theories to Experiments. *Magnetic Resonance in Medicine* **1991**, 22, (2), 178-182.

46. Bulte, J. W. M.; Brooks, R. A.; Moskowitz, B. M.; Bryant, L. H.; Frank, J. A., Relaxometry, magnetometry, and EPR evidence for three magnetic

phases in the MR contrast agent MION-46L. *Journal of Magnetism and Magnetic Materials* **1999**, 194, (1-3), 217-223.

47. Moghimi, S. M., Prolonging the circulation time and modifying the body distribution of intravenously injected polystyrene nanospheres by prior intravenous administration of poloxamine-908. A 'hepatic-blockade' event or manipulation of nanosphere surface in vivo? *Biochimica Et Biophysica Acta-General Subjects* **1997**, 1336, (1), 1-6.

48. Brusentsov, N. A.; Brusentsova, T. N.; Filinova, E. Y.; Jurchenko, N. Y.; Kupriyanov, D. A.; Pirogov, Y. A.; Dubina, A. I.; Shumskikh, M. N.; Shumakov, L. I.; Anashkina, E. N.; Shevelev, A. A.; Uchevatkin, A. A., Magnetohydrodynamic thermochemotherapy and MRI of mouse tumors. *Journal of Magnetism and Magnetic Materials* **2007**, 311, (1), 176-180.

49. Widder, K. J.; Senyei, A. E.; Scarpelli, D. G., Magnetic Microspheres - Model System for Site Specific Drug Delivery Invivo. *Proceedings of the Society for Experimental Biology and Medicine* **1978**, 158, (2), 141-146.

50. Shinkai, M., Functional magnetic particles for medical application. *Journal of Bioscience and Bioengineering* **2002**, 94, (6), 606-613.

51. Lubbe, A. S.; Alexiou, C.; Bergemann, C., Clinical applications of magnetic drug targeting. *Journal of Surgical Research* **2001**, 95, (2), 200-206.

52. Alexiou, C.; Jurgons, R.; Schmid, R.; Hilpert, A.; Bergemann, C.; Parak, F.; Iro, H., In vitro and in vivo investigations of targeted chemotherapy

with magnetic nanoparticles. *Journal of Magnetism and Magnetic Materials* **2005**, 293, (1), 389-393.

53. Brusentsov, N. A.; Brusentsova, T. N.; Filinova, E. Y.; Kuznetsov, V. D.; Shumakov, L. I.; Jurchenko, N. Y., Magnetic fluid thermo chemotherapy of murine tumors. *Journal of Magnetism and Magnetic Materials* **2005**, 293, (1), 450-454.

54. Brusentsova, T. N.; Brusentsov, N. A.; Kuznetsov, V. D.; Nikiforov, V. N., Synthesis and investigation of magnetic properties of Gd-substituted Mn-Zn ferrite nanoparticles as a potential low-T-C agent for magnetic fluid hyperthermia. *Journal of Magnetism and Magnetic Materials* **2005**, 293, (1), 298-302.

55. Brusentsov, N. A.; Kuznetsov, V. D.; Brusentsova, T. N.; Gendler, T. S.; Novakova, A. A.; Volter, E. R.; Haliulina, E. A.; Danilkin, M. I., Magnetisation of ferrifluids and effects of intracellular deposition of ferrite nanoparticles. *Journal of Magnetism and Magnetic Materials* **2004**, 272-76, (3), 2350-2351.

56. Brusentsov, N. A.; Nikitin, L. V.; Brusentsova, T. N.; Kuznetsov, A. A.; Bayburtskiy, F. S.; Shumakov, L. I.; Jurchenko, N. Y., Magnetic fluid hyperthermia of the mouse experimental tumor. *Journal of Magnetism and Magnetic Materials* **2002**, 252, (1-3), 378-380.

57. Mikkelsen, C.; Hansen, M. F.; Bruns, H., Theoretical comparison of magnetic and hydrodynamic interactions between magnetically tagged

particles in microfluidic systems. *Journal of Magnetism and Magnetic Materials* **2005**, 293, (1), 578-583.

58. Kim, J.; Lee, J. E.; Lee, J.; Yu, J. H.; Kim, B. C.; An, K.; Hwang, Y.; Shin, C. H.; Park, J. G.; Kim, J.; Hyeon, T., Magnetic fluorescent delivery vehicle using uniform mesoporous silica spheres embedded with monodisperse magnetic and semiconductor nanocrystals. *Journal of the American Chemical Society* **2006**, 128, (3), 688-689.

59. Moore, A., Brave small world - Biotechnology and nanotechnology may give rise to a completely new industry. *Embo Reports* **2001**, 2, (2), 86-88.

60. Marler, J. R., Tissue plasminogen activator for acute ischemic stroke - Reply. *New England Journal of Medicine* **1996**, 334, (21), 1406-1406.

61. Adams, H. P.; Adams, R. J.; Brott, T.; del Zoppo, G. J.; Furlan, A.; Goldstein, L. B.; Grubb, R. L.; Higashida, R.; Kidwell, C.; Kwiatkowski, T. G.; Marler, J. R.; Hademenos, G. J., Guidelines for the early management of patients with ischemic stroke - A scientific statement from the Stroke Council of the American Stroke Association. *Stroke* **2003**, 34, (4), 1056-1083.

62. Ma, Y. H.; Hsu, Y. W.; Chang, Y. J.; Hua, M. Y.; Chen, J. P.; Wu, T., Intra-arterial application of magnetic nanoparticles for targeted thrombolytic therapy: A rat embolic model. *Journal of Magnetism and Magnetic Materials* **2007**, 311, (1), 342-346.

63. Brown, D. C.; Gatter, K. C., Monoclonal antibody Ki-67: its use in histopathology. *Histopathology* **1990**, 17, (6), 489-503.

64. Luxton, R.; Badesha, J.; Kiely, J.; Hawkins, P., Use of External Magnetic Fields To Reduce Reaction Times in an Immunoassay Using Micrometer-Sized Paramagnetic Particles as Labels (Magnetoimmunoassay). *Analytical Chemistry* **2004**, 76, (6), 1715-1719.

65. Mitchels, J.; Hawkins, P.; Luxton, R.; Rhodes, A., Quantification in histopathology - Can magnetic particles help? *Journal of Magnetism and Magnetic Materials* **2007**, 311, (1), 264-268.

66. Plank, C.; Scherer, F.; Rudolph, C., *DNA Pharmaceuticals*. Wiley-VCH: Weinheim, 2005; p 55-116.

67. Scherer, F.; Anton, M.; Schillinger, U.; Henkel, J.; Bergemann, C.; Kruger, A.; Gansbacher, B.; Plank, C., Magnetofection: enhancing and targeting gene delivery by magnetic force in vitro and in vivo. *Gene Therapy* **2002**, 9, (2), 102-109.

68. Hughes, C.; Galea-Lauri, J.; Farzaneh, F.; Darling, D., Streptavidin paramagnetic particles provide a choice of three affinity-based capture and magnetic concentration strategies for retroviral vectors. *Molecular Therapy* **2001**, 3, (4), 623-630.

69. Mah, C.; Fraites, T. J.; Zolotukhin, I.; Song, S. H.; Flotte, T. R.; Dobson, J.; Batich, C.; Byrne, B. J., Improved method of recombinant AAV2 delivery for systemic targeted gene therapy. *Molecular Therapy* **2002**, 6, (1), 106-112.

70. Dobson, J., Gene therapy progress and prospects: magnetic nanoparticle-based gene delivery. *Gene Therapy* **2006**, 13, (4), 283-287.

71. McBain, S. C.; Yiu, H. H. P.; Dobson, J., Magnetic nanoparticles for gene and drug delivery. *International Journal of Nanomedicine* **2008**, 3, (2), 169-180.

72. Plank, C.; Schillinger, U.; Scherer, F.; Bergemann, C.; Remy, J. S.; Krotz, F.; Anton, M.; Lausier, J.; Rosenecker, J., The magnetofection method: Using magnetic force to enhance gene delivery. *Biological Chemistry* **2003**, 384, (5), 737-747.

73. Huth, S.; Lausier, J.; Gersting, S. W.; Rudolph, C.; Plank, C.; Welsch, U.; Rosenecker, J., Insights into the mechanism of magnetofection using PEI-based magnetofectins for gene transfer. *Journal of Gene Medicine* **2004**, 6, (8), 923-936.

74. Schillinger, U.; Brill, T.; Rudolph, C.; Huth, S.; Gersting, S.; Krotz, F.; Hirschberger, J.; Bergemann, C.; Plank, C., Advances in magnetofection - magnetically guided nucleic acid delivery. *Journal of Magnetism and Magnetic Materials* **2005**, 293, (1), 501-508.

75. McBain, S. C.; Yiu, H. H. P.; El Haj, A.; Dobson, J., Polyethyleneimine functionalized iron oxide nanoparticles as agents for DNA delivery and transfection. *Journal of Materials Chemistry* **2007**, 17, (24), 2561-2565.

76. Krotz, F.; de Wit, C.; Sohn, H. Y.; Zahler, S.; Gloe, T.; Pohl, U.; Plank, C., Magnetofection - A highly efficient tool for antisense oligonucleotide delivery in vitro and in vivo. *Molecular Therapy* **2003**, 7, (5), 700-710.

77. Li, W. Z.; Nesselmann, C.; Zhou, Z. H.; Ong, L. L.; Ori, F.; Tang, G. P.; Kaminski, A.; Lutzow, K.; Lendlein, A.; Liebold, A.; Stamm, C.; Wang,

J.; Steinhoff, G.; Ma, N., Gene delivery to the heart by magnetic nanobeads. *Journal of Magnetism and Magnetic Materials* **2007**, 311, (1), 336-341.

78. Zhao, X. J.; Tapec-Dytioco, R.; Wang, K. M.; Tan, W. H., Collection of trace amounts of DNA/mRNA molecules using genomagnetic nanocapturers. *Analytical Chemistry* **2003**, 75, (14), 3476-3483.

79. Mykhaylyk, O.; Antequera, Y. S.; Vlaskou, D.; Plank, C., Generation of magnetic nonviral gene transfer agents and magnetofection in vitro. *Nature Protocols* **2007**, 2, (10), 2391-2411.

80. Grief, A. D.; Richardson, G., Mathematical modelling of magnetically targeted drug delivery. *Journal of Magnetism and Magnetic Materials* **2005**, 293, (1), 455-463.

81. Giddings, J. C., Field-Flow Fractionation - Analysis of Macromolecular, Colloidal, and Particulate Materials. *Science* **1993**, 260, (5113), 1456-1465.

82. Carpino, F.; Zborowski, M.; Williams, P. S., Quadrupole magnetic field-flow fractionation: A novel technique for the characterization of magnetic nanoparticles. *Journal of Magnetism and Magnetic Materials* **2007**, 311, (1), 383-387.

83. Kennedy, D. J.; Todd, P.; Logan, S.; Becker, M.; Papas, K. K.; Moore, L. R., Engineering quadrupole magnetic flow sorting for the isolation of pancreatic islets. *Journal of Magnetism and Magnetic Materials* **2007**, 311, (1), 388-395.

84. Hering, B. J., Achieving and maintaining insulin independence in human islet transplant recipients. *Transplantation* **2005**, 79, (10), 1296-1297.

85. Bulte, J. W. M., Magnetic nanoparticles as markers for cellular MR imaging. *Journal of Magnetism and Magnetic Materials* **2005**, 289, 423-427.

86. Bulte, J. W. M.; Zhang, S. C.; van Gelderen, P.; Herynek, V.; Jordan, E. K.; Duncan, I. D.; Frank, J. A., Neurotransplantation of magnetically labeled oligodendrocyte progenitors: Magnetic resonance tracking of cell migration and myelination. *Proceedings of the National Academy of Sciences of the United States of America* **1999**, 96, (26), 15256-15261.

87. Walczak, P.; Zhang, J.; Gilad, A. A.; Kedziorek, D. A.; Ruiz-Cabello, J.; Young, R. G.; Pittenger, M. F.; Van Zijl, P. C. M.; Huang, J.; Bulte, J. W. M., Dual-modality monitoring of targeted intraarterial delivery of mesenchymal stem cells after transient ischemia. *Stroke* **2008**, 39, (5), 1569-1574.

88. Jendelova, P.; Herynek, V.; Urdzikova, L.; Glogarova, K.; Kroupova, J.; Andersson, B.; Bryja, V.; Burian, M.; Hajek, M.; Sykova, E., Magnetic resonance tracking of transplanted bone marrow and embryonic stem cells labeled by iron oxide nanoparticles in rat brain and spinal cord. *Journal of Neuroscience Research* **2004**, 76, (2), 232-243.

89. Bulte, J. W. M.; Arbab, A. S.; Douglas, T.; Frank, J. A., Preparation of magnetically labeled cells for cell tracking by magnetic resonance imaging. *Imaging in Biological Research, Pt B* **2004**, 386, 275-299.

90. Kostura, L.; Kraitchman, D. L.; Mackay, A. M.; Pittenger, M. F.; Bulte, J. W. M., Feridex labeling of mesenchymal stem cells inhibits chondrogenesis but not adipogenesis or osteogenesis. *Nmr in Biomedicine* **2004**, 17, (7), 513-517.

91. Flynn, E. R.; Bryant, H. C.; Bergemann, C.; Larson, R. S.; Lovato, D.; Sergatskov, D. A., Use of a SQUID array to detect T-cells with magnetic nanoparticles in determining transplant rejection. *Journal of Magnetism and Magnetic Materials* **2007**, 311, (1), 429-435.

92. Hattersley, S. R.; Pankhurst, Q. A.; Brazdeikis, A. Magnetic properties sensing system. Pat. No. GB20050008886 20050429, 2006-11-01 2006.

93. Muthana, M.; Scott, S. D.; Farrow, N.; Morrow, F.; Murdoch, C.; Grubb, S.; Brown, N.; Dobson, J.; Lewis, C. E., A novel magnetic approach to enhance the efficacy of cell-based gene therapies. *Gene Therapy* **2008**, 15, (12), 902-910.

94. Tartaj, P.; Morales, M. P.; Veintemillas-Verdaguer, S.; Gonzalez-Carreno, T.; Serna, C. J., *Handbook of Magnetic Materials*. Elsevier: Amsterdam, 2006; Vol. 16, p 403-482.

95. Morales, M. P.; Gonzalezcarreno, T.; Serna, C. J., The Formation of Alpha-Fe2O3 Monodispersed Particles in Solution. *Journal of Materials Research* **1992**, 7, (9), 2538-2545.

96. Ocana, M.; Rodriguezclemente, R.; Serna, C. J., Uniform Colloidal Particles in Solution - Formation Mechanisms. *Advanced Materials* **1995**, 7, (2), 212-216.

97. Puntes, V. F.; Krishnan, K. M.; Alivisatos, A. P., Colloidal nanocrystal shape and size control: The case of cobalt. *Science* **2001**, 291, (5511), 2115-2117.

98. Ma, W. W.; Yang, Y.; Chong, C. T.; Eggeman, A.; Piramanayagam, S. N.; Zhou, T. J.; Song, T.; Wang, J. P., Synthesis and magnetic behavior of self-assembled Co nanorods and nanoballs. *Journal of Applied Physics* **2004**, 95, (11), 6801-6803.

99. Jana, N. R.; Chen, Y. F.; Peng, X. G., Size- and shape-controlled magnetic (Cr, Mn, Fe, Co, Ni) oxide nanocrystals via a simple and general approach. *Chemistry of Materials* **2004**, 16, (20), 3931-3935.

100. Park, J.; An, K. J.; Hwang, Y. S.; Park, J. G.; Noh, H. J.; Kim, J. Y.; Park, J. H.; Hwang, N. M.; Hyeon, T., Ultra-large-scale syntheses of monodisperse nanocrystals. *Nature Materials* **2004**, 3, (12), 891-895.

101. Park, J.; Lee, E.; Hwang, N. M.; Kang, M. S.; Kim, S. C.; Hwang, Y.; Park, J. G.; Noh, H. J.; Kini, J. Y.; Park, J. H.; Hyeon, T., One-nanometer-scale size-controlled synthesis of monodisperse magnetic iron oxide nanoparticles. *Angewandte Chemie-International Edition* **2005**, 44, (19), 2872-2877.

102. Xu, X. Q.; Shen, H.; Xu, J. R.; Xu, J.; Li, X. J.; Xiong, X. M., Core-shell structure and magnetic properties of magnetite magnetic fluids stabilized with dextran. *Applied Surface Science* **2005**, 252, (2), 494-500.

103. Hu, F. Q.; Wei, L.; Zhou, Z.; Ran, Y. L.; Li, Z.; Gao, M. Y., Preparation of biocompatible magnetite nanocrystals for in vivo magnetic resonance detection of cancer. *Advanced Materials* **2006**, 18, (19), 2553-+.

104. Butter, K.; Philipse, A. P.; Vroege, G. J., Synthesis and properties of iron ferrofluids. *Journal of Magnetism and Magnetic Materials* **2002**, 252, (1-3), 1-3.

105. Dumestre, F.; Chaudret, B.; Amiens, C.; Renaud, P.; Fejes, P., Superlattices of iron nanocubes synthesized from $Fe[N(SiMe_3)_{(2)}]_{(2)}$. *Science* **2004**, 303, (5659), 821-823.

106. Puntes, V. F.; Zanchet, D.; Erdonmez, C. K.; Alivisatos, A. P., Synthesis of hcp-Co nanodisks. *Journal of the American Chemical Society* **2002**, 124, (43), 12874-12880.

107. Dumestre, F.; Chaudret, B.; Amiens, C.; Fromen, M. C.; Casanove, M. J.; Renaud, P.; Zurcher, P., Shape control of thermodynamically stable cobalt nanorods through organometallic chemistry. *Angewandte Chemie-International Edition* **2002**, 41, (22), 4286-4289.

108. Dumestre, F.; Chaudret, B.; Amiens, C.; Respaud, M.; Fejes, P.; Renaud, P.; Zurcher, P., Unprecedented crystalline super-lattices of monodisperse cobalt nanorods. *Angewandte Chemie-International Edition* **2003**, 42, (42), 5213-5216.

109. Bonnemann, H.; Brijoux, W.; Brinkmann, R.; Matoussevitch, N.; Waldofner, N.; Palina, N.; Modrow, H., A size-selective synthesis of air

stable colloidal magnetic cobalt nanoparticles. *Inorganica Chimica Acta* **2003**, 350, 617-624.

110. Yamada, Y.; Suzuki, T.; Abarra, E. N., Magnetic properties of electron beam evaporated CoPt alloy thin films. *Ieee Transactions on Magnetics* **1998**, 34, (2), 343-345.

111. Perera, S. C.; Tsoi, G.; Wenger, L. E.; Brock, S. L., Synthesis of MnP nanocrystals by treatment of metal carbonyl complexes with phosphines: A new, versatile route to nanoscale transition metal phosphides. *Journal of the American Chemical Society* **2003**, 125, (46), 13960-13961.

112. Stamm, K. L.; Gamo, J. C.; Liu, G. Y.; Brock, S. L., A general methodology for the synthesis of transition metal pnictide nanoparticles from pnictate precursors and its application to iron-phosphorus phases. *Journal of the American Chemical Society* **2003**, 125, (14), 4038-4039.

113. Luo, F.; Su, H. L.; Song, W.; Wang, Z. M.; Yan, Z. G.; Yan, C. H., Magnetic and magnetotransport properties of Fe2P nanocrystallites via a solvothermal route. *Journal of Materials Chemistry* **2004**, 14, (1), 111-115.

114. Tegus, O.; Bruck, E.; Buschow, K. H. J.; de Boer, F. R., Transition-metal-based magnetic refrigerants for room-temperature applications. *Nature* **2002**, 415, (6868), 150-152.

115. Grimes, C. A.; Horn, J. L.; Bush, G. G.; Allen, J. L.; Eklund, P. C., Curie temperature enhancement in Fe3C nanoparticles made by laser pyrolysis. *Ieee Transactions on Magnetics* **1997**, 33, (5), 3736-3738.

116. Zhao, X. Q.; Veintemillas-Verdaguer, S.; Bomati-Miguel, O.; Morales, M. P.; Xu, H. B., Thermal history dependence of the crystal structure of Co fine particles. *Physical Review B: Condensed Matter* **2005**, 71, (2), 024106 1-7.

117. Moras, K.; Schaarschuch, R.; Riehemann, W.; Zinoveva, S.; Modrow, H.; Eberbeck, D., Production and characterisation of magnetic nanoparticles produced by laser evaporation for ferrofluids. *Journal of Magnetism and Magnetic Materials* **2005**, 293, (1), 119-126.

118. Bomati-Miguel, O.; Leconte, Y.; Morales, M. P.; Herlin-Boime, N.; Veintemillas-Verdaguer, S., Laser pyrolysis preparation of SiO_2-coated magnetic nanoparticles for biomedical applications. *Journal of Magnetism and Magnetic Materials* **2005**, 290, (1), 272-275.

119. Kurland, H. D.; Grabow, J.; Staupendahl, G.; Andra, W.; Dutz, S.; Bellemann, M. E., Magnetic iron oxide nanopowders produced by CO_2 laser evaporation. *Journal Magnetism and Magnetic Materials* **2007**, 311, (1), 73-77.

120. Wang, C. Y.; Fang, J. Y.; He, J. B.; O'Connor, C. J., Synthesis of one-dimensional magnetic Co nanoparticles in a novel solution system. *Journal of Colloid and Interface Science* **2003**, 259, (2), 411-413.

121. Goia, D. V., Preparation and formation mechanisms of uniform metallic particles in homogeneous solutions. *Journal of Materials Chemistry* **2004**, 14, (4), 451-458.

122. Lu, L. T.; Tung, L. D.; Robinson, I.; Ung, D.; Tan, B.; Long, J.; Cooper, A. I.; Fernig, D. G.; Thanh, N. T. K., Size and shape control for water-soluble magnetic cobalt nanoparticles using polymer ligands. *Journal of Materials Chemistry* **2008**, 18, (21), 2453 - 2458.

123. Kodama, D.; Shinoda, K.; Sato, K.; Konno, Y.; Joseyphus, R. J.; Motomiya, K.; Takahashi, H.; Matsumoto, T.; Sato, Y.; Tohji, K.; Jeyadevan, B., Chemical synthesis of sub-micrometer- to nanometer-sized magnetic FeCo dice. *Advanced Materials* **2006**, 18, (23), 3154-3159.

124. Chaubey, G. S.; Barcena, C.; Poudyal, N.; Rong, C. B.; Gao, J. M.; Sun, S. H.; Liu, J. P., Synthesis and stabilization of FeCo nanoparticles. *Journal of the American Chemical Society* **2007**, 129, (23), 7214-7215.

125. Sun, S. H.; Anders, S.; Thomson, T.; Baglin, J. E. E.; Toney, M. F.; Hamann, H. F.; Murray, C. B.; Terris, B. D., Controlled synthesis and assembly of FePt nanoparticles. *Journal of Physical Chemistry B* **2003**, 107, (23), 5419-5425.

126. Faeder, J.; Ladanyi, B. M., Molecular dynamics simulations of the interior of aqueous reverse micelles. *Journal of Physical Chemistry B* **2000**, 104, (5), 1033-1046.

127. Carpenter, E. E.; Sangregorio, C.; O'Connor, C. J., Effects of shell thickness on blocking temperature of nanocomposites of metal particles with gold shells. *Ieee Transactions on Magnetics* **1999**, 35, (5), 3496-3498.

128. Lin, J.; Zhou, W. L.; Kumbhar, A.; Wiemann, J.; Fang, J. Y.; Carpenter, E. E.; O'Connor, C. J., Gold-coated iron (Fe@Au) nanoparticles: Synthesis, characterization, and magnetic field-induced self-assembly. *Journal of Solid State Chemistry* **2001**, 159, (1), 26-31.

129. Cho, S. J.; Idrobo, J. C.; Olamit, J.; Liu, K.; Browning, N. D.; Kauzlarich, S. M., Growth mechanisms and oxidation resistance of gold-coated iron nanoparticles. *Chemistry of Materials* **2005**, 17, (12), 3181-3186.

130. Mikhaylova, M.; Kim, D. K.; Bobrysheva, N.; Osmolowsky, M.; Semenov, V.; Tsakalakos, T.; Muhammed, M., Superparamagnetism of magnetite nanoparticles: Dependence on surface modification. *Langmuir* **2004**, 20, (6), 2472-2477.

131. Mandal, M.; Kundu, S.; Ghosh, S. K.; Panigrahi, S.; Sau, T. K.; Yusuf, S. M.; Pal, T., Magnetite nanoparticles with tunable gold or silver shell. *Journal of Colloid and Interface Science* **2005**, 286, (1), 187-194.

132. Carpenter, E. E.; Seip, C. T.; O'Connor, C. J., Magnetism of nanophase metal and metal alloy particles formed in ordered phases. *Journal of Applied Physics* **1999**, 85, (8), 5184-5186.

133. Liu, C.; Zou, B. S.; Rondinone, A. J.; Zhang, Z. J., Reverse micelle synthesis and characterization of superparamagnetic MnFe2O4 spinel ferrite nanocrystallites. *Journal of Physical Chemistry B* **2000**, 104, (6), 1141-1145.

134. Woo, K.; Lee, H. J.; Ahn, J. P.; Park, Y. S., Sol-gel mediated synthesis of Fe2O3 nanorods. *Advanced Materials* **2003**, 15, (20), 1761-+.

135. Pileni, M. P., Reverse micelles as microreactors. *Journal of Physical Chemistry* **1993**, 97, (6961-6973).

136. Wang, X.; Zhuang, J.; Peng, Q.; Li, Y. D., A general strategy for nanocrystal synthesis. *Nature* **2005**, 437, (7055), 121-124.

137. Cote, L. J.; Teja, A. S.; Wilkinson, A. P.; Zhang, Z. J., Continuous hydrothermal synthesis of CoFe2O4 nanoparticles. *Fluid Phase Equilibria* **2003**, 210, (2), 307-317.

138. Ji, G. B.; Tang, S. L.; Ren, S. K.; Zhang, F. M.; Gu, B. X.; Du, Y. W., Simplified synthesis of single-crystalline magnetic CoFe2O4 nanorods by a surfactant-assisted hydrothermal process. *Journal of Crystal Growth* **2004**, 270, (1-2), 156-161.

139. Zubris, M.; King, R. B.; Garmestani, H.; Tannenbaum, R., FeCo nanoalloy formation by decomposition of their carbonyl precursors. *Journal of Materials Chemistry* **2005**, 15, (12), 1277-1285.

140. Hutten, A.; Sudfeld, D.; Ennen, I.; Reiss, G.; Hachmann, W.; Heinzmann, U.; Wojczykowski, K.; Jutzi, P.; Saikaly, W.; Thomas, G., New magnetic nanoparticles for biotechnology. *Journal of Biotechnology* **2004**, 112, (1-2), 47-63.

141. Ung, D.; Tung, L. D.; Carnutu, G.; Delaprtas, D.; Alexandruo, I.; Prior, I. A.; Thanh, N. T. K., Variant shape and growth of nanoparticles of metallic Fe-Pt, Fe-Pd and Fe-Pt alloys *CrystEngComm* **2009**, 11, 1309-1316.

142. Euliss, L. E.; Grancharov, S. G.; O'Brien, S.; Deming, T. J.; Stucky, G. D.; Murray, C. B.; Held, G. A., Cooperative assembly of magnetic nanoparticles and block copolypeptides in aqueous media. *Nano Letters* **2003**, 3, (11), 1489-1493.

143. Liu, X. Q.; Guan, Y. P.; Ma, Z. Y.; Liu, H. Z., Surface modification and characterization of magnetic polymer nanospheres prepared by miniemulsion polymerization. *Langmuir* **2004**, 20, (23), 10278-10282.

144. Hong, R.; Fischer, N. O.; Emrick, T.; Rotello, V. M., Surface PEGylation and ligand exchange chemistry of FePt nanoparticles for biological applications. *Chemistry of Materials* **2005**, 17, (18), 4617-4621.

145. Sahoo, Y.; Pizem, H.; Fried, T.; Golodnitsky, D.; Burstein, L.; Sukenik, C. N.; Markovich, G., Alkyl phosphonate/phosphate coating on magnetite nanoparticles: A comparison with fatty acids. *Langmuir* **2001**, 17, (25), 7907-7911.

146. Yoon, M.; Kim, Y.; Kim, Y. M.; Volkov, V.; Song, H. J.; Park, Y. J.; Park, I. W., Superparamagnetic properties of nickel nanoparticles in an ion-exchange polymer film. *Materials Chemistry and Physics* **2005**, 91, (1), 104-107.

147. Kobayashi, Y.; Horie, M.; Konno, M.; Rodriguez-Gonzalez, B.; Liz-Marzan, L. M., Preparation and properties of silica-coated cobalt nanoparticles. *Journal of Physical Chemistry B* **2003**, 107, (30), 7420-7425.

148. Lu, A. H.; Li, W. C.; Matoussevitch, N.; Spliethoff, B.; Bonnemann, H.; Schuth, F., Highly stable carbon-protected cobalt nanoparticles and graphite shells. *Chemical Communications* **2005**, (1), 98-100.

149. Sobal, N. S.; Hilgendorff, M.; Mohwald, H.; Giersig, M.; Spasova, M.; Radetic, T.; Farle, M., Synthesis and structure of colloidal bimetallic nanocrystals: The non-alloying system Ag/Co. *Nano Letters* **2002**, 2, (6), 621-624.

150. Liu, Q. X.; Xu, Z. H.; Finch, J. A.; Egerton, R., A novel two-step silica-coating process for engineering magnetic nanocomposites. *Chemistry of Materials* **1998**, 10, (12), 3936-3940.

151. Liao, M. H.; Chen, D. H., Immobilization of yeast alcohol dehydrogenase on magnetic nanoparticles for improving its stability. *Biotechnology Letters* **2001**, 23, (20), 1723-1727.

152. Park, J. I.; Cheon, J., Synthesis of "solid solution" and "core-shell" type cobalt-platinum magnetic nanoparticles via transmetalation reactions. *Journal of the American Chemical Society* **2001**, 123, (24), 5743-5746.

153. Nunez, N. O.; Tartaj, P.; Morales, M. P.; Bonville, P.; Serna, C. J., Yttria-coated FeCo magnetic nanoneedles. *Chemistry of Materials* **2004**, 16, (16), 3119-3124.

154. Fan, J.; Lu, J. G.; Xu, R. S.; Jiang, R.; Gao, Y., Use of water-dispersible Fe2O3 nanoparticles with narrow size distributions in isolating avidin. *Journal of Colloid and Interface Science* **2003**, 266, (1), 215-218.

155. Xu, C. J.; Xu, K. M.; Gu, H. W.; Zheng, R. K.; Liu, H.; Zhang, X. X.; Guo, Z. H.; Xu, B., Dopamine as a robust anchor to immobilize functional molecules on the iron oxide shell of magnetic nanoparticles. *Journal of the American Chemical Society* **2004**, 126, (32), 9938-9939.

156. Gu, H. W.; Ho, P. L.; Tsang, K. W. T.; Wang, L.; Xu, B., Using biofunctional magnetic nanoparticles to capture vancomycin-resistant enterococci and other gram-positive bacteria at ultralow concentration. *Journal of the American Chemical Society* **2003**, 125, (51), 15702-15703.

157. Ho, K. C.; Tsai, P. J.; Lin, Y. S.; Chen, Y. C., Using biofunctionalized nanoparticles to probe pathogenic bacteria. *Analytical Chemistry* **2004**, 76, (24), 7162-7168.

158. Gruttner, C.; Muller, K.; Teller, J.; Westphal, F.; Foreman, A.; Ivkov, R., Synthesis and antibody conjugation of magnetic nanoparticles with improved specific power absorption rates for alternating magnetic field cancer therapy. *Journal of Magnetism and Magnetic Materials* **2007**, 311, (1), 181-186.

159. Shen, L. F.; Laibinis, P. E.; Hatton, T. A., Bilayer surfactant stabilized magnetic fluids: Synthesis and interactions at interfaces. *Langmuir* **1999**, 15, (2), 447-453.

160. Sousa, M. H.; Tonrinho, F. A.; Depeyrot, J.; da Silva, G. J.; Lara, M. C. F. L., New electric double-layered magnetic fluids based on copper, nickel, and zinc ferrite nanostructures. *Journal of Physical Chemistry B* **2001**, 105, (6), 1168-1175.

161. Lu, A. H.; Salabas, E. L.; Schuth, F., Magnetic nanoparticles: Synthesis, protection, functionalization, and application. *Angewandte Chemie-International Edition* **2007**, 46, (8), 1222-1244.

162. Berry, C. C.; Wells, S.; Charles, S.; Aitchison, G.; Curtis, A. S. G., Cell response to dextran-derivatised iron oxide nanoparticles post internalisation. *Biomaterials* **2004**, 25, (23), 5405-5413.

163. Aslam, M.; Schultz, E. A.; Sun, T.; Meade, T.; Dravid, V. P., Synthesis of amine-stabilized aqueous colloidal iron oxide nanoparticles. *Crystal Growth & Design* **2007**, 7, (3), 471-475.

164. Mondini, S.; Cenedese, S.; Marinoni, G.; Molteni, G.; Santo, N.; Bianchi, C. L.; Ponti, A., One-step synthesis and functionalization of hydroxyl-decorated magnetite nanoparticles. *Journal of Colloid and Interface Science* **2008**, 322, (1), 173-179.

165. Harris, L. A.; Goff, J. D.; Carmichael, A. Y.; Riffle, J. S.; Harburn, J. J.; St Pierre, T. G.; Saunders, M., Magnetite nanoparticle dispersions stabilized with triblock copolymers. *Chemistry of Materials* **2003**, 15, (6), 1367-1377.

166. Thunemann, A. F.; Schutt, D.; Kaufner, L.; Pison, U.; Mohwald, H., Maghemite nanoparticles protectively coated with poly(ethylene imine) and poly(ethylene oxide)-block-poly(glutamic acid). *Langmuir* **2006**, 22, (5), 2351-2357.

167. Dresco, P. A.; Zaitsev, V. S.; Gambino, R. J.; Chu, B., Preparation and properties of magnetite and polymer magnetite nanoparticles. *Langmuir* **1999**, 15, (6), 1945-1951.

168. Deng, J. G.; Ding, X. B.; Zhang, W. C.; Peng, Y. X.; Wang, J. H.; Long, X. P.; Li, P.; Chan, A. S. C., Magnetic and conducting Fe3O4-cross-linked polyaniline nanoparticles with core-shell structure. *Polymer* **2002**, 43, (8), 2179-2184.

169. Vestal, C. R.; Zhang, Z. J., Effects of surface coordination chemistry on the magnetic properties of MnFe2O4 spinel ferrite nanoparticles. *Journal of the American Chemical Society* **2003**, 125, (32), 9828-9833.

170. Robinson, I.; Alexander, C.; Lu, L. T.; Tung, L. D.; Fernig, D. G.; Thanh, N. T. K., One-step synthesis of monodisperse water-soluble 'dual-responsive' magnetic nanoparticles. *Chemical Communications* **2007**, (44), 4602-4604.

171. Ang, K. H.; Alexandrou, I.; Mathur, N. D.; Amaratunga, G. A. J.; Haq, S., The effect of carbon encapsulation on the magnetic properties of Ni nanoparticles produced by arc discharge in de-ionized water. *Nanotechnology* **2004**, 15, (5), 520-524.

172. Teunissen, W.; de Groot, F. M. F.; Geus, J.; Stephan, O.; Tence, M.; Colliex, C., The structure of carbon encapsulated NiFe nanoparticles. *Journal of Catalysis* **2001**, 204, (1), 169-174.

173. Hayashi, T.; Hirono, S.; Tomita, M.; Umemura, S., Magnetic thin films of cobalt nanocrystals encapsulated in graphite-like carbon. *Nature* **1996**, 381, (6585), 772-774.

174. Nesper, R.; Ivantchenko, A.; Krumeich, F., Synthesis and characterization of carbon-based nanoparticles and highly magnetic nanoparticles with carbon coatings. *Advanced Functional Materials* **2006**, 16, (2), 296-305.

175. Nikitenko, S. I.; Koltypin, Y.; Markovich, V.; Rozenberg, E.; Gorodetsky, G.; Gedanken, A., Synthesis of air-stable iron-iron carbide nanocrystalline particles showing very high saturation magnetization. *Ieee Transactions on Magnetics* **2002**, 38, (5), 2592-2594.

176. Geng, J. F.; Jefferson, D. A.; Johnson, B. F. G., Direct conversion of iron stearate into magnetic Fe and Fe3C nanocrystals encapsulated in polyhedral graphite cages. *Chemical Communications* **2004**, (21), 2442-2443.

177. Baranauskas, V. V.; Zalich, M. A.; Saunders, M.; St Pierre, T. G.; Riffle, J. S., Poly(styrene-b-4-vinylphenoxyphthalonitrile) - Cobalt complexes and their conversion to oxidatively stable cobalt nanoparticles. *Chemistry of Materials* **2005**, 17, (21), 5246-5254.

178. Lu, A. H.; Li, W. C.; Salabas, E. L.; Spliethoff, B.; Schuth, F., Low temperature catalytic pyrolysis for the synthesis of high surface area, nanostructured graphitic carbon. *Chemistry of Materials* **2006**, 18, (8), 2086-2094.

179. Ban, Z. H.; Barnakov, Y. A.; Golub, V. O.; O'Connor, C. J., The synthesis of core-shell iron@gold nanoparticles and their characterization. *Journal of Materials Chemistry* **2005**, 15, (43), 4660-4662.

180. Lu, Z. H.; Prouty, M. D.; Guo, Z. H.; Golub, V. O.; Kumar, C. S. S. R.; Lvov, Y. M., Magnetic switch of permeability for polyelectrolyte microcapsules embedded with Co@Au nanoparticles. *Langmuir* **2005**, 21, (5), 2042-2050.

181. Peng, D. L.; Sumiyama, K.; Hihara, T.; Yamamuro, S.; Konno, T. J., Magnetic properties of monodispersed Co/CoO clusters. *Physical Review B* **2000**, 61, (4), 3103-3109.

182. Boyen, H. G.; Kastle, G.; Zurn, K.; Herzog, T.; Weigl, F.; Ziemann, P.; Mayer, O.; Jerome, C.; Moller, M.; Spatz, J. P.; Garnier, M. G.; Oelhafen, P., A micellar route to ordered arrays of magnetic nanoparticles: From size-selected pure cobalt dots to cobalt-cobalt oxide core-shell systems. *Advanced Functional Materials* **2003**, 13, (5), 359-364.

183. Ulman, A., Formation and structure of self-assembled monolayers. *Chemical Reviews* **1996**, 96, (4), 1533-1554.

184. Lu, Y.; Yin, Y. D.; Mayers, B. T.; Xia, Y. N., Modifying the surface properties of superparamagnetic iron oxide nanoparticles through a sol-gel approach. *Nano Letters* **2002**, 2, (3), 183-186.

185. Zhao, W. R.; Gu, J. L.; Zhang, L. X.; Chen, H. R.; Shi, J. L., Fabrication of uniform magnetic nanocomposite spheres with a magnetic

core/mesoporous silica shell structure. *Journal of the American Chemical Society* **2005**, 127, (25), 8916-8917.

186. Tartaj, P.; Serna, C. J., Synthesis of monodisperse superparamagnetic Fe/silica nanospherical composites. *Journal of the American Chemical Society* **2003**, 125, (51), 15754-15755.

187. Santra, S.; Tapec, R.; Theodoropoulou, N.; Dobson, J.; Hebard, A.; Tan, W. H., Synthesis and characterization of silica-coated iron oxide nanoparticles in microemulsion: The effect of nonionic surfactants. *Langmuir* **2001**, 17, (10), 2900-2906.

188. Yi, D. K.; Lee, S. S.; Papaefthymiou, G. C.; Ying, J. Y., Nanoparticle architectures templated by SiO2/Fe2O3 nanocomposites. *Chemistry of Materials* **2006**, 18, (3), 614-619.

189. Vestal, C. R.; Zhang, Z. J., Synthesis and magnetic characterization of Mn and Co spinel ferrite-silica nanoparticles with tunable magnetic core. *Nano Letters* **2003**, 3, (12), 1739-1743.

190. Ung, T.; Liz-Marzan, L. M.; Mulvaney, P., Controlled method for silica coating of silver colloids. Influence of coating on the rate of chemical reactions. *Langmuir* **1998**, 14, (14), 3740-3748.

191. LizMarzan, L. M.; Giersig, M.; Mulvaney, P., Homogeneous silica coating of vitreophobic colloids. *Chemical Communications* **1996**, (6), 731-732.

192. Stoeva, S. I.; Huo, F. W.; Lee, J. S.; Mirkin, C. A., Three-layer composite magnetic nanoparticle probes for DNA. *Journal of the American Chemical Society* **2005**, 127, (44), 15362-15363.

193. Yi, D. K.; Selvan, S. T.; Lee, S. S.; Papaefthymiou, G. C.; Kundaliya, D.; Ying, J. Y., Silica-coated nanocomposites of magnetic nanoparticles and quantum dots. *Journal of the American Chemical Society* **2005**, 127, (14), 4990-4991.

194. Gu, H. W.; Ho, P. L.; Tsang, K. W. T.; Yu, C. W.; Xu, B., Using biofunctional magnetic nanoparticles to capture Gram-negative bacteria at an ultra-low concentration. *Chemical Communications* **2003**, (15), 1966-1967.

195. Longmire, M.; Choyke, P. L.; Kobayashi, H., Clearance properties of nano-sized particles and molecules as imaging agents: considerations and caveats. *Nanomedicine* **2008**, 3, (5), 703 - 717.

196. Schild, H. G., Poly (N-Isopropylacrylamide) - Experiment, Theory and Application. *Progress in Polymer Science* **1992**, 17, (2), 163-249.

197. Jeyadevan, B.; Shinoda, K.; Justin, R. J.; Matsumot, T.; Sato, K.; Takahashi, H.; Sato, Y.; Tohji, K., Polyol process for Fe-based hard(fct-FePt) and soft(FeCo) magnetic nanoparticles. *Ieee Transactions on Magnetics* **2006**, 42, (10), 3030-3035.

198. Thunemann, A. F.; Schutt, D.; Sachse, R.; Schlaad, H.; Mohwald, H., Complexes of poly(ethylene oxide)-block-poly(L-glutamate) and diminazene. *Langmuir* **2006**, 22, (5), 2323-2328.

199. Robinson, I.; Alexander, C.; Tung, L. D.; Fernig, D. G.; Thanh, N. T. K., Fabrication of water-soluble magnetic nanoparticles by ligand-exchange with thermo-responsive polymers. *Journal of Magnetism and Magnetic Materials* **2009**, 321, (10), 1421-1423.

200. Kaiser, A.; Gelbrich, T.; Schmidt, A. M., Thermosensitive magnetic fluids. *Journal of Physics-Condensed Matter* **2006**, 18, (38), S2563-S2580.

201. Shamim, N.; Hong, L.; Hidajat, K.; Uddin, M. S., Thermosensitive-polymer-coated magnetic nanoparticles: Adsorption and desorption of bovine serum albumin. *Journal of Colloid and Interface Science* **2006**, 304, (1), 1-8.

202. Tadd, E.; Zeno, A.; Zubris, M.; Dan, N.; Tannenbaum, R., Adsorption and polymer film formation on metal nanoclusters. *Macromolecules* **2003**, 36, (17), 6497-6502.

203. Tannenbaum, R.; Zubris, M.; Goldberg, E. P.; Reich, S.; Dan, N., Polymer-directed nanocluster synthesis: Control of particle size and morphology. *Macromolecules* **2005**, 38, (10), 4254-4259.

204. David, V.; Vinas, C.; Teixidor, F., Poly(3,4-ethylenedioxythiophene) doped with a non-extrudable metallacarborane anion electroactive during synthesis. *Polymer* **2006**, 47, (13), 4694-4702.

205. Larsson, A.; Kuckling, D.; Schonhoff, M., 1H NMR of thermoreversible polymers in solution and at interfaces: the influence of charged groups on

the phase transition. *Colloids and Surfaces a-Physicochemical and Engineering Aspects* **2001**, 190, (1-2), 185-192.

206. Yim, H.; Kent, M. S.; Mendez, S.; Lopez, G. P.; Satija, S.; Seo, Y., Effects of grafting density and molecular weight on the temperature-dependent conformational change of poly(N-isopropylacrylamide) grafted chains in water. *Macromolecules* **2006**, 39, (9), 3420-3426.

207. Yim, H.; Kent, M. S.; Satija, S.; Mendez, S.; Balamurugan, S. S.; Balamurugan, S.; Lopez, C. P., Study of the conformational change of poly(N-isopropylacrylamide)-grafted chains in water with neutron reflection: Molecular weight dependence at high grafting density. *Journal of Polymer Science Part B: Polymer Physics* **2004**, 42, (17), 3302-3310.

208. Gil, E. S.; Hudson, S. M., Stimuli-reponsive polymers and their bioconjugates. *Progress in Polymer Science* **2004**, 29, (12), 1173-1257.

209. Guo, J.; Yang, W. L.; Wang, C. C.; He, J.; Chen, J. Y., Poly(N-isopropylacrylamide)-coated luminescent/magnetic silica microspheres: Preparation, characterization, and biomedical applications. *Chemistry of Materials* **2006**, 18, (23), 5554-5562.

210. Kurisawa, M.; Yokoyama, M.; Okano, T., Gene expression control by temperature with thermo-responsive polymeric gene carriers. *Journal of Controlled Release* **2000**, 69, (1), 127-137.

211. Meyer, D. E.; Shin, B. C.; Kong, G. A.; Dewhirst, M. W.; Chilkoti, A., Drug targeting using thermally responsive polymers and local hyperthermia. *Journal of Controlled Release* **2001**, 74, (1-3), 213-224.

212. O'Connor, C. J.; Lee, Y. S.; Tang, J.; John, V. T.; Kommareddi, N. S.; Tata, M.; Mcpherson, G. L.; Akkara, J. A.; Kaplan, D. L., Superparamagnetism of Ferrite Particles Dispersed in Spherical Polymeric Materials. *Ieee Transactions on Magnetics* **1994**, 30, (6), 4954-4956.

213. Murray, C. B.; Sun, S. H.; Gaschler, W.; Doyle, H.; Betley, T. A.; Kagan, C. R., Colloidal synthesis of nanocrystals and nanocrystal superlattices. *IBM Journal of Research and Development* **2001**, 45, (1), 47-56.

214. Sweany, R. L.; Brown, T. L., Matrix-Isolation Spectra of Thermal and Photochemical Decomposition Products of Dicobalt Octacarbonyl. *Inorganic Chemistry* **1977**, 16, (2), 421-424.

215. Abrahamson, H. B.; Frazier, C. C.; Ginley, D. S.; Gray, H. B.; Lilienthal, J.; Tyler, D. R.; Wrighton, M. S., Electronic-Spectra of Dinuclear Cobalt Carbonyl Complexes. *Inorganic Chemistry* **1977**, 16, (6), 1554-1556.

216. Moskovich, S.; Reuvenov, D.; Schultz, R. H., Microsecond UV flash photolysis of $Co_2(CO)_8$ in solution: Wavelength dependence of the $CO(CO)_4/Co_2(CO)_7$ branching ratio. *Chemical Physics Letters* **2006**, 431, (1-3), 62-66.

217. Privman, V.; Goia, D. V.; Park, J.; Matijevic, E., Mechanism of formation of monodispersed colloids by aggregation of nanosize precursors. *Journal of Colloid and Interface Science* **1999**, 213, (1), 36-45.

218. Simons, W. W., *The Sadtler Handbook of Ultraviolet Spectra*. Sadtler & Heyden: Philadelphia, 1979.

219. Wray, W. O.; Aida, T.; Dyer, R. B., *Appl. Phys. B* **2002**, 74, 57-66.

220. Murray, C. B.; Norris, D. J.; Bawendi, M. G., Synthesis and Characterization of Nearly Monodisperse Cde (E = S, Se, Te) Semiconductor Nanocrystallites. *Journal of the American Chemical Society* **1993**, 115, (19), 8706-8715.

221. Creighton, J. A.; Eadon, D. G., Ultraviolet Visible Absorption-Spectra of the Colloidal Metallic Elements. *Journal of the Chemical Society-Faraday Transactions* **1991**, 87, (24), 3881-3891.

222. Chen, G. X.; Hong, M. H.; Lan, B.; Wang, Z. B.; Lu, Y. F.; Chong, T. C., A convenient way to prepare magnetic colloids by direct Nd : YAG laser ablation. *Applied Surface Science* **2004**, 228, (1-4), 169-175.

223. Xie, C. S.; Hu, J. H.; Wu, R.; Xia, H., Structure transition comparison between the amorphous nanosize particles and coarse-grained polycrystalline of cobalt. *Nanostructured Materials* **1999**, 11, (8), 1061-1066.

224. Tracy, J. B.; Weiss, D. N.; Dinega, D. P.; Bawendi, M. G., Exchange biasing and magnetic properties of partially and fully oxidized colloidal cobalt nanoparticles. *Physical Review B* **2005**, 72, (6), 064404 1-8.

225. Behrens, S.; Bonnemann, H.; Matoussevitch, N.; Gorschinski, A.; Dinjus, E.; Habicht, W.; Bolle, J.; Zinoveva, S.; Palina, N.; Hormes, J.; Modrow, H.; Bahr, S.; Kempter, V., Surface engineering of Co and FeCo nanoparticles for biomedical application. *Journal of Physics-Condensed Matter* **2006**, 18, (38), S2543-S2561.

226. Sun, S. H.; Anders, S.; Hamann, H. F.; Thiele, J. U.; Baglin, J. E. E.; Thomson, T.; Fullerton, E. E.; Murray, C. B.; Terris, B. D., Polymer mediated self-assembly of magnetic nanoparticles. *Journal of the American Chemical Society* **2002**, 124, (12), 2884-2885.

227. Sun, S. H.; Murray, C. B.; Weller, D.; Folks, L.; Moser, A., Monodisperse FePt nanoparticles and ferromagnetic FePt nanocrystal superlattices. *Science* **2000**, 287, (5460), 1989-1992.

228. Sun, S. H.; Fullerton, E. E.; Weller, D.; Murray, C. B., Compositionally controlled FePt nanoparticle materials. *Ieee Transactions on Magnetics* **2001**, 37, (4), 1239-1243.

229. Kiely, C. J.; Fink, J.; Zheng, J. G.; Brust, M.; Bethell, D.; Schiffrin, D. J., Ordered colloidal nanoalloys. *Advanced Materials* **2000**, 12, (9), 640-643.

230. Toshima, N.; Kushihashi, K.; Yonezawa, T.; Hirai, H., Colloidal Dispersions of Palladium-Platinum Bimetallic Clusters Protected by Polymers - Preparation and Application to Catalysis. *Chemistry Letters* **1989**, (10), 1769-1772.

231. Toshima, N.; Harada, M.; Yonezawa, T.; Kushihashi, K.; Asakura, K., Structural-Analysis of Polymer-Protected Pd/Pt Bimetallic Clusters as Dispersed Catalysts by Using Extended X-Ray Absorption Fine-Structure Spectroscopy. *Journal of Physical Chemistry* **1991**, 95, (19), 7448-7453.

232. Toshima, N.; Yonezawa, T.; Kushihashi, K., Polymer-Protected Palladium-Platinum Bimetallic Clusters - Preparation, Catalytic

Properties and Structural Considerations. *Journal of the Chemical Society-Faraday Transactions* **1993**, 89, (14), 2537-2543.

233. Richard, D.; Couves, J. W.; Thomas, J. M., Structural and Electronic-Properties of Finely-Divided Supported Pt-Group Metals and Bimetals. *Faraday Discussions* **1991**, (92), 109-119.

234. Toshima, N.; Lu, P., Synthesis and catalysis of colloidal dispersions of Pd/Ni bimetallic clusters. *Chemistry Letters* **1996**, (9), 729-730.

235. Deshpande, V. M.; Narasimhan, C. S., Synthesis and Catalytic Activity of Palladium Tin Mixed Metal Colloid Sols. *Journal of Molecular Catalysis* **1989**, 53, (3), L21-L24.

236. Degani, Y.; Willner, I., Photoinduced Hydrogenation of Ethylene and Acetylene in Aqueous-Media - the Functions of Palladium and Platinum Colloids as Catalytic Charge Relays. *Journal of the Chemical Society-Perkin Transactions 2* **1986**, (1), 37-41.

237. Schmid, G.; Lehnert, A.; Malm, J. O.; Bovin, J. O., Ligand-Stabilized Bimetallic Colloids Identified by HRTEM and EDX. *Angewandte Chemie-International Edition in English* **1991**, 30, (7), 874-876.

238. Harada, M.; Asakura, K.; Toshima, N., Catalytic Activity and Structural-Analysis of Polymer-Protected Au/Pd Bimetallic Clusters Prepared by the Successive Reduction of $HAuCl_4$ and $PdCl_2$. *Journal of Physical Chemistry* **1993**, 97, (19), 5103-5114.

239. Wang, Y.; Toshima, N., Preparation of Pd-Pt bimetallic colloids with controllable core/shell structures. *Journal of Physical Chemistry B* **1997**, 101, (27), 5301-5306.

240. Reetz, M. T.; Helbig, W., Size-Selective Synthesis of Nanostructured Transition-Metal Clusters. *Journal of the American Chemical Society* **1994**, 116, (16), 7401-7402.

241. Reetz, M. T.; Helbig, W.; Quaiser, S. A.; Stimming, U.; Breuer, N.; Vogel, R., Visualization of Surfactants on Nanostructured Palladium Clusters by a Combination of Stm and High-Resolution Tem. *Science* **1995**, 267, (5196), 367-369.

242. Reetz, M. T.; Quaiser, S. A., A New Method for the Preparation of Nanostructured Metal-Clusters. *Angewandte Chemie-International Edition in English* **1995**, 34, (20), 2240-2241.

243. Henglein, A., Physicochemical Properties of Small Metal Particles in Solution - Microelectrode Reactions, Chemisorption, Composite Metal Particles, and the Atom-to-Metal Transition. *Journal of Physical Chemistry* **1993**, 97, (21), 5457-5471.

244. Katsikas, L.; Gutierrez, M.; Henglein, A., Bimetallic colloids: Silver and mercury. *Journal of Physical Chemistry* **1996**, 100, (27), 11203-11206.

245. Henglein, A.; Brancewicz, C., Absorption spectra and reactions of colloidal bimetallic nanoparticles containing mercury. *Chemistry of Materials* **1997**, 9, (10), 2164-2167.

246. Brenner, J. R.; Harkness, J. B. L.; Knickelbein, M. B.; Krumdick, G. K.; Marshall, C. L., Microwave plasma synthesis of carbon-supported ultrafine metal particles. *Nanostructured Materials* **1997**, 8, (1), 1-17.

247. Torigoe, K.; Esumi, K., Preparation of Bimetallic Ag-Pd Colloids from Silver(I) Bis(Oxalato)Palladate(Ii). *Langmuir* **1993**, 9, (7), 1664-1667.

248. Torigoe, K.; Nakajima, Y.; Esumi, K., Preparation and Characterization of Colloidal Silver Platinum Alloys. *Journal of Physical Chemistry* **1993**, 97, (31), 8304-8309.

249. Sudfeld, D.; Wojczykowski, K.; Hachmann, W.; Heitmann, S.; Rott, K.; Hempel, T.; Kammerer, S.; Jutzi, R.; Hutten, A.; Reiss, G., Magnetic cobalt nanocrystals organized in patches and chains. *Ieee Transactions on Magnetics* **2002**, 38, (5), 2601-2603.

250. Bonnemann, H.; Brand, R. A.; Brijoux, W.; Hofstadt, H. W.; Frerichs, M.; Kempter, V.; Maus-Friedrichs, W.; Matoussevitch, N.; Nagabhushana, K. S.; Voigts, F.; Caps, V., Air stable Fe and Fe-Co magnetic fluids - synthesis and characterization. *Applied Organometallic Chemistry* **2005**, 19, (6), 790-796.

251. Ichikawa, M., *Metal Clusters in Chemistry*. Wiley-VCH: Weinheim, 1999.

252. Schweyer-Tihay, F.; Estournes, C.; Braunstein, P.; Guille, J.; Paillaud, J. L.; Richard-Plouet, M.; Rose, J., On the nature of metallic nanoparticles obtained from molecular Co3Ru-carbonyl clusters in mesoporous silica matrices. *Physical Chemistry Chemical Physics* **2006**, 8, (34), 4018-4028.

253. Gates, B. C., Supported Metal-Clusters - Synthesis, Structure, and Catalysis. *Chemical Reviews* **1995**, 95, (3), 511-522.

254. Thomas, J. M.; Johnson, B. F. G.; Raja, R.; Sankar, G.; Midgley, P. A., High-performance nanocatalysts for single-step hydrogenations. *Accounts of Chemical Research* **2003**, 36, (1), 20-30.

255. Johnson, B. F. G.; Raynor, S. A.; Brown, D. B.; Shephard, D. S.; Mashmeyer, T.; Thomas, J. M.; Hermans, S.; Raja, R.; Sankar, G., New catalysts for clean technology. *Journal of Molecular Catalysis a-Chemical* **2002**, 182, (1), 89-97.

256. Dyson, P. J., Catalysis by low oxidation state transition metal (carbonyl) clusters. *Coordination Chemistry Reviews* **2004**, 248, (21-24), 2443-2458.

257. Albonetti, S.; Bonelli, R.; Mengou, J. E.; Femoni, C.; Tiozzo, C.; Zacchini, S.; Trifiro, F., Gold/iron carbonyl clusters as precursors for TiO_2 supported catalysts. *Catalysis Today* **2008**, 137, (2-4), 483-488.

258. Siani, A.; Captain, B.; Alexeev, O. S.; Stafyla, E.; Hungria, A. B.; Midgley, P. A.; Thomas, J. M.; Adams, R. D.; Amiridis, M. D., Improved CO oxidation activity in the presence and absence of hydrogen over cluster-derived $PtFe/SiO_2$ catalysts. *Langmuir* **2006**, 22, (11), 5160-5167.

259. Rutledge, R. D.; Morris, W. H.; Wellons, M. S.; Gai, Z.; Shen, J.; Bentley, J.; Wittig, J. E.; Lukehart, C. M., Formation of FePt nanoparticles having high coercivity. *Journal of the American Chemical Society* **2006**, 128, (44), 14210-14211.

260. Low, A. A.; Lauher, J. W., Tetraethylammonium dodecarbonyltricobaltferrate$^{(1-)}$ and (triphenylphosphine)gold$^{(1+)}$ dodecarbonyltricobaltferrate$^{(1-)}$. *Inorganic Syntheses* **1990**, 27, 188- 191.

261. Chini, P.; Colli, L.; Peraldo, M., Preparation and properties of the hydrocarbonyl $HFeCo_3(CO)_{12}$ and of compounds prepared from the anion $[FeCo_3(CO)_{12}]^-$. *Gazzetta Chimica Italiana* **1960**, 90, 1005-20.

262. Longoni, G.; Manassero, M.; Sansoni, M., Synthesis and Characterization of New Fe-Pd and Fe-Pt Carbonyl Anionic Clusters. *Journal of the American Chemical Society* **1980**, 102, (9), 3242-3244.

263. Della Pergola, R.; Diana, E.; Garlaschelli, L.; Peli, G.; Manassero, M.; Sansoni, M.; Strumolo, D., Iron-nickel mixed metal clusters: synthesis, reactivity and vibrational spectroscopy of $[FeNi_5(CO)_{(13)}]^{(2-)}$. Solid state structure of the anions $[FeNi_5(CO)_{(13)}]^{(2-)}$ and $[Fe_3Ni(CO)_{(12)}]^{(2-)}$. *Inorganica Chimica Acta* **2003**, 350, 107-113.

264. Keller, E. *SHAKAL99*, University of Freiburg, Germany, 1999.

265. LaMer, V. K.; Dinegar, R. H., Theory, Production and Mechanism of Formation of Monodispersed Hydrosols. *Journal of the American Chemical Society* **1950**, 72, (11), 4847-4854.

266. Inomata, K.; Sawa, T.; Hashimoto, S., Effect of Large Boron Additions to Magnetically Hard Fe-Pt Alloys. *Journal of Applied Physics* **1988**, 64, (5), 2537-2540.

267. Longoni, G.; Femoni, C.; Iapalucci, C.; Zanello, P., *Metal Clusters in Chemistry*. Wiley-VCH: Wienheim, 1999.

268. Longoni, G.; Iapalucci, C., *Clusters and Colloids*. Wiley-VCH: WeinHeim, 1994.

269. Femoni, C.; Iapalucci, M. C.; Kaswalder, F.; Longoni, G.; Zacchini, S., The possible role of metal carbonyl clusters in nanoscience and nanotechnologies. *Coordination Chemistry Reviews* **2006**, 250, (11-12), 1580-1604.

270. Narain, R.; Gonzales, M.; Hoffman, A. S.; Stayton, P. S.; Krishnan, K. M., Synthesis of monodisperse biotinylated p(NIPAAm)-coated iron oxide magnetic nanoparticles and their bioconjugation to streptavidin. *Langmuir* **2007**, 23, (11), 6299-6304.

271. Zhang, T. R.; Ge, J. P.; Hu, Y. P.; Yin, Y. D., A general approach for transferring hydrophobic nanocrystals into water. *Nano Letters* **2007**, 7, (10), 3203-3207.

272. Jun, Y. W.; Huh, Y. M.; Choi, J. S.; Lee, J. H.; Song, H. T.; Kim, S.; Yoon, S.; Kim, K. S.; Shin, J. S.; Suh, J. S.; Cheon, J., Nanoscale size effect of magnetic nanocrystals and their utilization for cancer diagnosis via magnetic resonance imaging. *Journal of the American Chemical Society* **2005**, 127, (16), 5732-5733.

273. Lee, S. Y.; Harris, M. T., Surface modification of magnetic nanoparticles capped by oleic acids: Characterization and colloidal stability in polar

solvents. *Journal of Colloid and Interface Science* **2006**, 293, (2), 401-408.

274. De Palma, R.; Peeters, S.; Van Bael, M. J.; Van den Rul, H.; Bonroy, K.; Laureyn, W.; Mullens, J.; Borghs, G.; Maes, G., Silane ligand exchange to make hydrophobic superparamagnetic nanoparticles water-dispersible. *Chemistry of Materials* **2007**, 19, (7), 1821-1831.

275. Qin, J.; Laurent, S.; Jo, Y. S.; Roch, A.; Mikhaylova, M.; Bhujwalla, Z. M.; Muller, R. N.; Muhammed, M., A high-performance magnetic resonance Imaging T-2 contrast agent. *Advanced Materials* **2007**, 19, (18), 2411-2411.

276. Boal, A. K.; Frankamp, B. L.; Uzun, O.; Tuominen, M. T.; Rotello, V. M., Modulation of spacing and magnetic properties of iron oxide nanoparticles through polymer-mediated "bricks and mortar" self-assembly. *Chemistry of Materials* **2004**, 16, (17), 3252-3256.

277. Bin Na, H.; Lee, I. S.; Seo, H.; Il Park, Y.; Lee, J. H.; Kim, S. W.; Hyeon, T., Versatile PEG-derivatized phosphine oxide ligands for water-dispersible metal oxide nanocrystals. *Chemical Communications* **2007**, (48), 5167-5169.

278. Teng, X. W.; Black, D.; Watkins, N. J.; Gao, Y. L.; Yang, H., Platinum-maghemite core-shell nanoparticles using a sequential synthesis. *Nano Letters* **2003**, 3, (2), 261-264.

279. Lyon, J. L.; Fleming, D. A.; Stone, M. B.; Schiffer, P.; Williams, M. E., Synthesis of Fe oxide core/Au shell nanoparticles by iterative hydroxylamine seeding. *Nano Letters* **2004**, 4, (4), 719-723.

280. Cheng, G. J.; Hight Walker, A. R., Synthesis and characterization of cobalt/gold bimetallic nanoparticles. *Journal of Magnetism and Magnetic Materials* **2007**, 311, (1), 31-35.

281. Tsaur, B. Y.; Lau, S. S.; Mayer, J. W., Ion-Beam-Induced Metastable Phases in the Au-Co System. *Philosophical Magazine B-Physics of Condensed Matter Statistical Mechanics Electronic Optical and Magnetic Properties* **1981**, 44, (1), 95-108.